(NASA-CR-140321) SPACE SHUTTLE ORBIT MANEUVERING ENGINE REUSABLE THRUST CHAMBER PROGRAM Tasks 5 and 8 Data Dump One Demonstrator Thrust Chamber Test Report (Rocketdyne) 112 p HC $5.25 CSCL 21H G3/20

N75-10167

Unclas
5302

Rocketdyne Division
Rockwell International

SPACE SHUTTLE

ORBIT MANEUVERING ENGINE

REUSABLE THRUST CHAMBER PROGRAM

TASKS V AND VIII DATA DUMP
OME DEMONSTRATOR THRUST CHAMBER
TEST REPORT

NAS 9-12802

Rocketdyne Division of Rockwell International
6633 Canoga Avenue; Canoga Park, California 91304

SPACE SHUTTLE

ORBIT MANEUVERING ENGINE

REUSABLE THRUST CHAMBER PROGRAM

TASKS V AND VIII DATA DUMP
OME DEMONSTRATOR THRUST CHAMBER
TEST REPORT

Prepared by

R. P. Pauckert

M. C. Yost

R. D. Tobin
Advanced Programs

Approved by

R. D. Paster
SS/OME Project Engineer
Advanced Programs

R. W. Helsel
Program Manager
SS/APS Programs

Rocketdyne Division of Rockwell International
6633 Canoga Avenue; Canoga Park, California 91304

CONTENTS

ILLUSTRATIONS

TABLES

INTRODUCTION

The Orbit Maneuvering Engine of the Space Shuttle will use a regeneratively cooled thrust chamber. Present plans call for using MMH as the fuel and coolant for the engine with NTO as the oxidizer. A 50-50 blend of hydrazine and UDMH is a possible alternate fuel. Under Tasks I and II of Contract NAS9-12802, Rocketdyne investigated, analytically, several thrust chamber cooling concepts and fuel coolants. Using the criteria of performance, reliability, safety, maintainability, cost, and development risk Rocketdyne concluded that the regeneratively cooled chambers using amine fuels was a superior combination.

Some experience with regeneratively cooled chambers using amine fuels was available. Rocketdyne performed some preliminary experiments using existing high thrust LOX/RP-1 engines and testing them with NTO/amine fuels. The engines used on the VEGA Program at JPL used amine cooled thrust chambers.

The thrust chambers for the Japanese upper stage space engine use 50-50 coolant. Rocketdyne is a consultant on this program. While this experience provided the base upon which the regeneratively cooled MMH thrust chamber was selected by Rocketdyne, operation at OME design operating conditions with man rated safety factors had never been accomplished. The purpose of this experimental program, was to verify the performance, thermal and stability characteristics analytically predicted for the OME and to provide data to supplement the analytical calculations.

Injectors used for the program were previously designed, fabricated, and tested under a company sponsored program. Injector performance, heat transfer and stability characteristics were obtained during this program. Recorded heat flux profiles were used for the design of the regeneratively cooled thrust chamber. The regeneratively cooled thrust chamber was designed and fabricated under Tasks II and IV of this Contract (NAS9-12802). The cooled chamber was designed with flight hot wall thickness and channel geometry to accurately determine cooling characteristics. The thrust chamber utilized non-flightweight manifolds for cost effectiveness and test flexibility.

SUMMARY

A total of 112 tests were conducted on the regenerative cooled demonstration chamber for an accumulated duration of 1042 seconds (Fig. 1) at Rocketdyne's Component Test Laboratory IV (CTL-IV), and NASA's White Sands Test Facility (WSTF). Initial checkout tests at CTL-IV were conducted with bypass cooling to allow independent control of regenerative jacket coolant flow and injector fuel flow. The chamber was then replumbed to provide completely regenerative cooling for the remainder of the tests. A total of 32 tests were conducted at CTL-IV for a total duration of 439 seconds, including one test of 185 seconds duration. These tests demonstrated thrust chamber operation over the nominal ranges of chamber pressure and mixture ratio. Variations in auxiliary film coolant flowrate were also demonstrated.

The remaining 80 tests were conducted at the White Sands Test Facility, where a total duration of 603 seconds was accumulated. These tests were conducted with both MMH and 50-50 fuels, and demonstrated performance, safety, and stability over the nominal chamber pressure and mixture ratio ranges. The effects of helium saturation were demonstrated with both propellants. Several tests were conducted without boundary layer cooling over the range of chamber pressures and mixture ratios. Operation under conditions simulating a vehicle propellant tank pressurization system failure was also demonstrated. Finally, high pressure tests at the facility upper pressure limit were conducted to demonstrate thrust chamber operation at conditions approaching the design chamber pressure for an OME derivative Space Tug application, designed to operate with NTO/MMH propellants.

The demonstration chamber after these tests was in good condition. The thrust chamber had been slightly damaged due to a facility malfunction at CTL-IV, but was repaired and used for the WSTF tests without further incidents.

FIGURE 1

DEMONSTRATION CHAMBER TEST SUMMARY

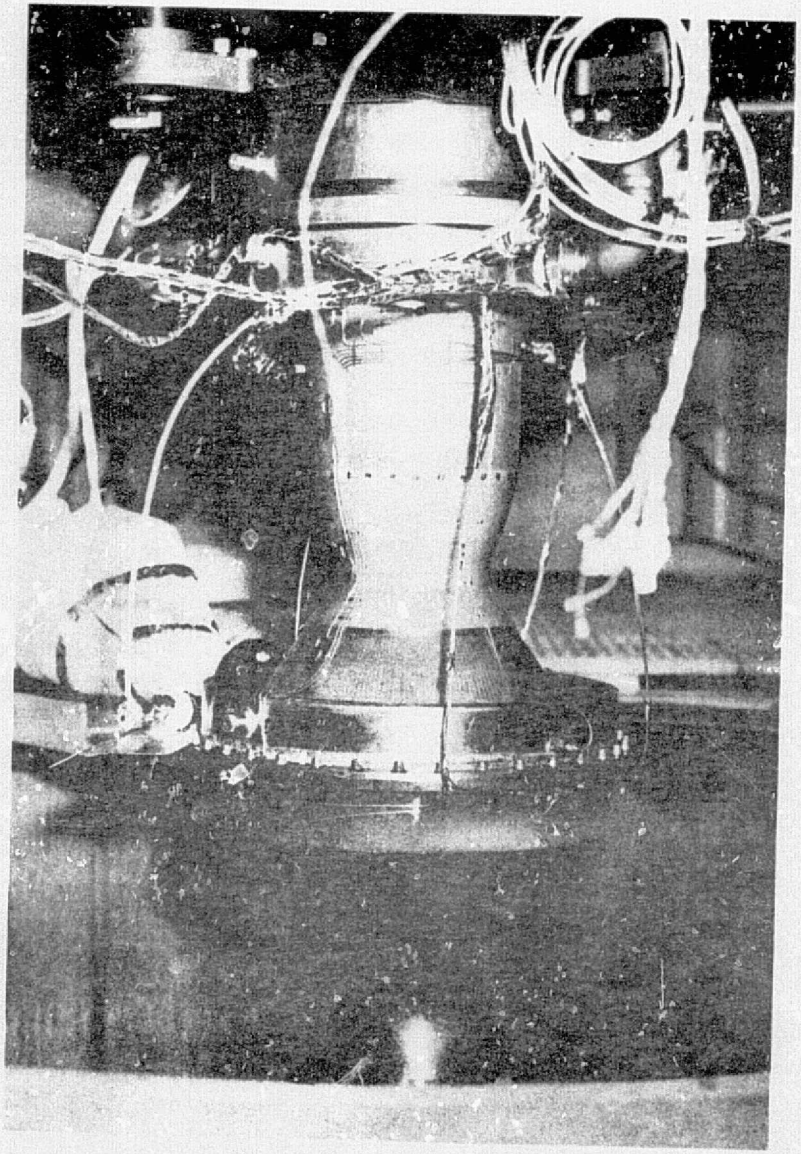

- 112 TESTS
- 1042 SEC TOTAL DURATION
- 100-178 PSIA CHAMBER PRESSURE
- 1.40-1.88 O/F MIXTURE RATIO
- 0-3% FILM COOLANT
- MMH AND 50-50 FUELS

334-178

Rocketdyne Division
Rockwell International

Based on the test data, the engine performance extrapolated to vacuum test conditions with a high area ratio (72:1) nozzle attached, is 310 seconds at nominal conditions. Performance measured at CTL-IV and WSTF agreed within 1 percent. The coolant temperature rise was 131 F, approximately 25 percent less than predicted based on earlier injector heat sink data. Radiation cooled nozzle temperatures were significantly lower than predicted. The regenerative coolant pressure drop was approximately the value predicted, 15 psi. All tests with regeneratively cooled thrust chambers were stable with respect to both high and low frequency. Stability was achieved without baffles by using acoustic cavities.

From the results of these tests, it may be concluded that the Orbit Maneuvering Engine regeneratively cooled thrust chamber designed by Rocketdyne, will operate safely at nominal and off-design operating conditions. Additional design and testing is recommended to develop increased performance and to demonstrate operation with flightweight hardware which simulates engine hydraulic characteristics such that start and shutdown characteristics as well as duty cycle constraints (minimum on and off times0 can be defined.

TEST HARDWARE

The hardware used for the test program consisted of a regeneratively cooled thrust chamber, a short radiation cooled nozzle, an auxiliary film coolant ring, and two like doublet injectors. The hardware was designed to provide maximum test flexibility. All components were bolted together and sealed with either metallic or elastomeric O-rings, as appropriate.

A drawing of the thrust chamber assembly is shown in Fig. 2. Table 1 provides a summary of the regenerative cooled chamber design characteristics. The combustion chamber length is 14.7 inches and has a contraction ratio of 2:1 with a throat diameter of 5.820. The expansion area ratio of the regeneratively cooled nozzle is 7:1. The inner wall and the lands of the chamber are 321 CRES and the channels are closed out with electroformed nickel. The CRES liner with 180 coolant channels is shown in the photograph of Fig. 3. The thrust chamber was designed for the heat flux profile shown in Fig. 4. Channel sizes are such that the minimum safety factor is approximately 1.5 at the most severe off design conditions, namely, the fuel inlet temperature of 100 F, the chamber pressure of 112 psia, and a propellant mixture ratio of 1.85. The coolant jacket itself is flight-weight with nickel closeout thicknesses as thin as 0.020 inches at the throat. The inlet and outlet manifolds are heavy weight configurations to reduce cost. The completed regeneratively cooled thrust chamber is shown in Fig. 5.

The radiation cooled nozzle shown in Fig. 6 is Columbium 103 and extends the area ratio to $\epsilon = 9:1$. The nozzle is coated with a VAC-HYD coating of silicide (V-101). The nozzle is contoured externally to simulate the transient soakback characteristics of the full length nozzle. A separately fed auxiliary film coolant ring is bolted between the injector manifold and the coolant discharge manifold of the thrust chamber. The ring has 180 coolant orifices and, during regeneratively cooled chamber operation, is fed from the chamber discharge manifold line with an orifice to control flow. During the

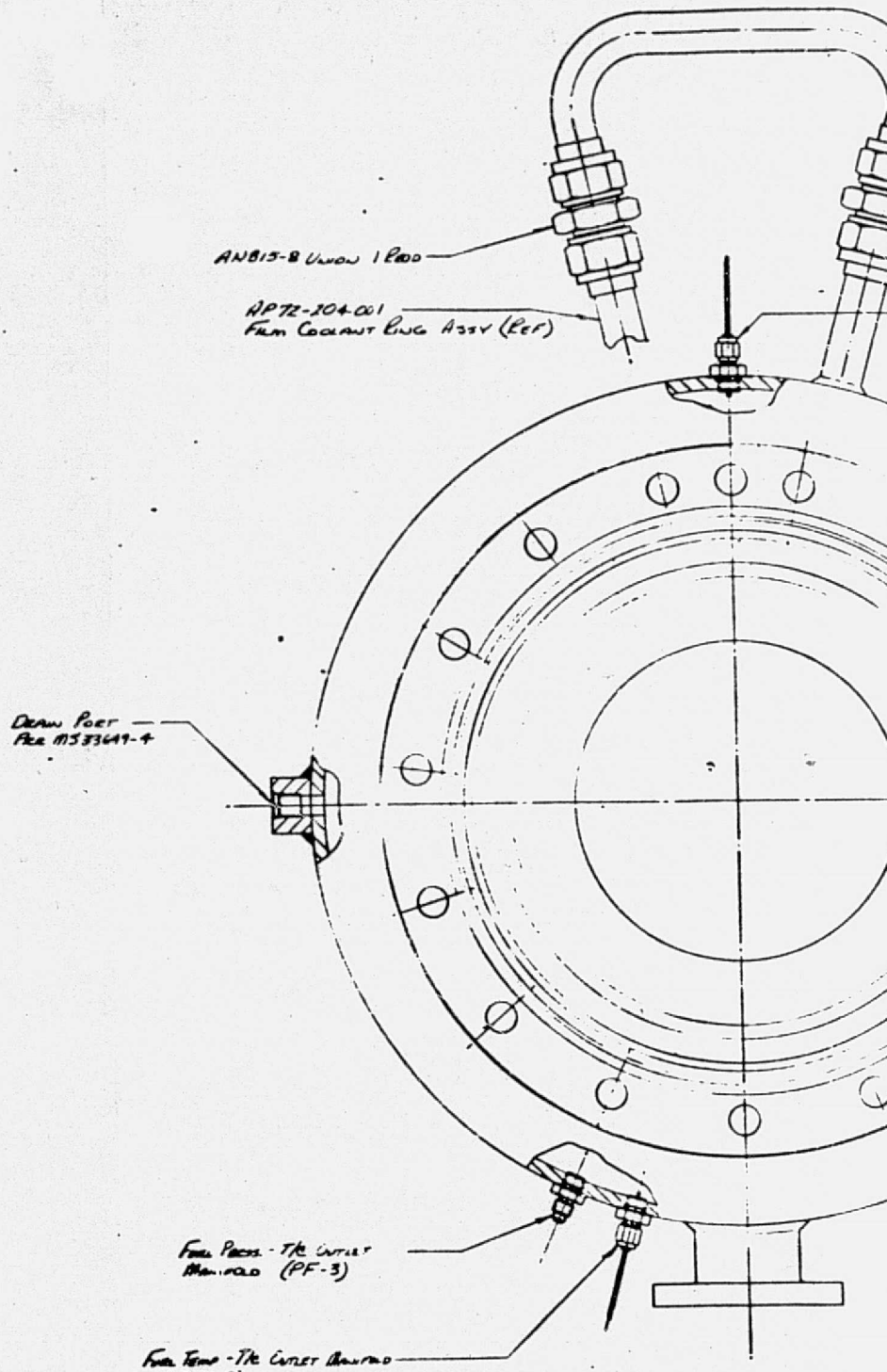

View 13-13
(Thrust Chamber Only)

MICROFILM OVERLAP AREA

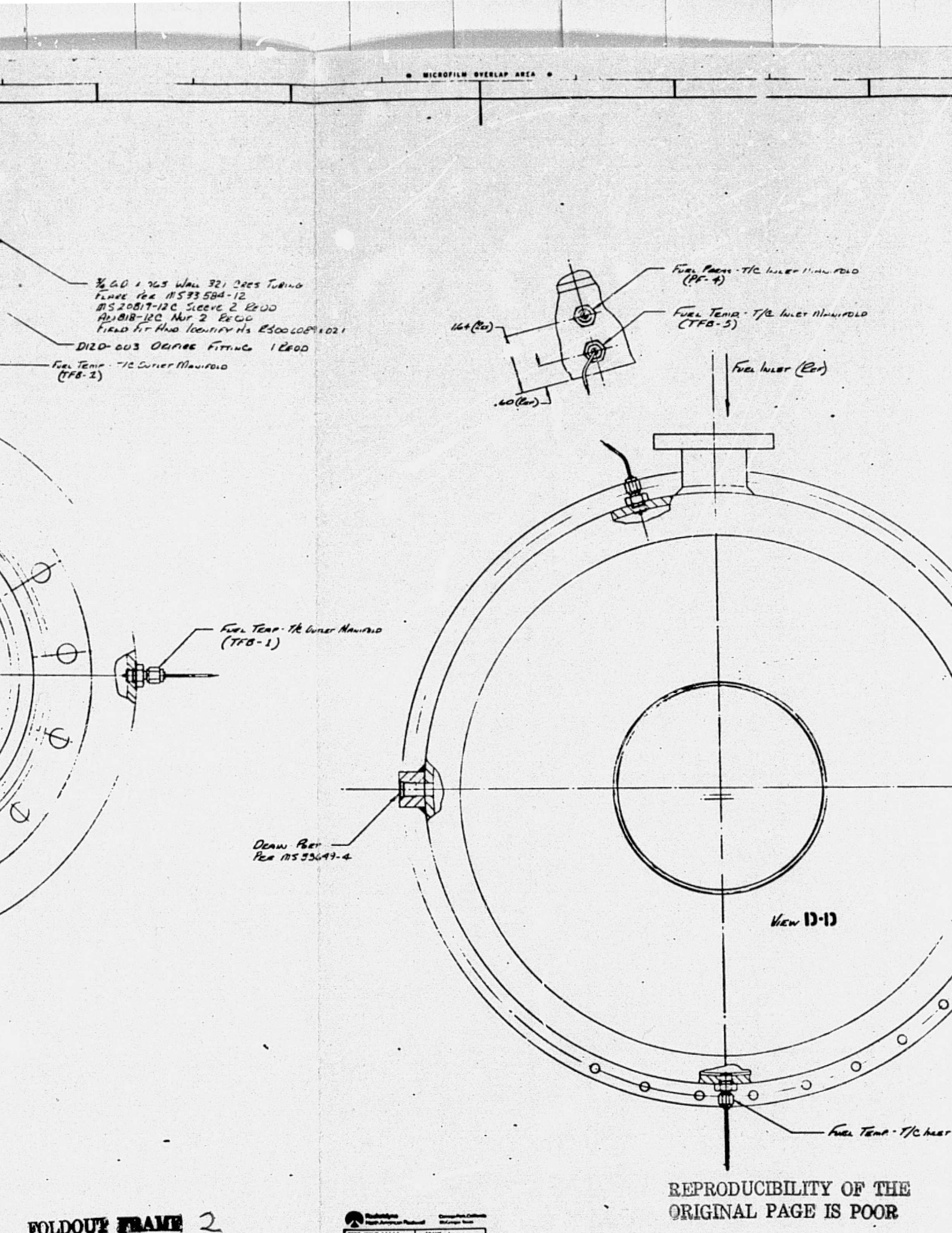

REPRODUCIBILITY OF THE ORIGINAL PAGE IS POOR

FOLDOUT FRAME 2

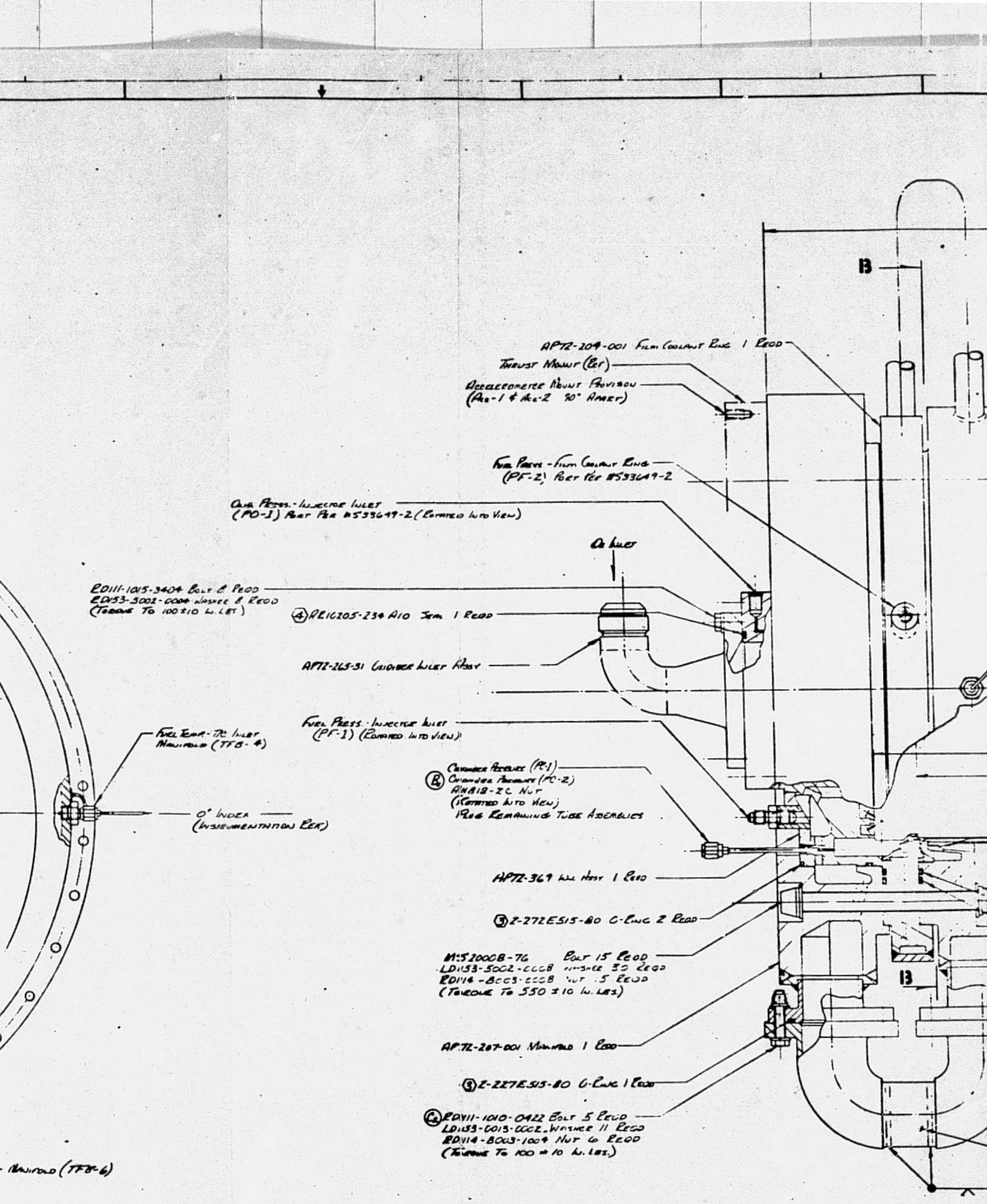

FOLDOUT FRAME 3

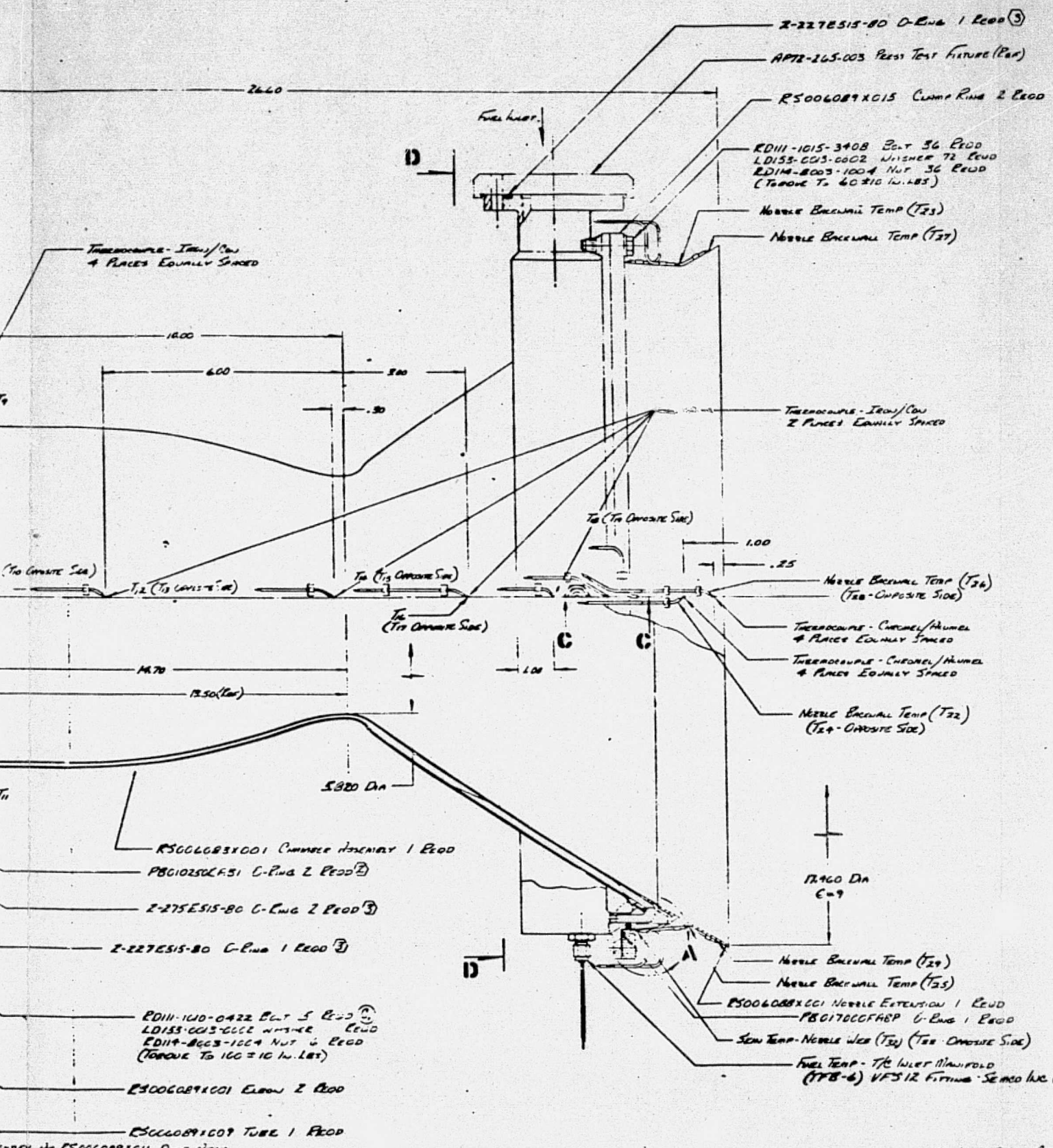

PLAN VIEW - FACILITY MOUNTED (Ref)

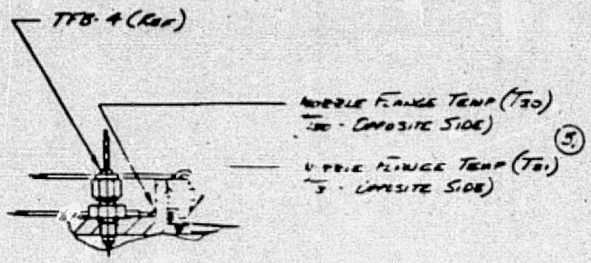

VIEW C-C

ASSEMBLY CONFIG	
DETAIL PART NO.	DETAIL PART NAME
AP72-369	INJECTOR ASSY
R500C689X021	TUBE ASSY
AP72-207-001	MANIFOLD ASSY
AP72-265-21	INLET ASSY
NP72-204-001	RING ASSY
R500C083C001	CHAMBER ASSY
R500C689X001	NOZZLE EXTENSION
R500C689X015	CLAMP RING
R500C689X011	DUCT ASSY

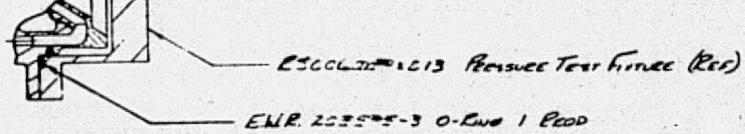

DETAIL A
(LEAK CHECK ASSY)

FOLDOUT FRAME 5

THIS IS NOT A RELEASE COPY

Figure 2

1. LEAK CHECK ASSEMBLY WITH GN_2 TO 100±10 PSIG.
2. FIELD FIT AND WELD PER EA0167-027 USING 308 ELC FILLER WIRE WITH FLANGES BOLTED IN PLACE. CLEAN PER EA0116-018 PRIOR TO FINAL ASSY.
3. HARRISON MFG CO BURBANK, CALIF
4. AEROJET CORP SUPERIOR, CALIF
5. [illegible] SEAL CO CULVER CITY, CALIF

AEROJET-TRW[illegible] GK GM.E.

Table 1. Demonstrator Thrust Chamber Design Characteristics

Combustor	
Contraction Ratio	2:1
Length, in.	14.7
Contour	Tapered from 7 in. upstream of throat
Nozzle	
Regen Section Expansion Ratio	to 7:1
Contour	Flight parabolic
Nozzle Extension Expansion Ratio	7:1 to 9:1
Contour	30^{o} Conical
Coolant	
Circuit	Uppass
Number of Regen Coolant Channels	180
Coolant Pressure Drop, psid	15
Coolant Bulk Temperature Rise, F	178
Auxiliary Film Coolant	2.5% Total Propellant
Materials	
Hot Wall (0.030 in.) and Lands	Cres 321
Cold Wall (0.030 in.)	Electroformed Nickel
Nozzle Extension	Columbium 103 with Vac Hyd Silicide Coating

Figure 3. Slotted OME Chamber

FIGURE 4

DEMONSTRATOR CHAMBER HEAT FLUX PROFILE

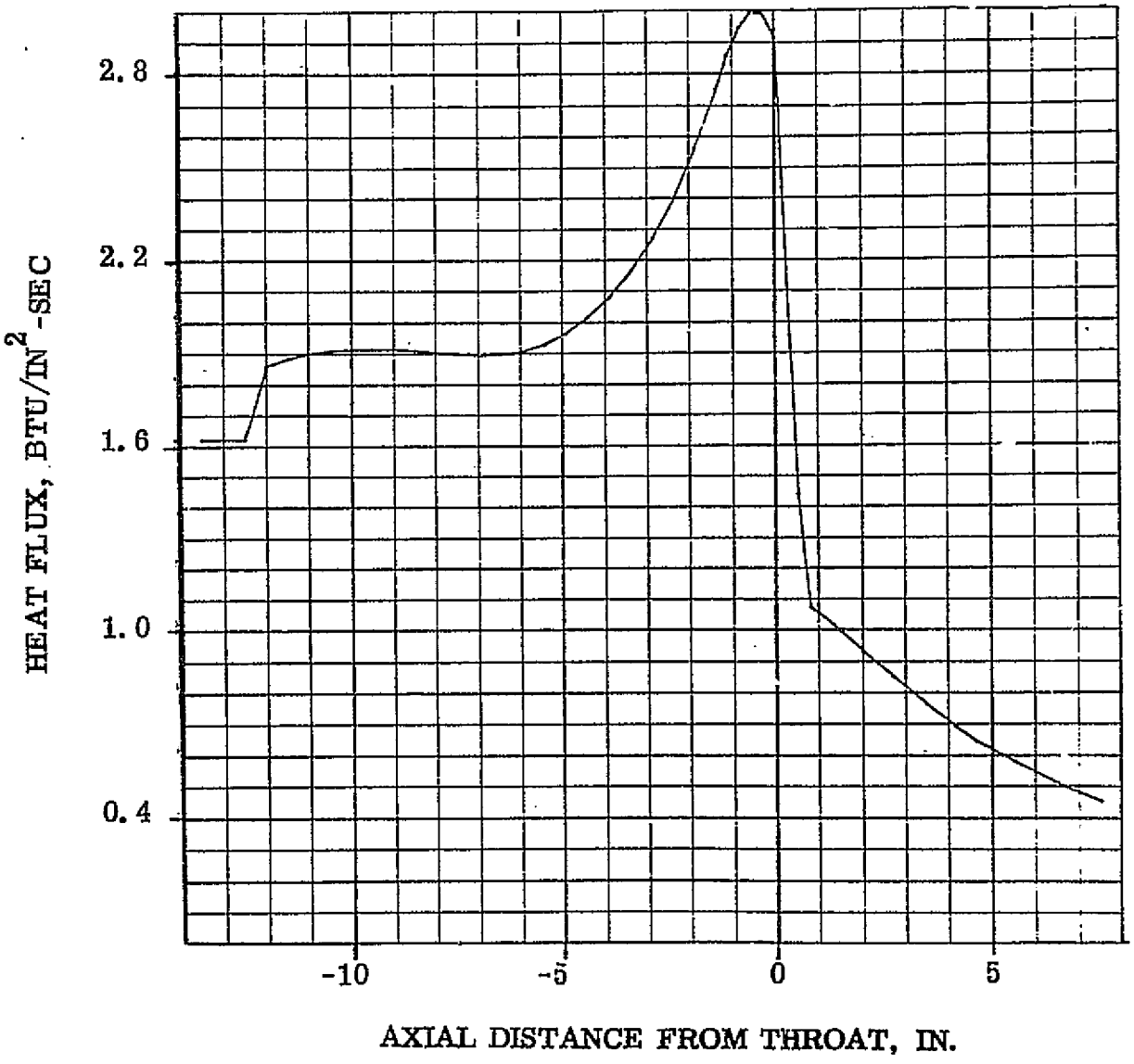

Figure 5. Demonstration Thrust Chamber

Figure 6. Nozzle Extension with Instrumentation

earlier bypass cooling tests, the film coolant was fed from the injector inlet line. The coolant ring also forms the outer walls and dams of the entrance to the acoustic cavities. The film coolant ring is shown in Fig. 7 and 8 .

Two like-doublet element injectors (Fig.9) were used with the thrust chamber. Table 2 summarizes their design characteristics. These injectors were designed by Rocketdyne under a company sponsored program and tested in solid wall thrust chambers to provide performance and stability data and heat flux profiles for design of the regeneratively cooled thrust chamber.

In the test hardware configuration, the acoustic cavities and the cavity dams were wholly contained within the injector body assembly, whereas a flight configuration assembly would use the regeneratively cooled chamber for the outer cavity walls and the cavity dams.

Provisions were made in the thrust chamber manifolds to measure the coolant inlet and outlet pressures. The coolant inlet and outlet temperatures were each measured at three locations on the inlet end of the manifolds. The locations at which thrust chamber and nozzle skin temperature measurements were made are shown in Fig. 2 and described in Table 3. Propellant pressures were measured in the injector and boundary layer coolant ring manifolds. Chamber pressure was measured in the acoustic cavities.

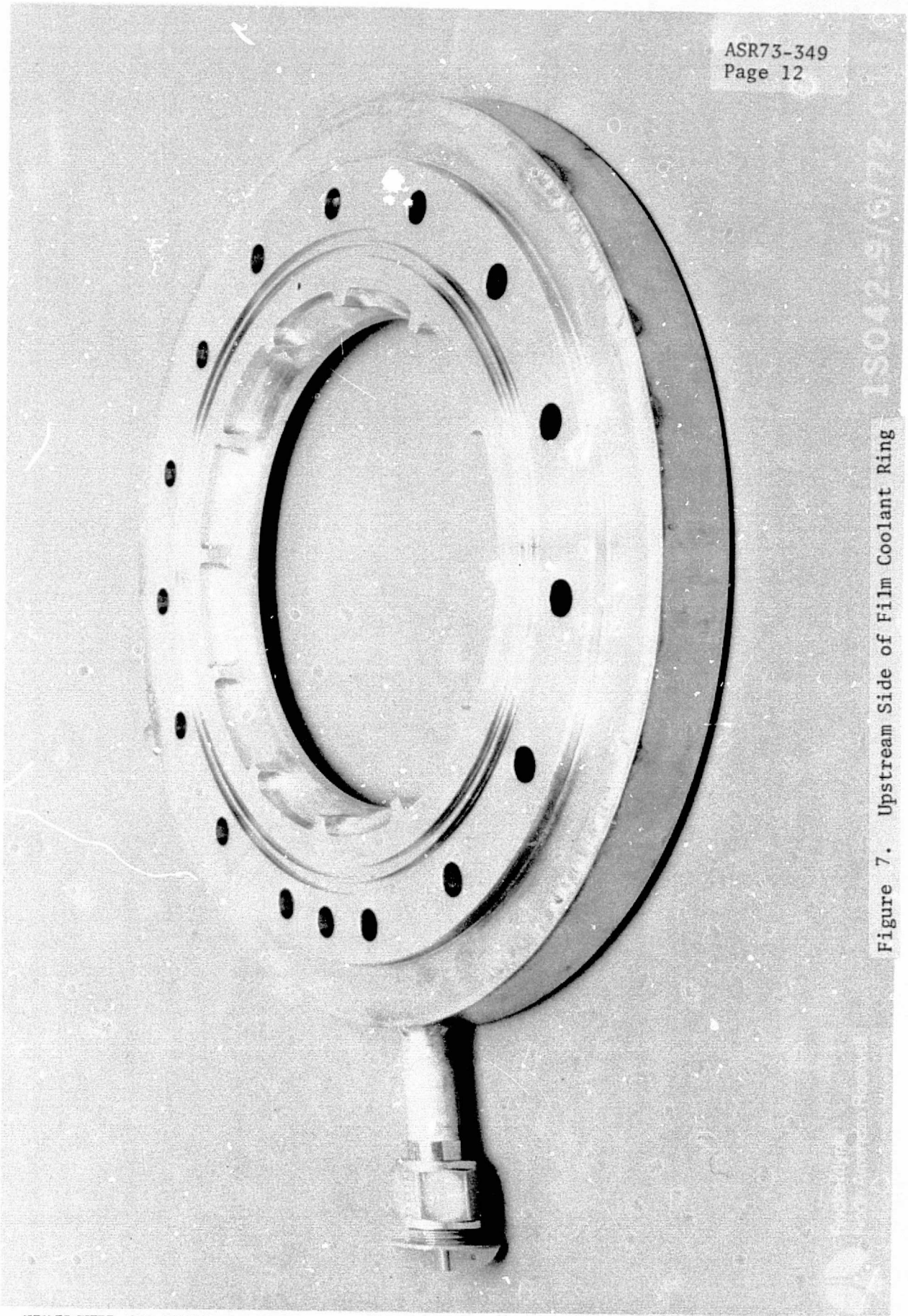

Figure 7. Upstream Side of Film Coolant Ring

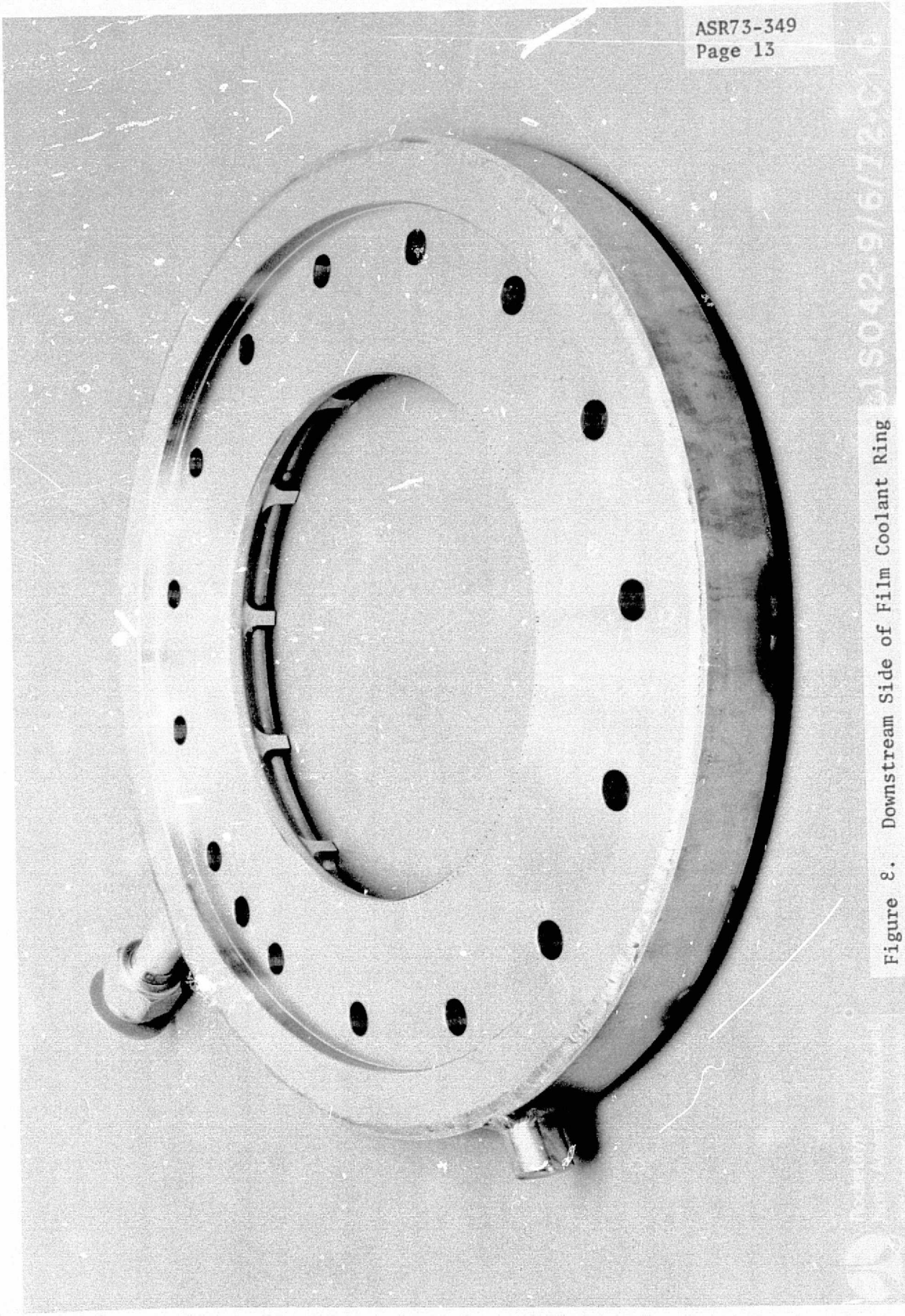

Figure 8. Downstream Side of Film Coolant Ring

FIGURE 9

OME LIKE DOUBLET INJECTORS

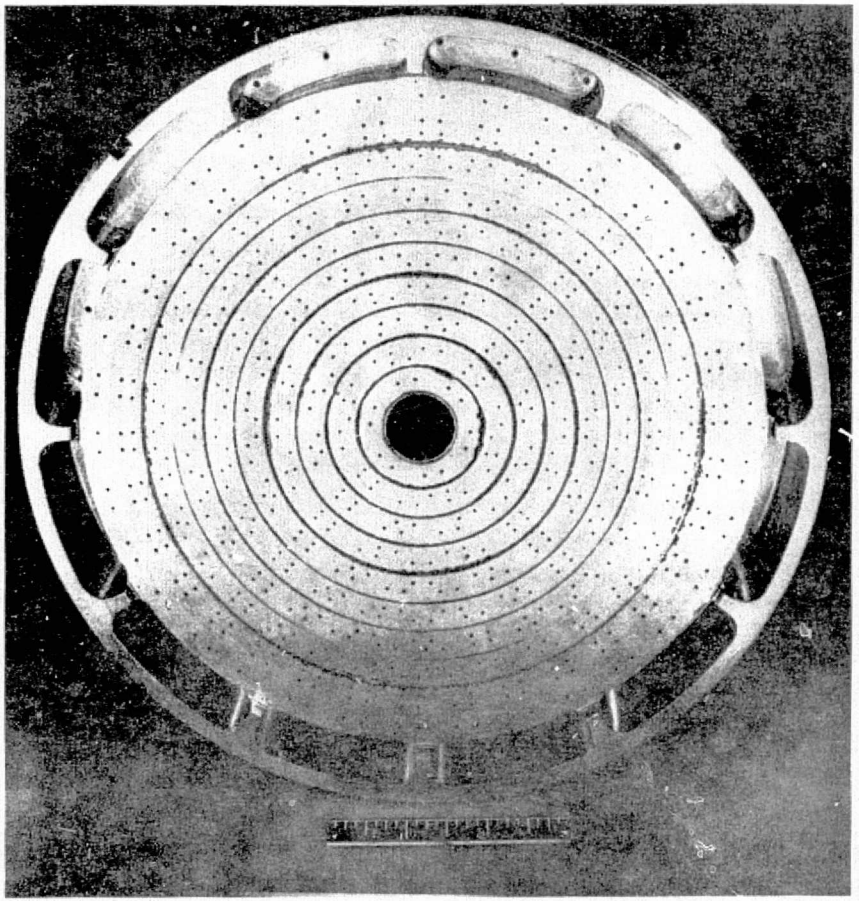

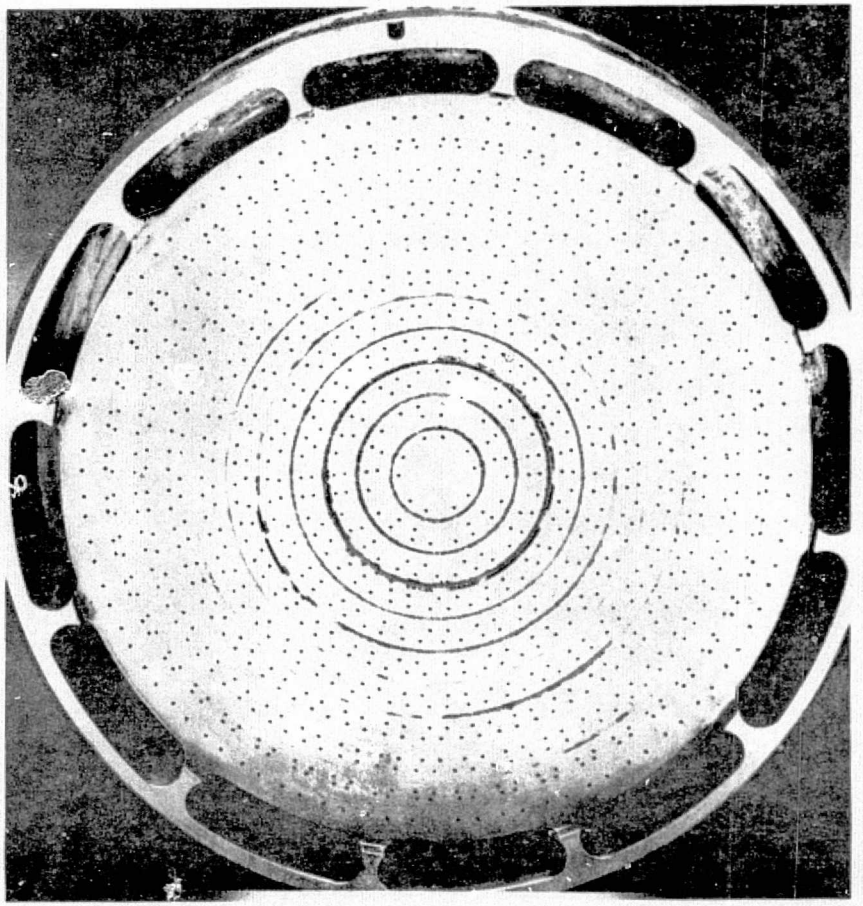

277-306

Rocketdyne Division
Rockwell International

Table 2. Injector Characteristics

	No. 1	No. 2
Diameter, in.	8.200	8.200
Number of Elements	186	286
Number of Rows	9	10
Type of Elements	Like Doublet	Like Doublet
Oxidizer Element Diameter, in. (minimum/maximum)	0.032/ 0.038	0.026 0.032
Fuel Element Diameter, in. (minimum/maximum)	0.028/ 0.033	0.025/ 0.031
Number of Acoustic Cavities	12	8/4
Mode Suppression	1st Tangential	1st Tang., 1st Rad., 3rd Tang.

TABLE 3

ENGINE INSTRUMENTATION LIST

(See Figure 5 for Instrumentation Location on Engine)

TEMPERATURE

TFB-1	Fuel Temp. - T/C Outlet Manifold	@ 0°
TFB-2	Fuel Temp. - T/C Outlet Manifold	@ 90°
TFB-3	Fuel Temp. - T/C Outlet Manifold	@ 255°
TFB-4	Fuel Temp. - T/C Inlet Manifold	@ 0°
TFB-5	Fuel Temp. - T/C Inlet Manifold	@ 105°
TFB-6	Fuel Temp. - T/C Inlet Manifold	@ 270°
T8	Ni. Back Wall Temp. @ STA-10.0	@ 0°
T9	Ni. Back Wall Temp. @ STA-10.0	@ 90°
T10	Ni. Back Wall Temp. @ STA-10.0	@ 180°
T11	Ni. Back Wall Temp. @ STA-10.0	@ 270°
T12	Ni. Back Wall Temp. @ STA-6.0	@ 0°
T13	Ni. Back Wall Temp. @ STA-6.0	@ 180°
T14	Ni. Back Wall Temp. @ STA-.30	@ 0°
T15	Ni. Back Wall Temp. @ STA-.30	@ 180°
T16	Ni. Back Wall Temp. @ STA+3.0	@ 0°
T17	Ni. Back Wall Temp. @ STA+3.0	@ 180°
T18	Skin Temp. - T/C Inlet Manifold	@ 0°
T19	Skin Temp. - T/C Inlet Manifold	@ 180°
T20	Nozzle Flange - T/C Side	@ 0°
T21	Nozzle Clamp Ring	@ 0°
T22	Nozzle Back Wall @ STA+8.3	@ 0°
T23	Nozzle Back Wall @ STA+8.3	@ 90°
T24	Nozzle Back Wall @ STA+8.3	@ 180°
T25	Nozzle Back Wall @ STA+8.3	@ 270°
T26	Nozzle Back Wall @ STA+9.0	@ 0°
T27	Nozzle Back Wall @ STA+9.0	@ 90°
T28	Nozzle Back Wall @ STA+9.0	@ 180°
T29	Nozzle Back Wall @ STA+9.0	@ 270°
T30	Nozzle Flange - T/C Side	@ 180°
T31	Nozzle Clamp Ring	@ 180°
T32	Skin Temp. - Nozzle Web	@ 90°
T33	Skin Temp. - Nozzle Web	@ 270°

PRESSURE

PC-1	Chamber Pressure
PC-2	Chamber Pressure
PO-1	Oxidizer Inlet Pressure Injector
PF-1	Fuel Inlet Pressure Injector
PF-2	Fuel Pressure - B.L.C. Ring
PF-3	Fuel Pressure - T/C Outlet Manifold @ 250°
PF-3	Fuel Pressure - T/C Inlet @ 105°
Acc-1	Accelerometer - Axial
Acc-2	Accelerometer - Axial

NOTE: 0° @ 12:00 Noon Facing Injector, Clockwise
STA. Location (±) From Throat With Aft (+)

TEST FACILITIES

The thrust chamber was tested at Rocketdyne's Santa Susana Field Laboratory in Cell 29-B of the Component Test Laboratory IV and at Test Cell 401 of the White Sands Test Facility. Both test sites are altitude facilities with complete instrumentation capability.

COMPONENT TEST LABORATORY IV

Figure 10 is a photograph of Rocketdyne's Component Test Laboratory IV. The engine is shown installed in this facility in Fig. 11. Two feed system arrangements were used for the engine in this facility. One of the configurations shown in Fig. 12 was used to provide a bypass cooling system in which coolant flowed through the regenerative jacket and was dumped into a catch tank. A separate feed system (from the same propellant tank) provided fuel for the injector. The fuel in this system was heated in a hot water heat exchanger to simulate the temperature of the propellant leaving the regeneratively cooled jacket. Oxidizer flow to the engine was controlled by regulating the oxidizer tank pressure to a predetermined value dependent upon the system and engine hydraulic resistance. The coolant flowrate and pressure levels were adjusted by the use of appropriately sized fixed orifices at the inlet and exit to the thrust chamber cooling jacket. Fuel flow for the injector was obtained from a branch (tee) in this line and the flowrate was adjusted by a variable area throttling servo-controlled valve. The injector fuel feed system and the oxidizer feed system contained dual flowmeters for measurement of propellant flowrates while a single flowmeter was used in the thrust chamber bypass cooling system. Boundary layer coolant flow was taken from the injector feed system and controlled and measured by means of a calibrated orifice. Gaseous nitrogen purges were supplied at the engine for all feed systems and a water flush was provided at the injector interface. Purges were operated manually at the end of each test series to permit safe inspection of the thrust chamber and injector.

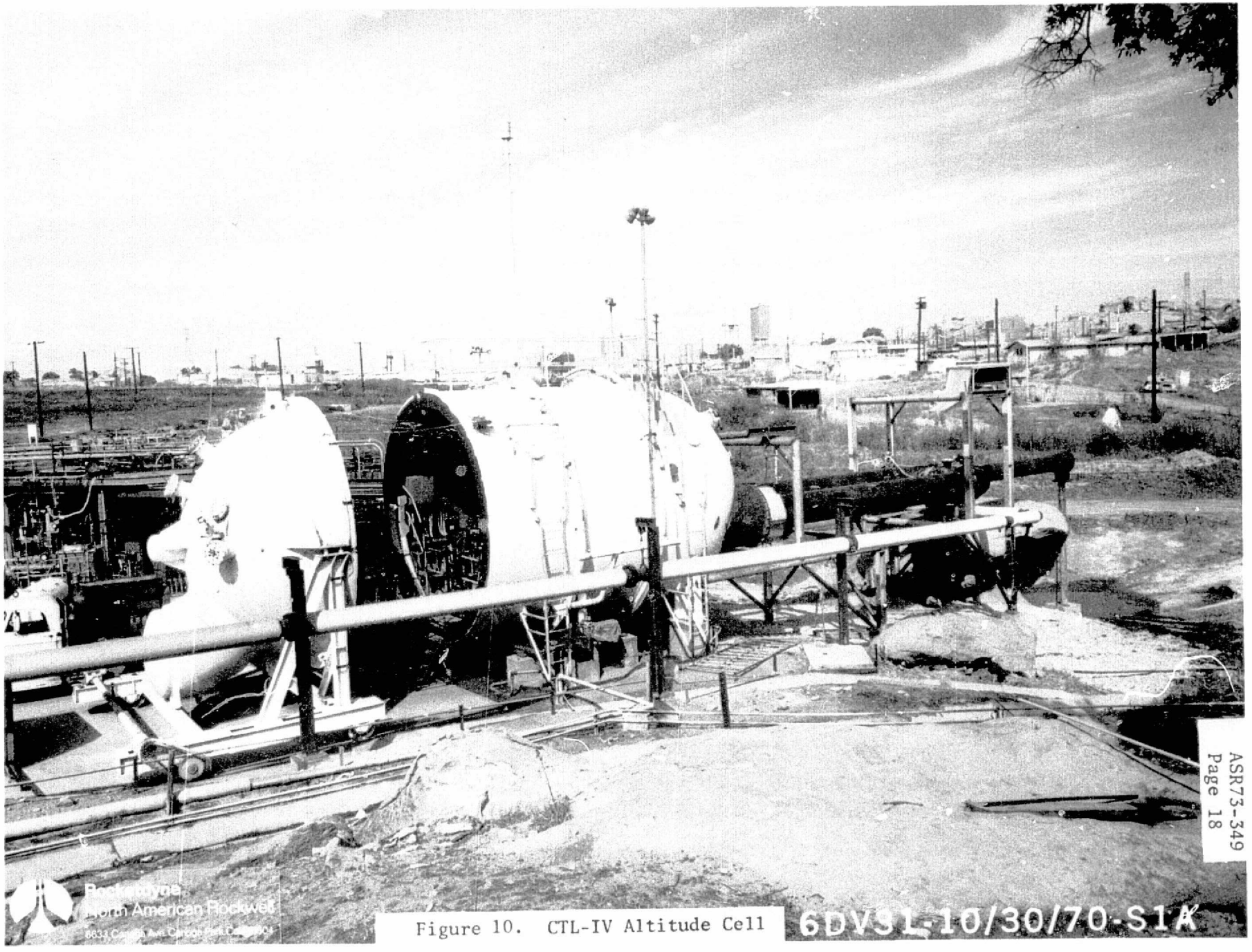

Figure 10. CTL-IV Altitude Cell

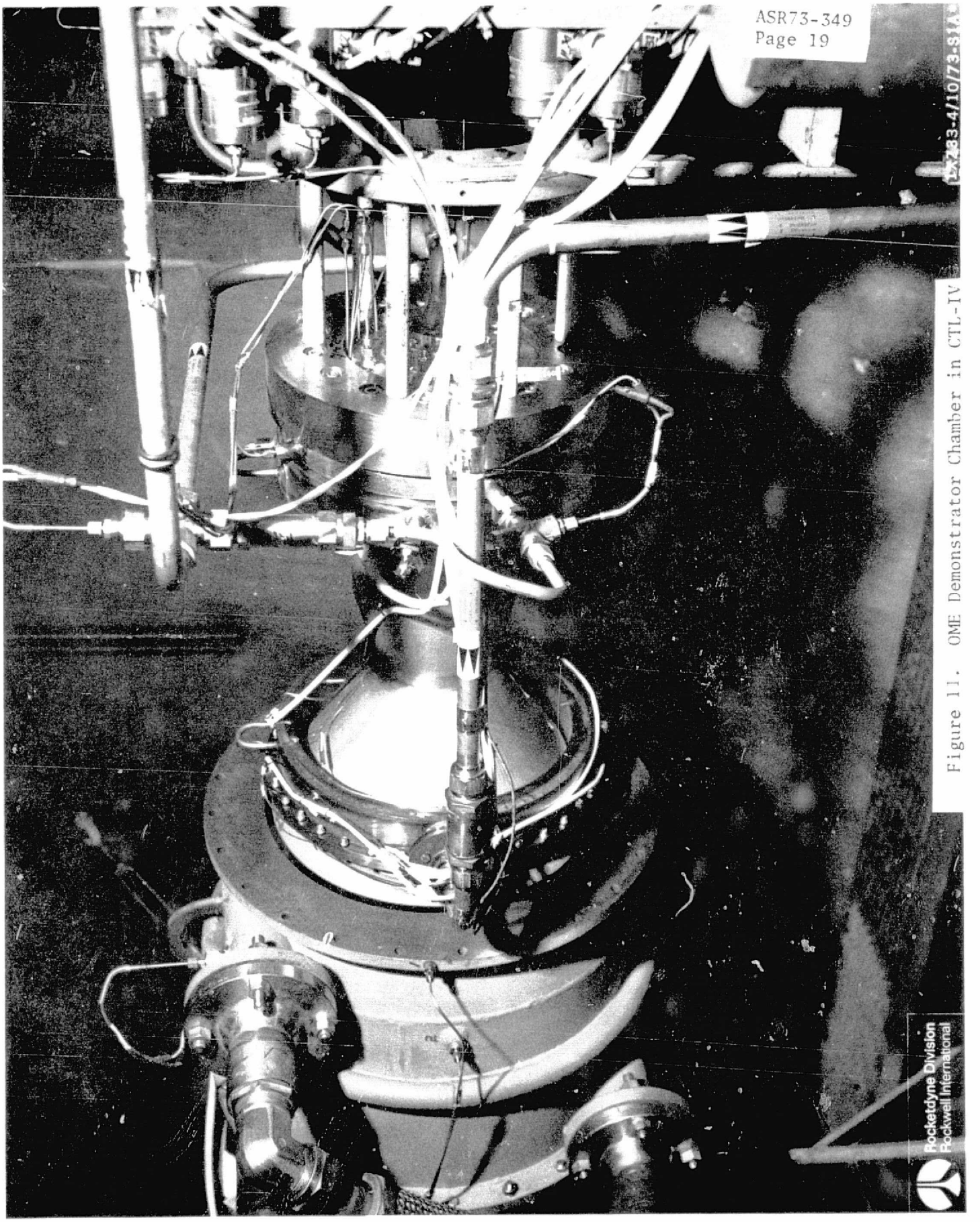

Figure 11. OME Demonstrator Chamber in CTL-IV

FIGURE 12

FACILITY AND INSTRUMENTATION SCHEMATIC FOR BYPASS COOLING

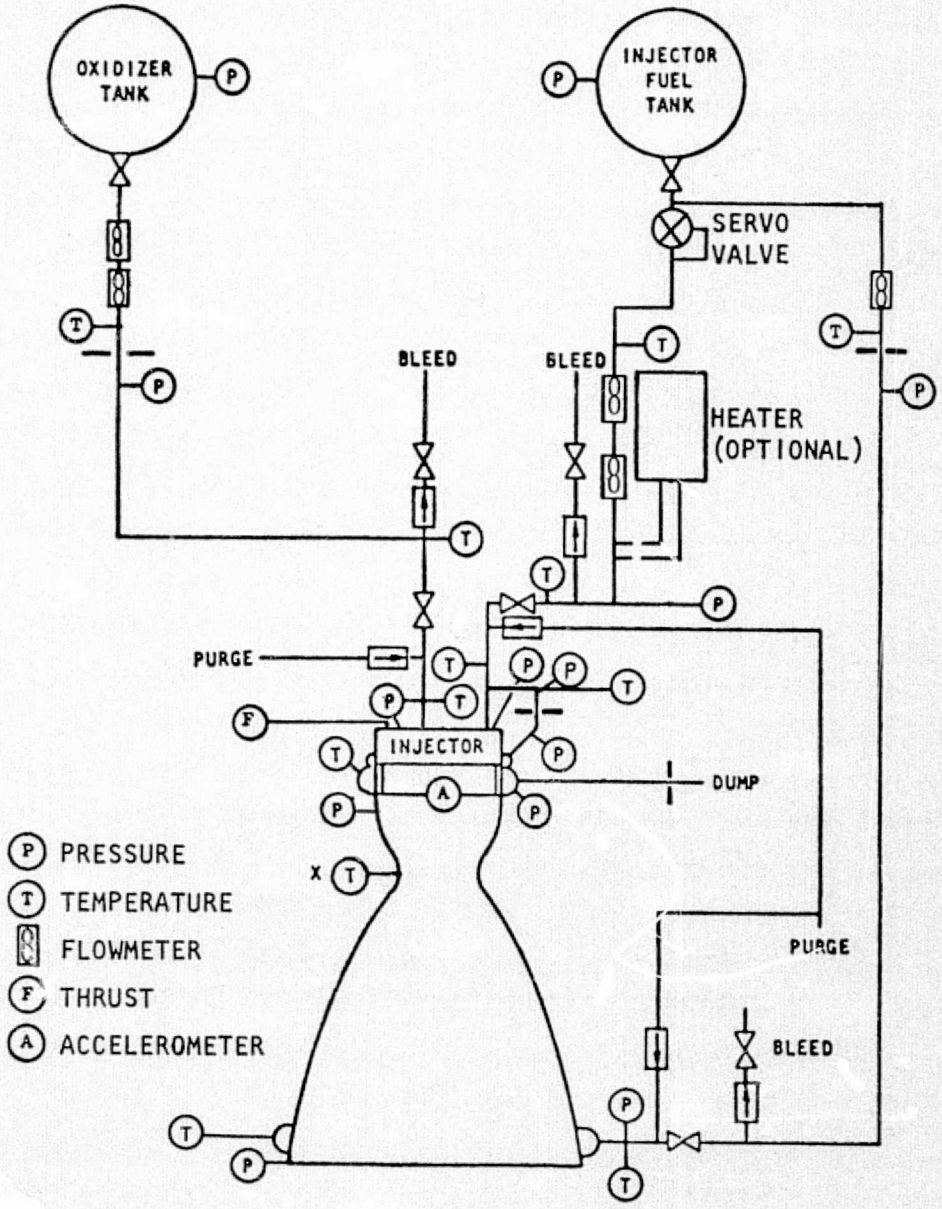

After the first checkout tests, the feed system was replumbed to the configuration shown in Fig. 13 , in which coolant exiting the regenerative jacket was ducted directly into the injector manifold. The servo valve was used to control the fuel flowrate. The oxidizer and fuel tanks were each rated at 665 psig and had capacities of 1600 and 1200 gallons, respectively. Several hundred seconds of operation at OME conditions were, therefore, possible with these propellant tanks.

The CTL-IV altitude facility in which the engine was tested is shown in schematically in Fig. 14 . The engine was mounted horizontally in the 16-foot diameter altitude capsule and fired into a water cooled diffuser duct. The capsule is 31 feet long with hemispherical ends, one of which is roller mounted to provide access to the engine. A gas generator driven ejector was initially fired to reduce the pressure in the altitude capsule with the 42-inch flapper valve closed. When the engine ignited, the valve was opened by a pneumatic actuator and the engine exhaust maintained the capsule at the low pressure. A simulated altitude of 75,000 feet (0.5 psia) is attainable with this configuration. At engine shutdown, the 42-inch valve was closed to minimize blowback into the altitude capsule.

The ejector was run continuously during the test and was shutdown after engine shutoff. When the ejector was shutdown, the isolation valve was closed and the capsule slowly brought up to pressure by bleeding in external air through the 6-inch vent valve. The gas generator system for the ejector has sufficient propellants to provide for 45 minutes of operation.

The complete list of all facility and engine mounted instrumentation is shown in Table 3 and 4. Thrust was measured by a single axis dual bridge load cell so that two thrust readings were obtained. Two independent flow measurements were made for each propellant entering the injector and a single flow measurement was made of the fuel coolant when the configuration was plumbed for bypass operation.

FIGURE 13

FACILITY AND INSTRUMENTATION SCHEMATIC FOR REGENERATIVE COOLING

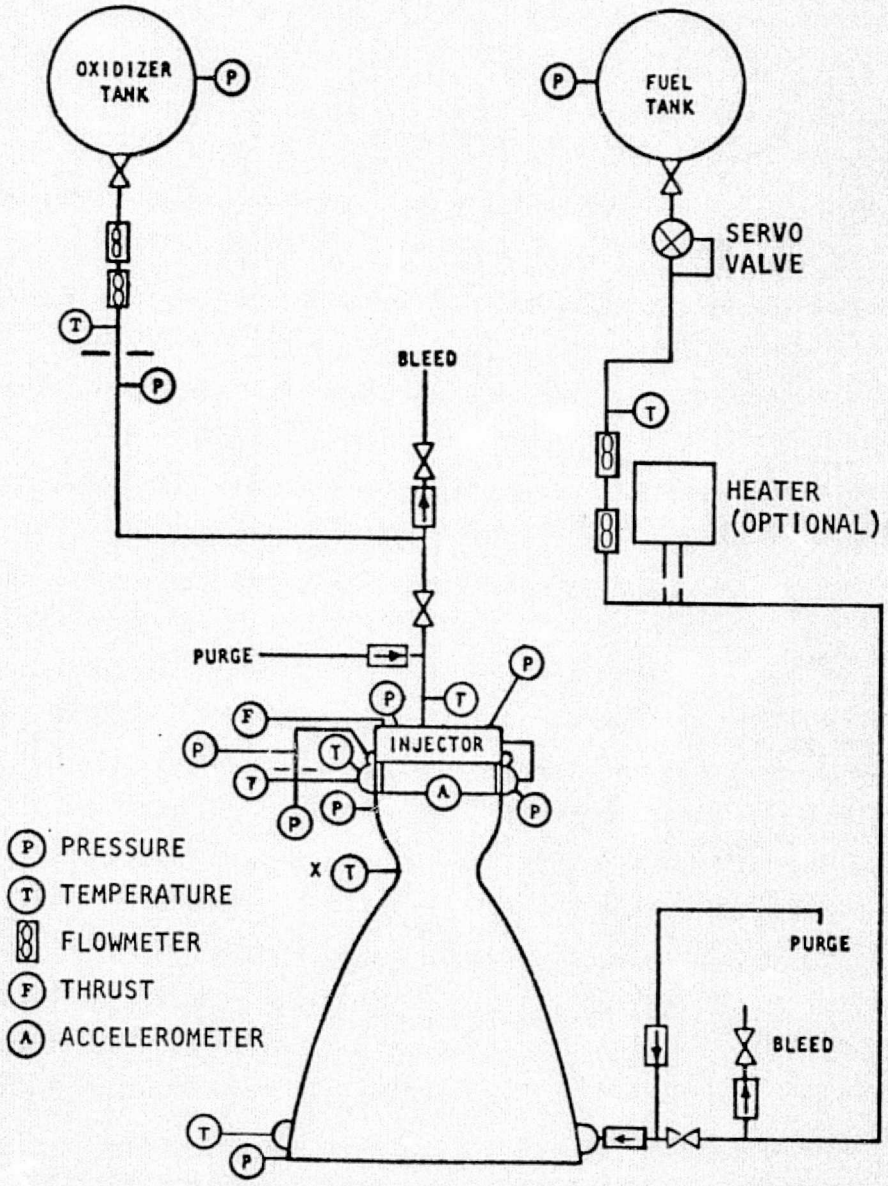

FIGURE 14

CELL 29 FACILITY SCHEMATIC

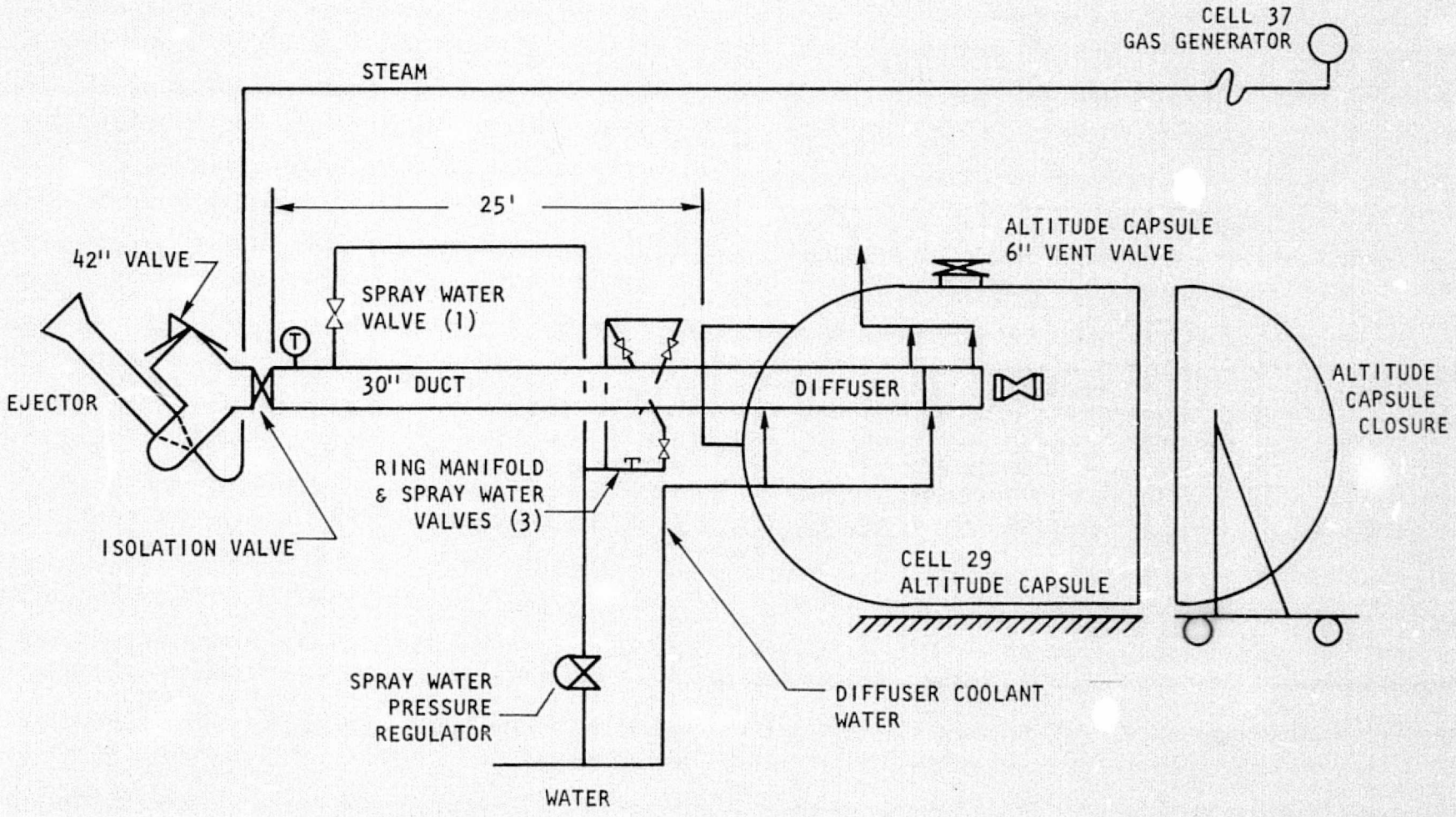

TABLE 4

TEST INSTRUMENTATION

PARAMETER	UNITS	RANGE * NOM	RANGE * MAX	PRECISION	RECORDER DIGR	RECORDER OSC	RECORDER STRIP	RECORDER DIGIT	EST. RESPONSE (CPS)
THRUST	LB	5100	6000	1/2	X				250
CHAMBER PRESSURE (2 EA)	PSI	125	150	1/2	X	X		X	90
OXID. INLET PRESSURE	PSI	175	225	1/2	X	X		X	90
OXID. P/V INLET PRESS	PSI	175	225	1/2	X			X	100
FUEL INLET PRESSURE	PSI	175	225	1/2	X	X		X	100
FUEL P/V INLET PRESS	PSI	175	225	1/2	X			X	100
BLC INLET PRESSURE	PSI	175	225	1/2	X	X		X	90
COOLANT INLET PRESS	PSI	200	250	1/2	X	X		X	50
COOLANT OUTLET PRESS	PSI	175	225	1/2	X	X		X	100
COOLANT P/V INLET PRESS	PSI	200	275	1/2	X			X	100
OXID. TANK PRESSURE	PSI	225	300	1/2	X			X	100
FUEL TANK PRESSURE	PSI	225	300	1/2	X			X	100
OXID. FLOW RATE (2 EA)	LB/SEC	11.97	14.2	1/2		X		X	
FUEL FLOW RATE INJECTOR (2 EA)	LB/SEC	7.2	9.0	1/2		X		X	
COOLANT (2 EA)	LB/SEC	7.2	9.0	1/2		X		X	
OXID. TEMPERATURE F/M	°F	80	100	3F	X			X	
OXID. TEMPERATURE INLET	°F	80	100	3F	X			X	
FUEL TEMPERATURE F/M	°F	80	100	3F	X			X	
FUEL TEMPERATURE INLET	°F	200	250	3F	X			X	
BLC TEMPERATURE	°F	200	250	3F	X			X	
COOLANT TEMPERATURE INLET	°F	70	150	3F	X			X	
COOLANT TEMPERATURE OUTLET	°F	200	250	3F	X			X	
CHAMBER WALL TEMPERATURE 1 THRU X (C/A)	°F	300	1000	20F	X			X	
OXID. VALVE TIMING						X	X		
FUEL VALVE TIMING						X	X		
COOLANT VALVE TIMING						X	X		
ALTITUDE CAPSULE PRESSURE	PSIA	.5	2.0	1	X			X	
ACCUMULATOR FUEL TEMP.	°F	200	275	3F	X			X	

*NOTE: These values are steady-state range values only and do not take into account start transients.

The testing at CTL-IV was initiated by preparing the engine test stand for operation by bringing the propellant tanks up to the required run pressure and assuring that the engine stand and the engine data acquisition systems were in readiness for the test. The hyperflow gas generator system was started and brought up to full operation. At this time the altitude capsule isolation valve was opened to permit the hyperflow action to pump down the altitude cell to the run pressure (0.5 psia).

Throughout the entire program, the engine valves were individually activated from a sequence timer so that signals to the valves could be controlled very closely as necessary.

During the bypass cooled phase of the program, three main propellant valves were used:

1. An oxidizer propellant valve.
2. A fuel propellant valve for controlling fuel flow to the injector.
3. A fuel valve for controlling fuel flow to the thrust chamber coolant jacket.

Test firing was initiated by opening the fuel coolant valve approximately 2 seconds prior to hot fire. The coolant outlet pressure was monitored by an automatic shutdown system so that if no coolant flow was observed, the propellant valves would not receive a signal to open. The 2 second time period allowed ample time for the coolant flow to establish and for manual observation of the flow on the "quick look" data recording system. The main oxidizer valve was then signaled to open and the fuel valve was signaled to open from 100 to 300 milliseconds later. This fuel valve delay assured that oxidizer would reach the injector prior to the fuel to assure an oxidizer-rich start and, thus, more nearly simulate an actual engine start sequence. The tests were automatically terminated after the predetermined duration by removing electrical power from the propellant valves. The oxidizer valve closed first and the fuel valve then closed within 100 milliseconds and the

fuel coolant valve closed about 1 second later. This shutdown sequence assured that the thrust chamber coolant passages would be full of fuel during the shutdown transient to eliminate a possible hazard to the chamber. There was no post test purge. The time required for each test was about 3 to 4 minutes, the variation dependent upon the tank pressure changes required and whether any difficulties were encountered making these changes.

The opening and closing sequence of the propellant valves was varied somewhat during the program to determine the effect of different oxidizer leads into the engine. The shortest oxidizer lead, as determined from review of the oxidizer injection pressure trace on the oscillogram, was less than 50 milliseconds, while the longest oxidizer lead was several hundred milliseconds. No significant difference in the engine ignition characteristics was observed with these different start transients.

Upon completion of the test series, the engine propellant manifolds were purged with GN_2 in order to clear the propellants from the engine for the post-test engine inspection. When the engine was sufficiently purged, the duct isolation valve was closed and the hyperflow gas generator was shut down. The altitude cell was returned to ambient pressure by opening a valve which allowed external air to bleed into the cell. After the cell was at ambient pressure and the cell door opened, additional engine purges were used to clear residual propellants from the engine.

The test sequence for regeneratively cooled operation was essentially the same except that there were only two propellant valves. The fuel was opened about 200 milliseconds prior to the oxidizer valve. With the additional distance traveled by the fuel in going through the engine regenerative cooling jacket, this resulted in a nominal oxidizer lead of about 200 milliseconds. There were no variations in the start sequence.

WHITE SANDS TEST FACILITY

The thrust chamber assembly was also tested at the NASA White Sands Test Facility at Las Cruces, New Mexico. The installation is shown schematically

in Fig. 15 , and is similar to the setup used at CTL-IV. Figure 16 is a photograph of the installation in the White Sands Test Facility. Facility pressure drops under rated flow conditions were 40 psi for the oxidizer side, and 35 psi for the fuel side. Propellant tank capacities were 2000 gallons for both the fuel and oxidizer. Propellant tank pressures were limited to 372 psia on the oxidizer fuel sides. The altitude system was initially pumped down to a pressure of approximately 0.1 psia, and then a gas generator-driven ejector system pumped the capsule down to a pressure of 0.06 to 0.07 psia, equivalent to an altitude in excess of 100,000 feet.

Thrust measurements were made using a multi-axis measuring system with three axial dual bridge load cells for recording the main thrust. A complete list of facility and engine instrumentation is given in Table 4 and 5 , respectively. Instrumentation was similar to that used at Rocketdyne's CTL-IV, except that accelerometers were used to monitor the stability of the engine.

The test operation at WSTF was initiated with a vacuum pump evacuation of test stand 401. This operation was performed about 2-3 hours prior to the actual test operation. The engine test stand was then readied for operation by bringing the propellant tanks up to the required run pressure and assuring that the engine stand and the engine instrumentation were in readiness for the test. With this assurance that the engine was ready for testing, the hyperflow gas generator system was started and brought up to full operation. At this time the altitude capsule isolation valve was opened to permit the hyperflow action to pump down the altitude cell to the final run pressure.

The cell pressure was continuously monitored and when it reached 0.1 psia, engine test activity commenced. The first event, at sequence time equals zero, was activation of the "fire switch". At this time the electrical signal was simultaneously applied to both fuel and oxidizer main propellant valves.

During the course of the program, as discussed elsewhere, the opening times of these valves varied slightly, but the sequencing used for the bulk of the testing was as shown in Fig. 17 . This plot shows the typical operation and relative timing of valve position microswitches located on the valve actuators.

FIGURE 15

FACILITY AND INSTRUMENTATION SCHEMATIC

Regeneratively Cooled Engine
with ILC

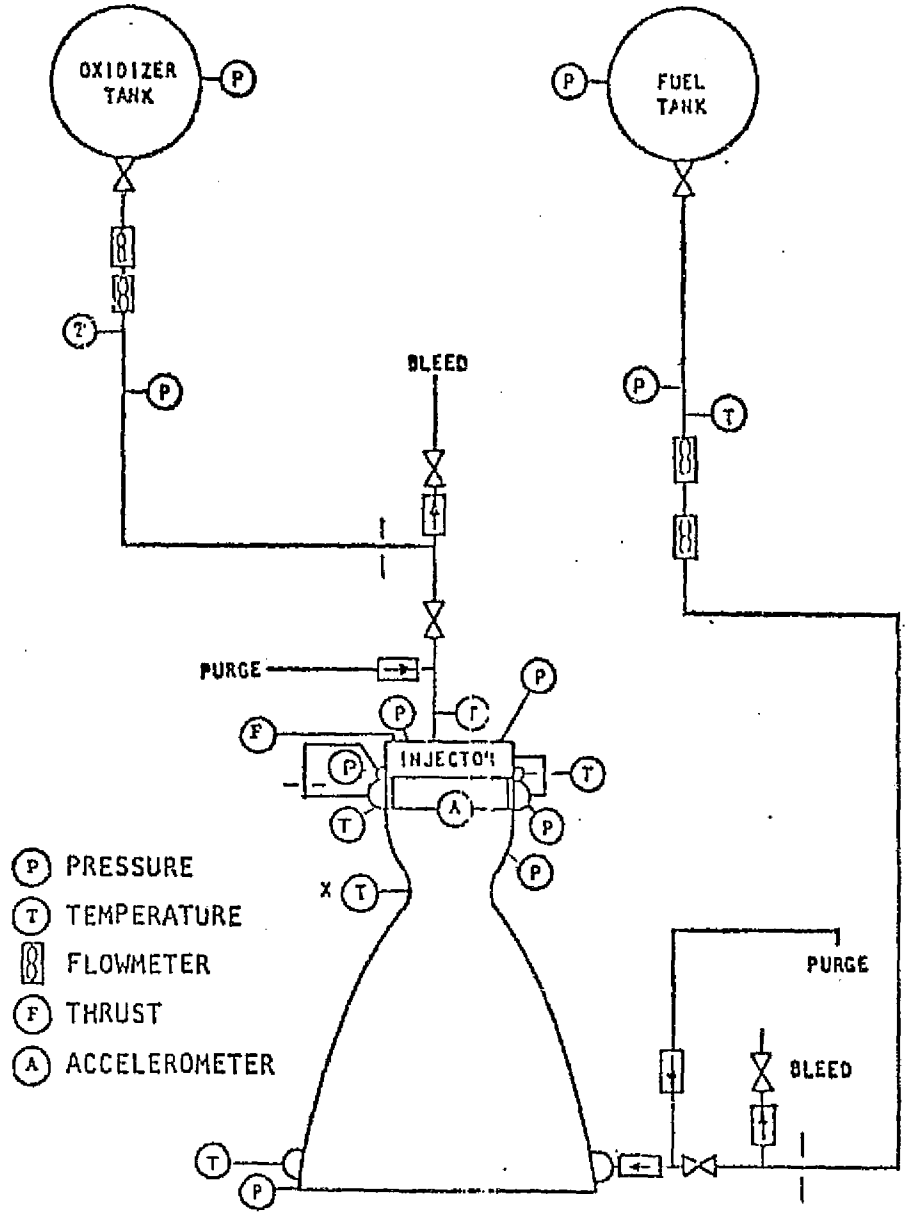

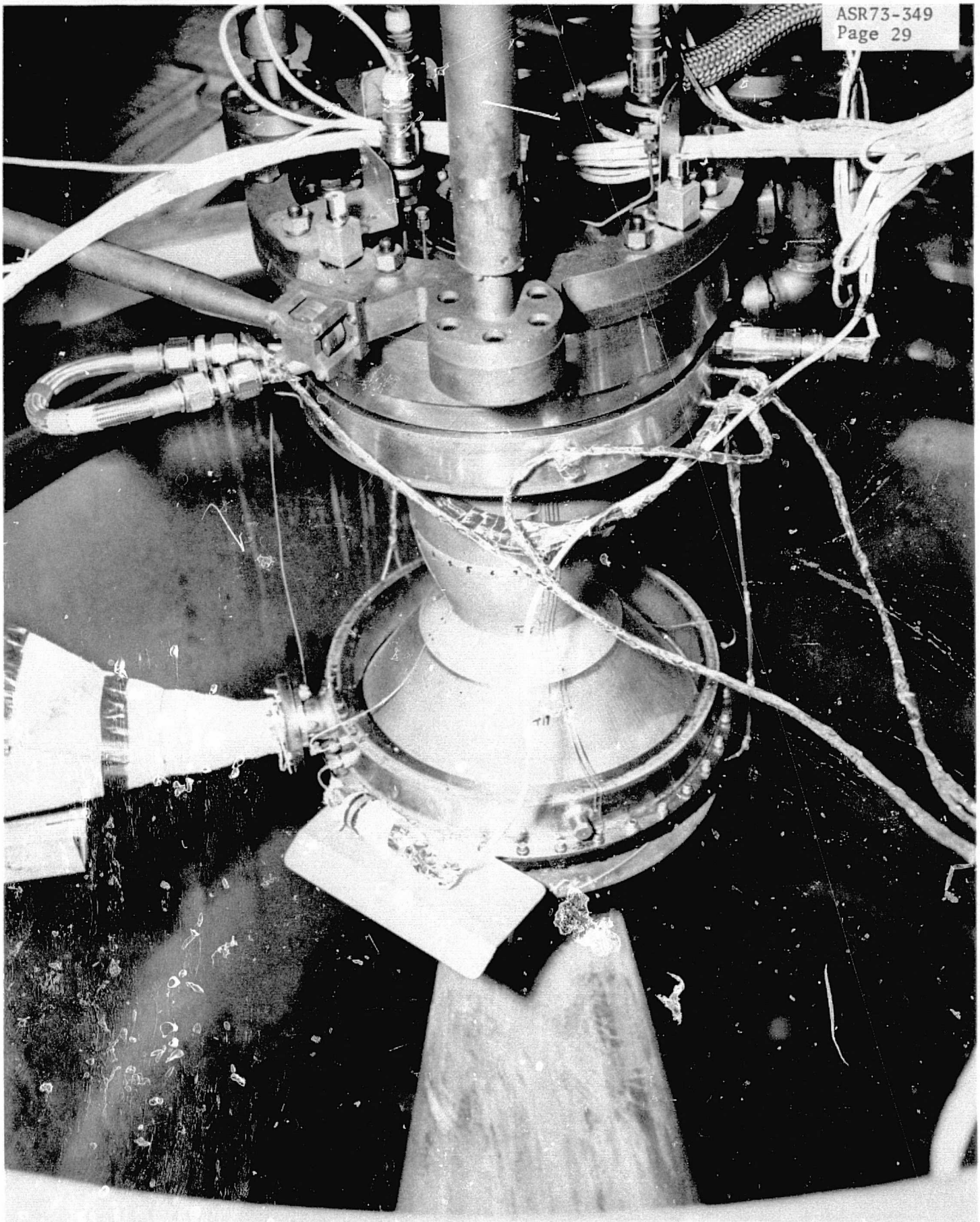

Figure 16. OME Demonstrator Chamber in WSTF

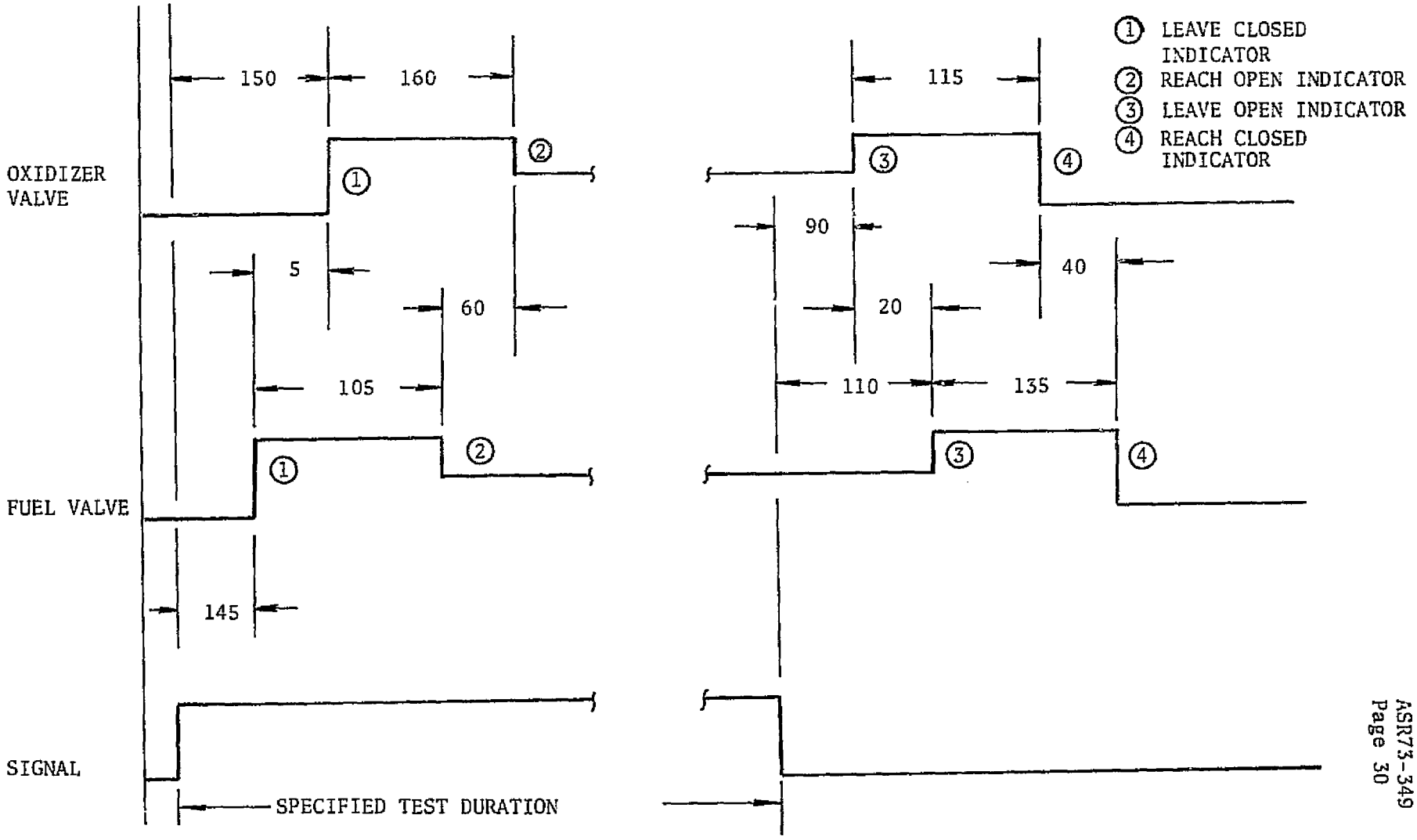

Figure 17. OME Test Valve Sequencing (All Times in Milliseconds)

Propellant flow, thus, started very nearly simultaneously. With the oxidizer valve located very close to the oxidizer injector manifold and the fuel valve located close to the thrust chamber coolant manifold inlet, a substantial oxidizer lead into the thrust chamber was obtained for all tests (with the exception of the one test for which the oxidizer valve malfunctioned and opened approximately two seconds late). The oxidizer lead was generally about 150 to 200 milliseconds.

The tests were automatically terminated after the predetermined duration by simultaneously removing power from the main propellant valves. The oxidizer valve closed first and the fuel valve then closed within 40 milliseconds as shown in Fig. 17 . This shutdown sequence assured that the thrust chamber coolant passages would be full of fuel during the shutdown transient to eliminate a possible hazard to the chamber.

Following each test, the engine was purged with gaseous nitrogen. At 5 seconds after shutdown, the oxidizer side purge was turned on to empty the oxidizer side of the injector. Then 5 seconds later, the fuel side purge was activated to clear residual fuel from the thrust chamber coolant passages and from the injector manifold. Then the two purges were alternately cycled on and off at 5-second intervalves until no propellant vapors could be seen, usually about 20 to 25 seconds after test shutdown. During this purge cycle, the propellant tank pressures were reset to the predetermined levels for the next test. The time required for each test was between 30 and 120 seconds, the variation generally dependent upon the magnitude of the tank pressure change. Following the last test of a sequence, the engine was purged as before. On completion of the purge, the altitude cell isolation valve was closed and the hyperflow steam generator system shut down. The altitude cell pressure was then returned to ambient by bleeding in gaseous nitrogen.

TEST PROGRAMS

The basic objective of test programs conducted at both facilities was to evaluate performance, heat flux and operating characteristics of the OME thrust chamber assembly over the anticipated range of operating conditions. The test programs were broken down into groups of tests, called test sequences, having specific detailed objectives.

CTL-IV TESTS

A total of nine sequences were planned to be conducted at Rocketdyne's CTL-IV. of which three were completed (Table 5). A facility malfunction resulted in delay of subsequent planned tests until the WSTF test program. The L/D #1 injector was used in all sequences. Sequence 1 consisted of seven tests conducted in the bypass coolant mode with decreasing amounts of coolant, increasing duration, and increasing mixture ratio during the sequence. Sequence 2 was a series of 12 ten-second tests in the bypass cooling mode covering the complete ranges of chamber pressure (110-140 psia) and mixture ratio (1.45-1.85). The 19 tests conducted for sequences 1 and 2 in the bypass mode were generally successful except that three tests at low chamber pressure gave indications of flow separation in the nozzle rendering the thrust measurement invalid.

For Sequence 3 the engine was plumbed to the regenerative cooling configuration and four tests were made of varying duration at the nominal conditions. These were followed by a nine-test matrix covering the complete chamber pressure and mixture ratio range. Operation of these tests were successful except for three low-pressure tests, where separation again took place; and one test in which the digital data system was inoperative. The last test of this sequence was to be a 250 second duration test; however, a facility malfunction occurred, which damaged the chamber and prematurely ended this phase of the test program.

TABLE 5. TEST PROGRAM SUMMARY

Test Sequence	No. of Tests	Hardware Configuration	Test Purpose
Tests at CTL-IV			
1	7	L/D #1 Injector; Bypass Cooling	Checkout
2	12	↓ Same	Chamber Pressure and Mixture Ratio Survey
3		L/D #1 Injector; Regenerative Cooling	Checkout
4	9	↓ Same	Chamber Pressure and Mixture Ratio Survey
Tests at WSTF			
1-1	6	L/D #2 Injector Regenerative Cooling	Checkout
1-2	12	L/D #2 Injector w/o Aux Film Cooling	Chamber Pressure and Mixture Ratio Survey
1-4	5	↓ Same	Same with no Film Coolant
2-1	3	L/D #1 Injector w/o Aux Film Cooling	Checkout
2-2	6	↓ Same	Pc and O/F Survey with No Film Coolant
2-3	12	L/D #1 Injector Regenerative Cooling	Chamber Pressure and Mixture Ratio Survey
2-4	10	↓ Same	Pc and O/F Saturated Propellant
2-9	11	↓ Same	High and Low Pressure Survey
2-5	15	↓ Same	Pc and O/F Survey with 50-50 Fuel

The engine was mounted in a vacuum can where altitude was maintained by a LOX/alcohol hyperflow system (Fig. 14). The engine was mounted with the nozzle exit nearly flush with a duct through which the hot gas was expelled. During the test the water-cooled duct overheated and expanded against the inlet manifold of the regenerative chamber (Fig. 18), placing a load in excess of 6000 pounds on the engine, as indicated by the thrust measurement. The test was terminated, at which time the duct collapsed and imparted a shock load on the engine inlet in excess of 10,000 pounds (thrust pegged off scale). Subsequent to this failure, the cell closure blew off due to an overpressure in the test cell.

Inspection of the chamber indicated that the outer wall was damaged locally but the hot wall did not crack. The non-axisymmetric load caused the throat to deform one percent in diameter; and one of the channels deformed, causing a 33 percent restriction in flow area. The nickel back wall was repaired by electroforming (Fig. 19). Thermal analysis of the engine indicated that it would operate satisfactorily with the deformed channel, which effectively simulates a partially plugged channel condition. Figure 20 shows the thrust chamber at conclusion of the test program after cleaning. The discoloration at the combustor end represents the liquid length of the auxiliary film coolant.

Tests which were scheduled but not completed due to the facility malfunction were tests with saturated propellants, cycle testing, and off-limits tests simulating vehicle malfunctions resulting in extremely low pressure operation. These tests were completed at the White Sands Facility.

FIGURE 18

CTL IV - CELL 29B

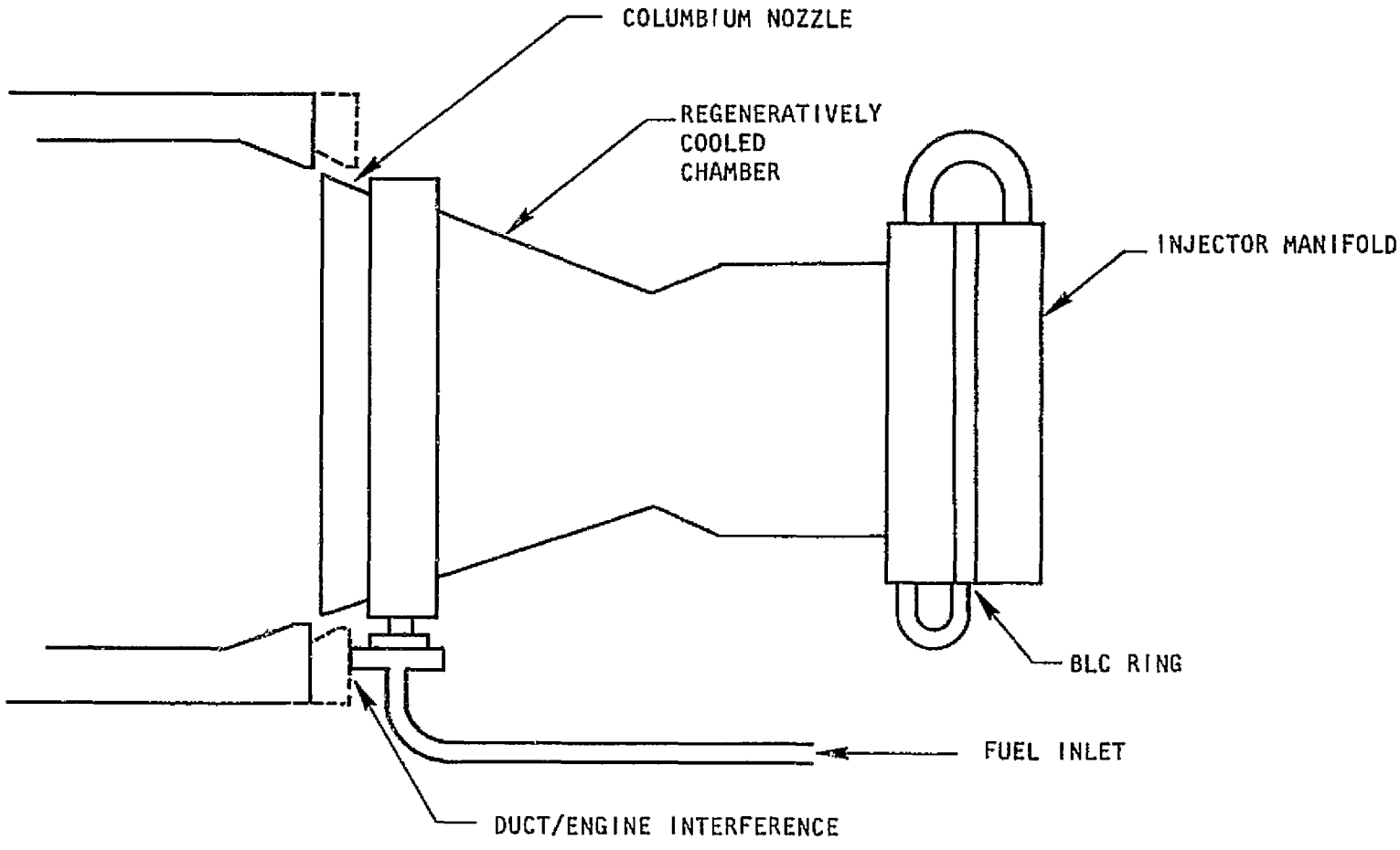

277-701

Rocketdyne Division
Rockwell International

FIGURE 19

REWORKED DEMONSTRATION CHAMBER

FIGURE 20

DEMONSTRATION CHAMBER POST TEST CONDITION AFTER CLEANING

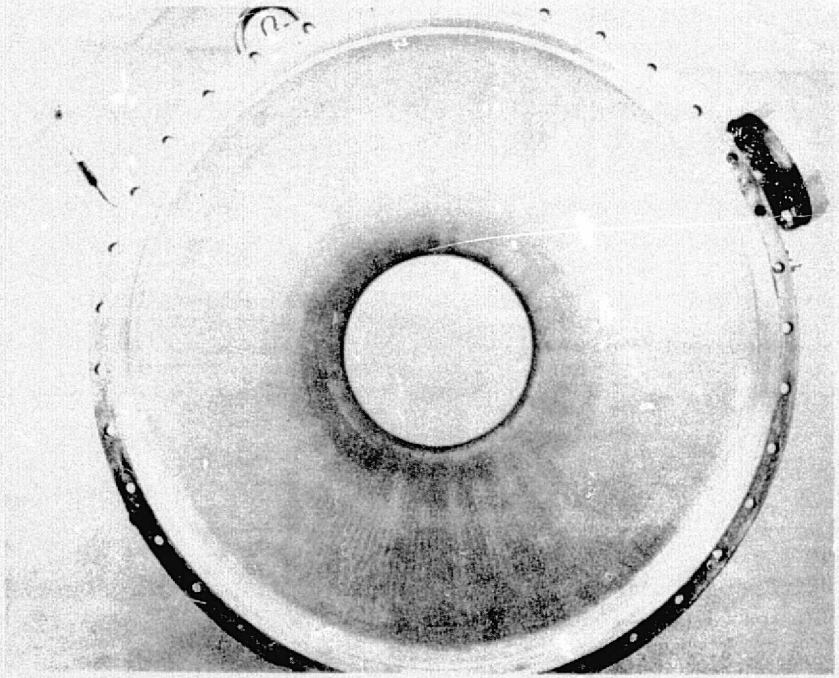

NOZZLE END

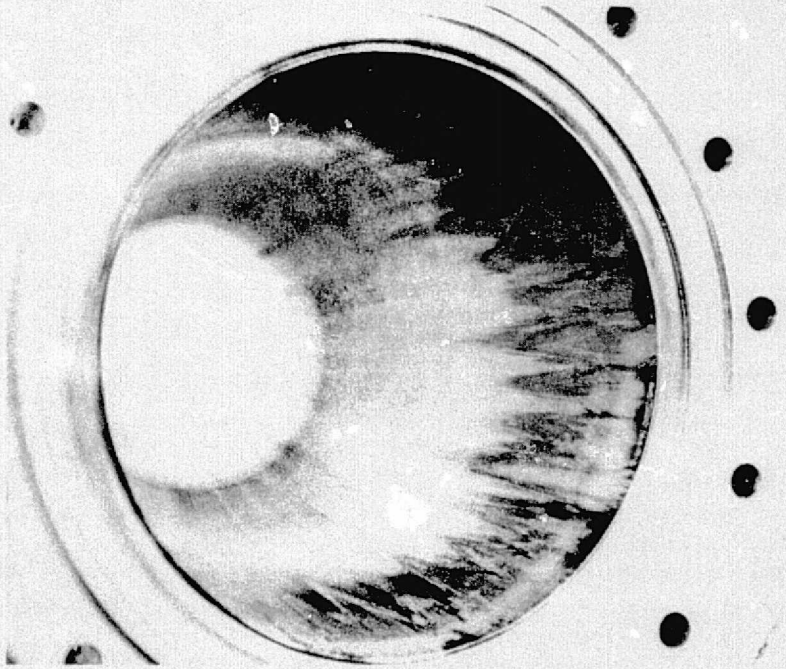

COMBUSTOR END

WHITE SANDS TESTS

The tests conducted at WSTF included several engine configurations (Table). The repaired regeneratively cooled thrust chamber shown in Fig. 19 was used for all tests. The first tests were conducted with the L/D #2 injector with the film coolant ring flowing fuel at approximately 2 percent of the total propellant flow rate. A total of six tests were conducted during the first sequence with durations ranging up to 10 seconds at nominal conditions. Satisfactory operation of the repaired thrust chamber was demonstrated at nominal and under abnormal operating conditions. Particularly, the nominal start sequence included an oxidizer injection lead and the shutdown sequence consisted of a fuel rich shutdown. Due to a facility malfunction, an excessively fuel rich start caused by a 1½ second oxidizer valve opening delay occurred. In addition, during later tests, a slow closing oxidizer valve caused several 100 millisecond oxidizer rich shutdowns. The thrust chamber operated smoothly during these tests and the hardware was in excellent condition after the tests. Also, on two tests, the oxidizer flow meters were erratic, indicating the possibility of residual gas bubbles in the oxidizer feed system; however, no instabilities were observed in engine operation. Test data appeared to be valid on four of these checkout tests, with the exception that a small oxidizer leak in the facility could have degraded performance by approximately 1 percent. The second sequence consisted of 12 tests over the complete chamber pressure and mixture ratio range. Posttest inspection showed that the film coolant ring had been slightly eroded and the acoustic cavity insert ring had been warped.

The film coolant ring was not a flight configuration and was included only to permit test flexibility. In the flight hardware, film coolant will be supplied from the injector. Also, an uncooled acoustic cavity insert, which would not be used in the flight hardware configuration, was warped. The engine was reassembled with an uncooled spacer in place of the boundary layer coolant ring, and a series of five tests conducted to explore engine performance without boundary layer coolant. The test data indicated that fuel was leaking into the thrust chamber and posttest hardware inspection revealed that the

injector indeed had become sufficiently distorted at the O-ring seal to permit massive fuel leakage to the chamber. Data analysis, delayed until after completion of this test sequence, indicated that leakage was present as early as the fifth test of the first (checkout) test sequence at WSTF.

The thrust chamber was in no way damaged during these tests, and was reassembled with the L/D #1 injector and the solid spacer ring in place of the film coolant ring. Three checkout tests and six performance survey tests were made without auxiliary film coolant. Data from these tests indicated a variation and discrepancy in oxidizer flow. Subsequent facility checkouts after completion of the non-film cooled test series indicated a check valve failure allowing oxidizer leakage into a nitrogen purge line. Performance data is somewhat questionable, because the leak occurred downstream of the oxidizer flow meters.

The engine was reassembled with the repaired film coolant ring. The repair consisted of sealing the leaking area of the coolant ring and Rokide coating the surface exposed to combustion chamber gases. Twelve tests were conducted to complete a performance survey over the ranges of chamber pressure and mixture ratio. This was followed by a ten-test sequence covering the same ranges with the propellants saturated with helium at 225 psia. A series of eleven tests was then conducted with chamber pressures ranging up to 178 psia (the facility limit) to demonstrate operation of the thrust chamber at conditions near the Space Tug design for Space Storable engines. The series also included tests down to 100 psia chamber pressure to simulate the blow-down conditions resulting from a vehicle pressurization system failure. Both propellants were saturated with helium at 165 psia for these tests.

The final test series was conducted with 50-50 as the fuel. The propellants were again saturated with helium at 165 psia for these 15 tests. The tests were conducted at chamber pressures ranging from 100 to 179 psia and mixture ratios ranging from 1.48 to 1.86. One test was conducted for a duration of 30 seconds. The duration was limited to 30 seconds because of the

susceptibility of the film coolant ring to overheating. Longer duration tests are planned for the integrated thrust chamber which does not use a separate coolant ring.

After the tests, the thrust chamber and injector were in excellent condition, while the film coolant ring was again slightly eroded in three places.

TEST RESULTS

The test conditions and a steady state data summary for all the tests conducted on the regeneratively cooled demonstration thrust chamber are summarized in Table 6. A total of 112 tests was conducted for a cumulative duration of 1042 seconds. Chamber pressures ranged from 100 psi to almost 180 psi and mixture ratios from 1:4 to 1:9. Figure 21 is a graphic presentation of the distribution of chamber pressure and mixture ratio points tested during the program.

START AND SHUTDOWN CHARACTERISTICS

The thrust and chamber pressure transients depend on valve sequencing, facility and engine flow resistances, facility and engine volumes, ambient pressure, and steady-state operating conditions. Some oscillating of the servo controlled fuel throttling valve at the CTL-IV facility generally occurred distorting the start transients, so that the transients demonstrated at the White Sands Test Facility are more typical of vehicle operation. A typical start sequence for the demonstration chamber with the L/D #1 injector is shown in Fig. 22.

The first major rise in the oxidizer injector pressure leads the fuel injector pressure rise by approximately 300 milliseconds. There is no overshoot in chamber pressure, although some damping of the trace is probable due to the configuration of the tube from the chamber to the transducer. The thrust overshoot is approximately 60 percent of the steady-state value and the oxidizer pressure overshoot is approximately 30 percent of its steady-state value.

A start transient for a similar oxidizer lead with the No. 2 like-doublet injector is shown in Fig. 23 and 24, showing the similarity in the transient characteristics.

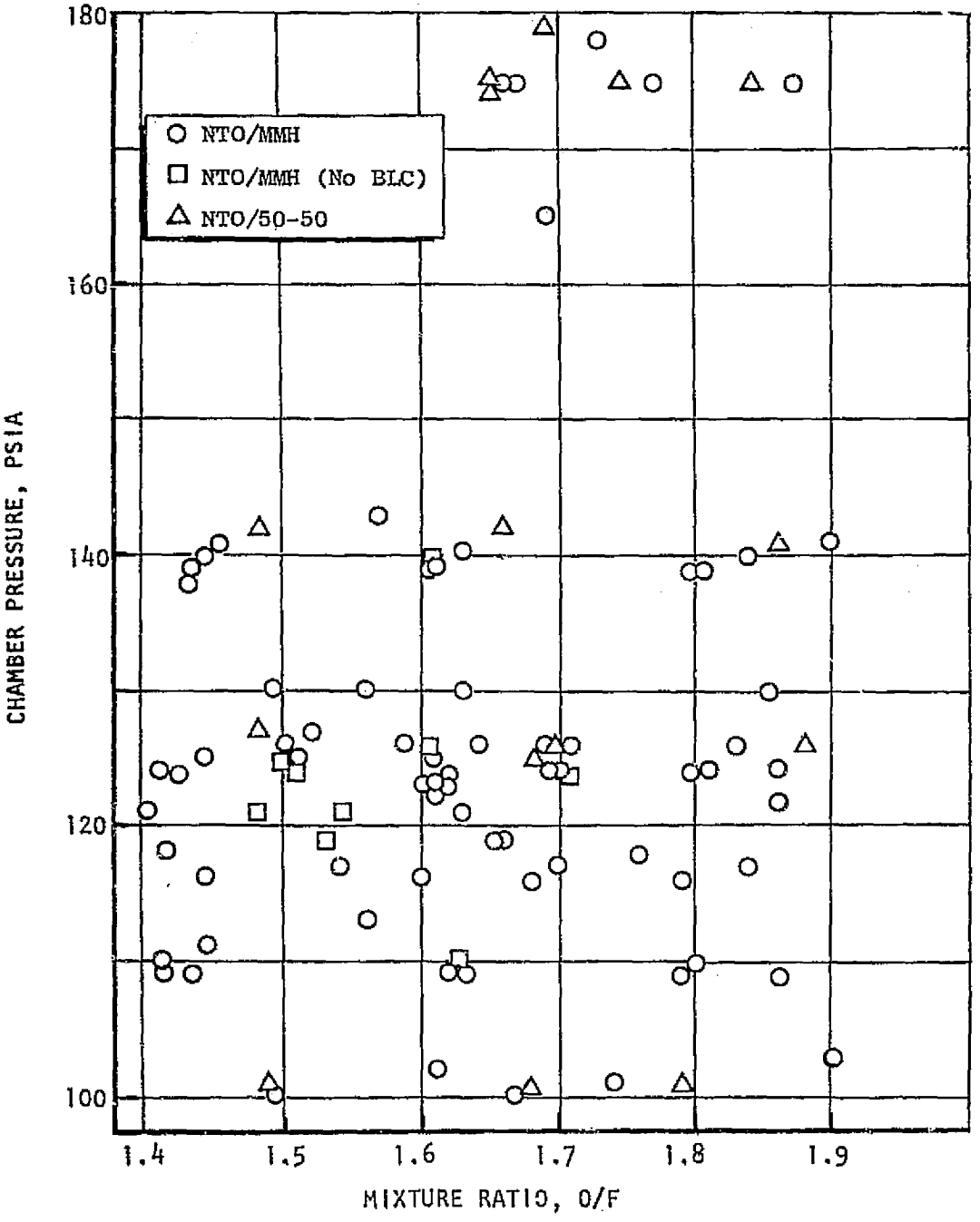

Figure 21. Demonstrator OME Thrust Chamber Operating Conditions

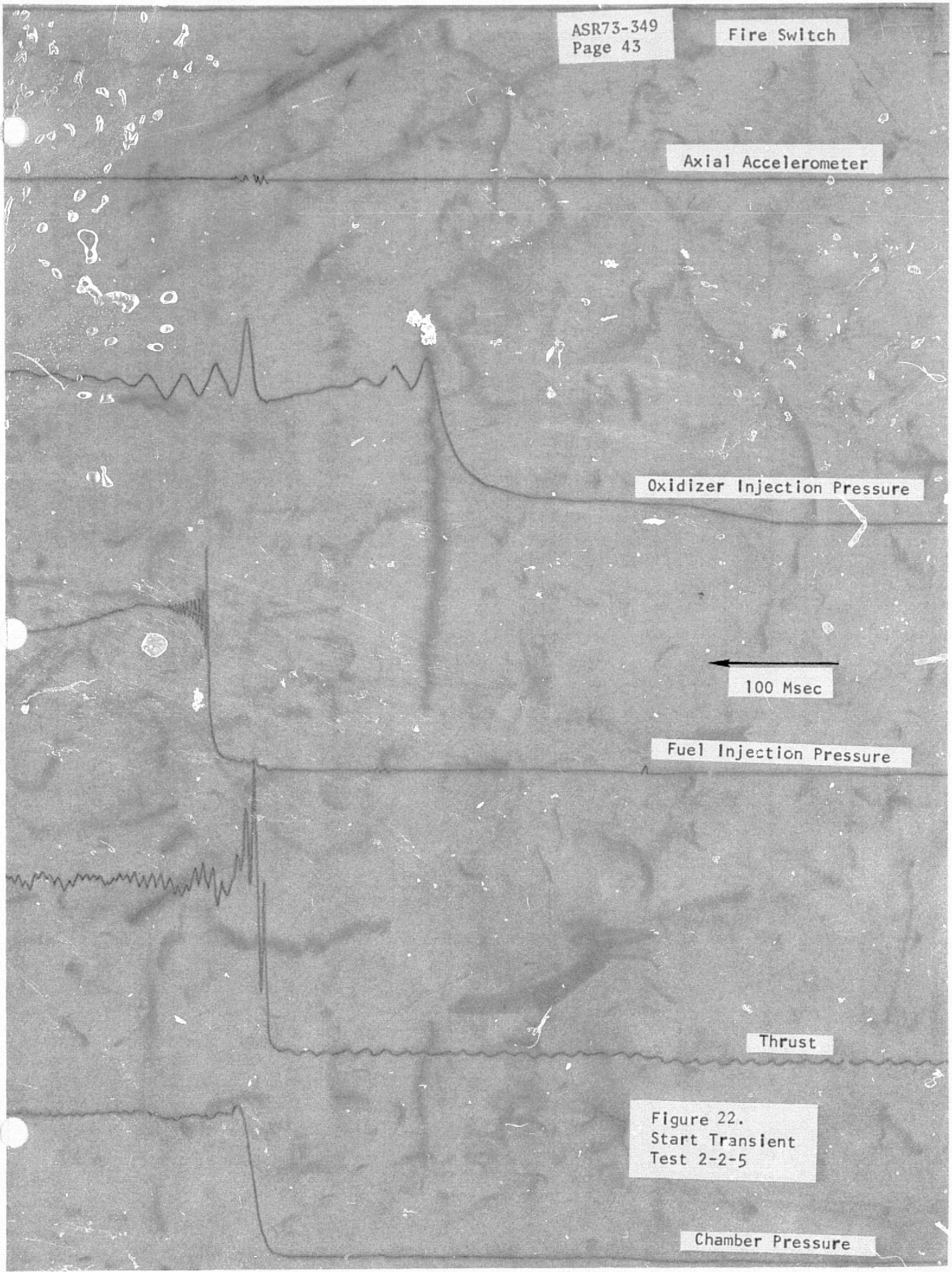

Figure 22.
Start Transient
Test 2-2-5

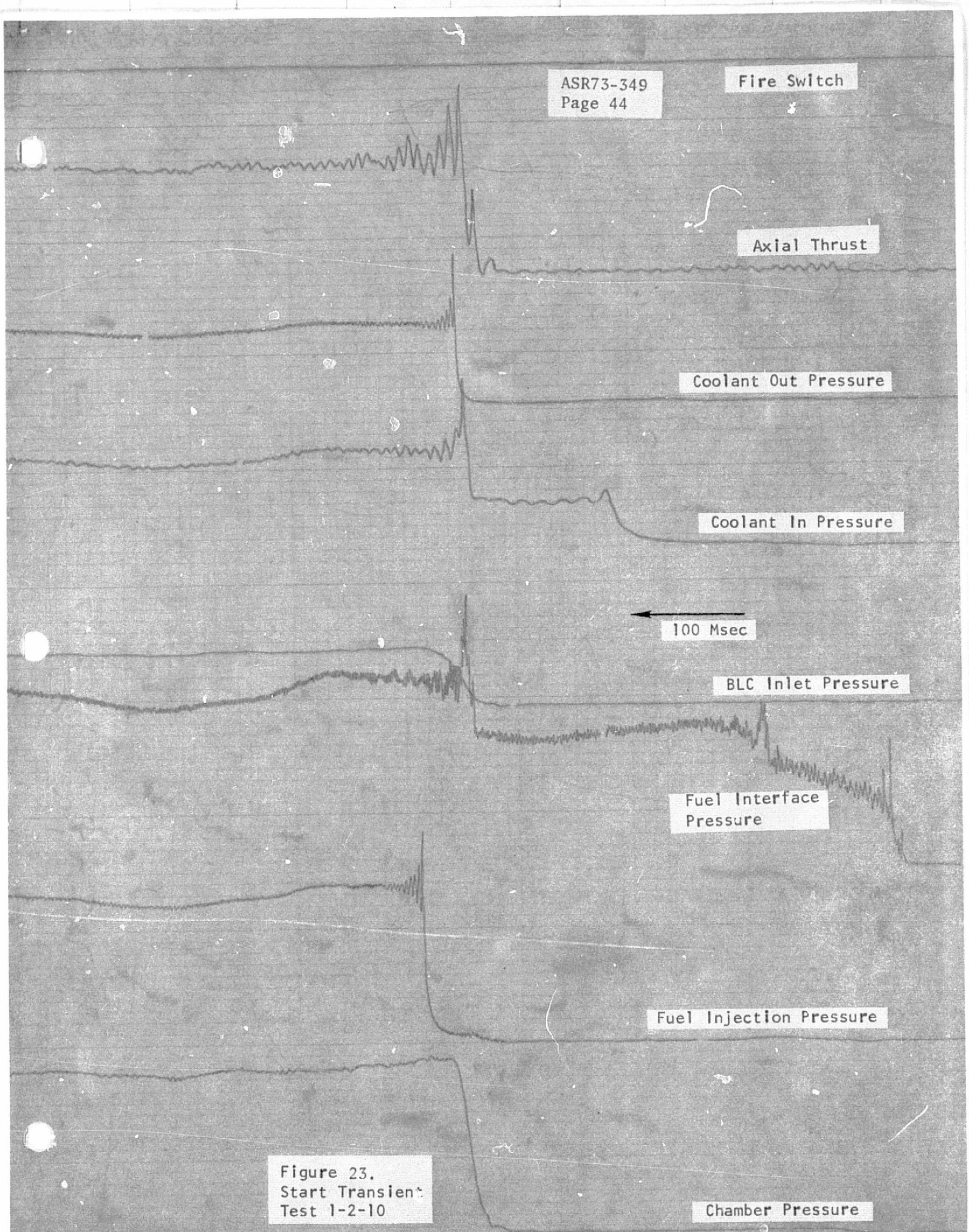

Figure 23.
Start Transient
Test 1-2-10

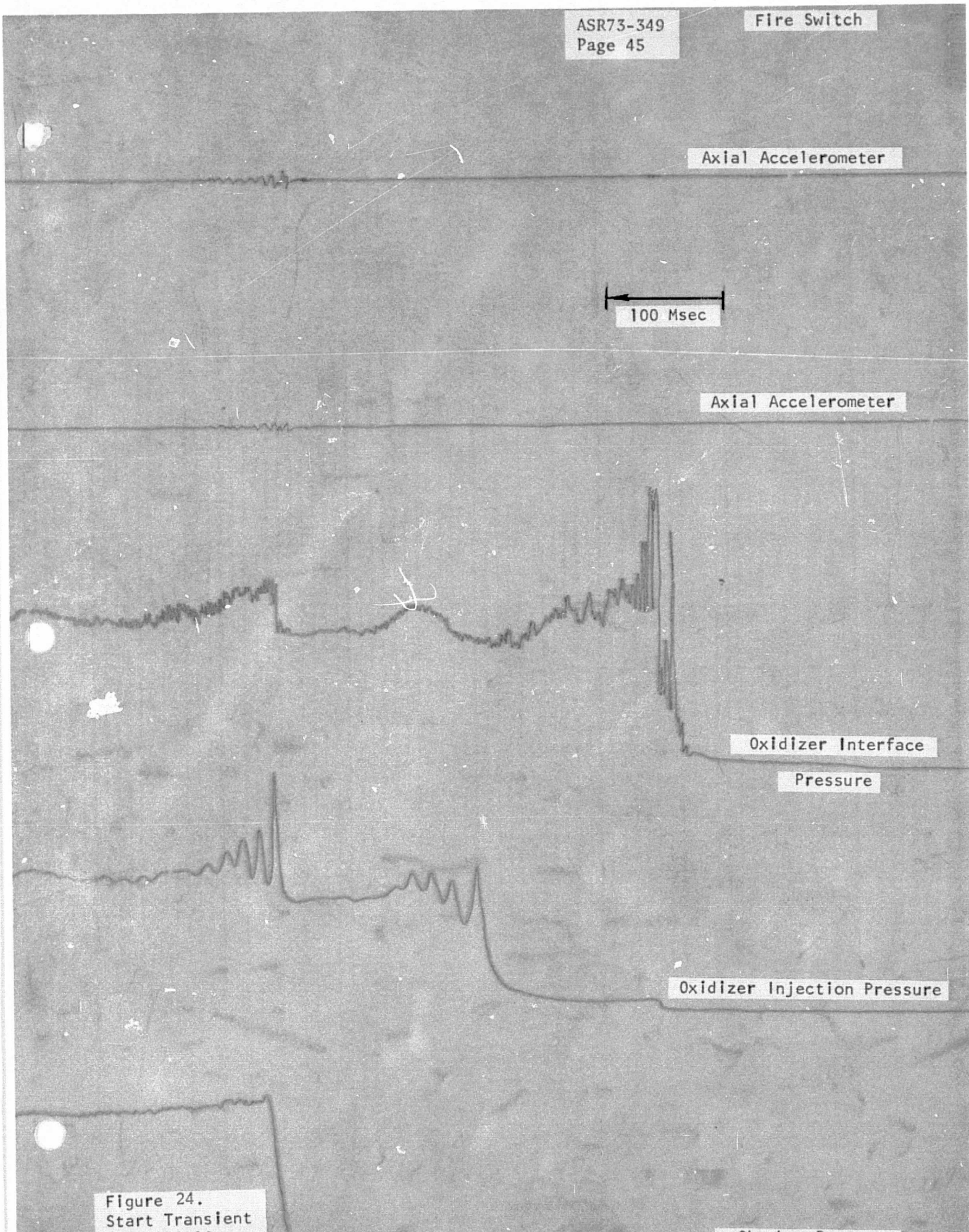

Figure 24.
Start Transient

The injector/thrust chamber combinations tested in this program have demonstrated the ability to start safely over a range of propellant inlet conditions and sequences, which allows considerable flexibility in design of flight valve and ducting configurations.

The oxidizer valve was scheduled to close prior to the fuel valve so that the heat input to the regeneratively cooled jacket would decay before the coolant flow decayed. In the typical shutdown transient shown in Fig. 25, the oxidizer injection pressure decayed slightly before the fuel injection pressure as planned. Due to a facility malfunction on Test 1-1B-3, the fuel valve closed approximately 100 milliseconds before the oxidizer valve closed, resulting in an oxidizer-rich shutdown. However, posttest inspection indicated no hardware damage resulted from this shutdown. Not only was the thrust chamber undamaged by this shutdown sequence, but the shutdown transient shown in Fig. 26 and 27 indicates that severe exothermic overheating of the fuel did not occur during this shutdown transient.

The heat sink capability of the channel wall design is sufficient to tolerate oxidizer rich shutoffs of this magnitude. Since chamber pressure and, consequently, heat flux, decay significantly with the reduction of fuel injection pressure, it is probable that even longer oxidizer rich shutdowns could be tolerated.

STABILITY CHARACTERISTICS

No high or low frequency instability was recorded over the entire range of chamber prossures and mixture ratios tested with either MMH or 50-50 fuels with either the L/D #1 or L/D #2 injector. All configurations relied on acoustic cavities without baffles to maintain stable operation. Axial accelerometers installed on the engine thrust mount typically showed disturbances of 10-20 g's RMS at at start and no significant activity during the tests.

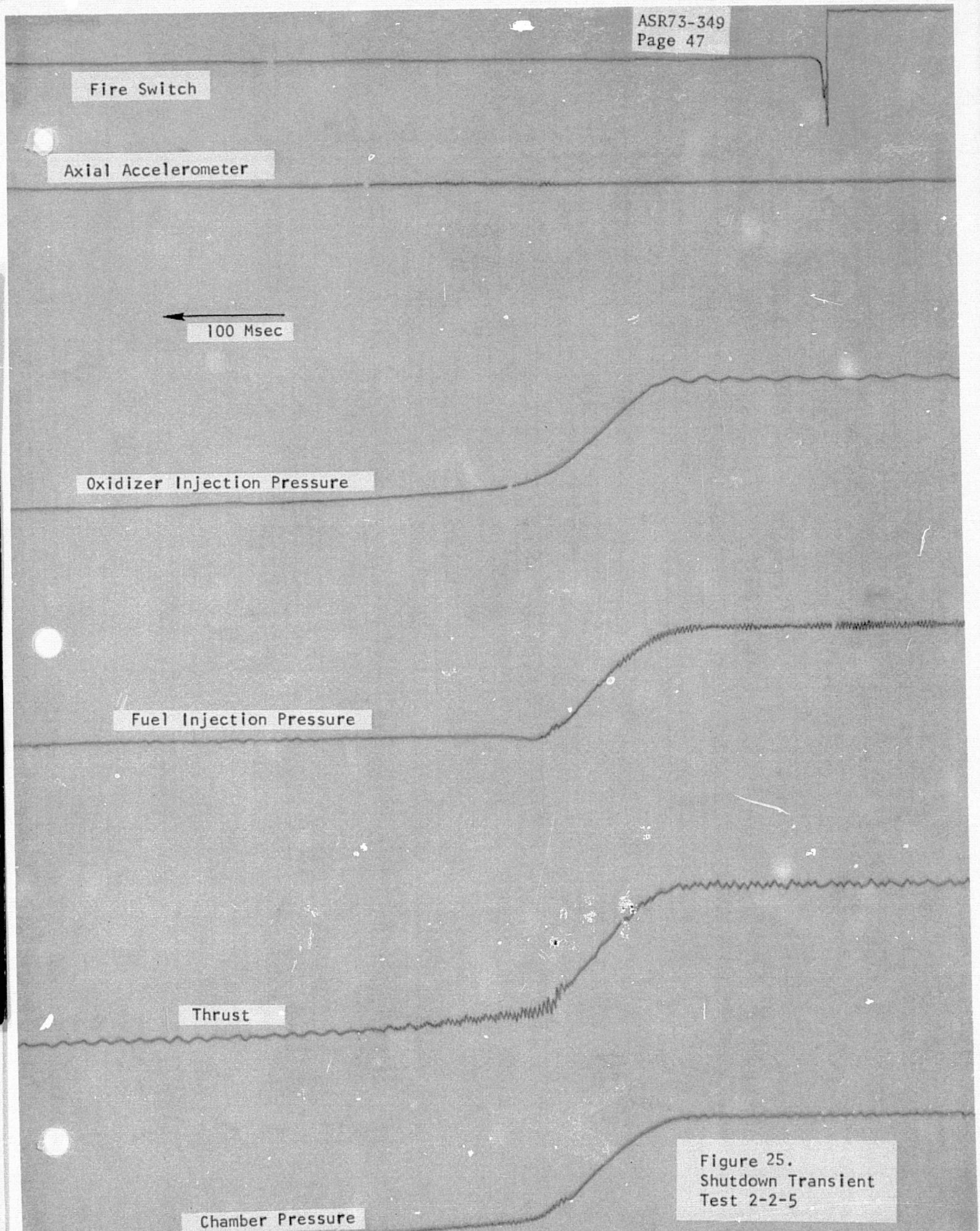

Figure 25.
Shutdown Transient
Test 2-2-5

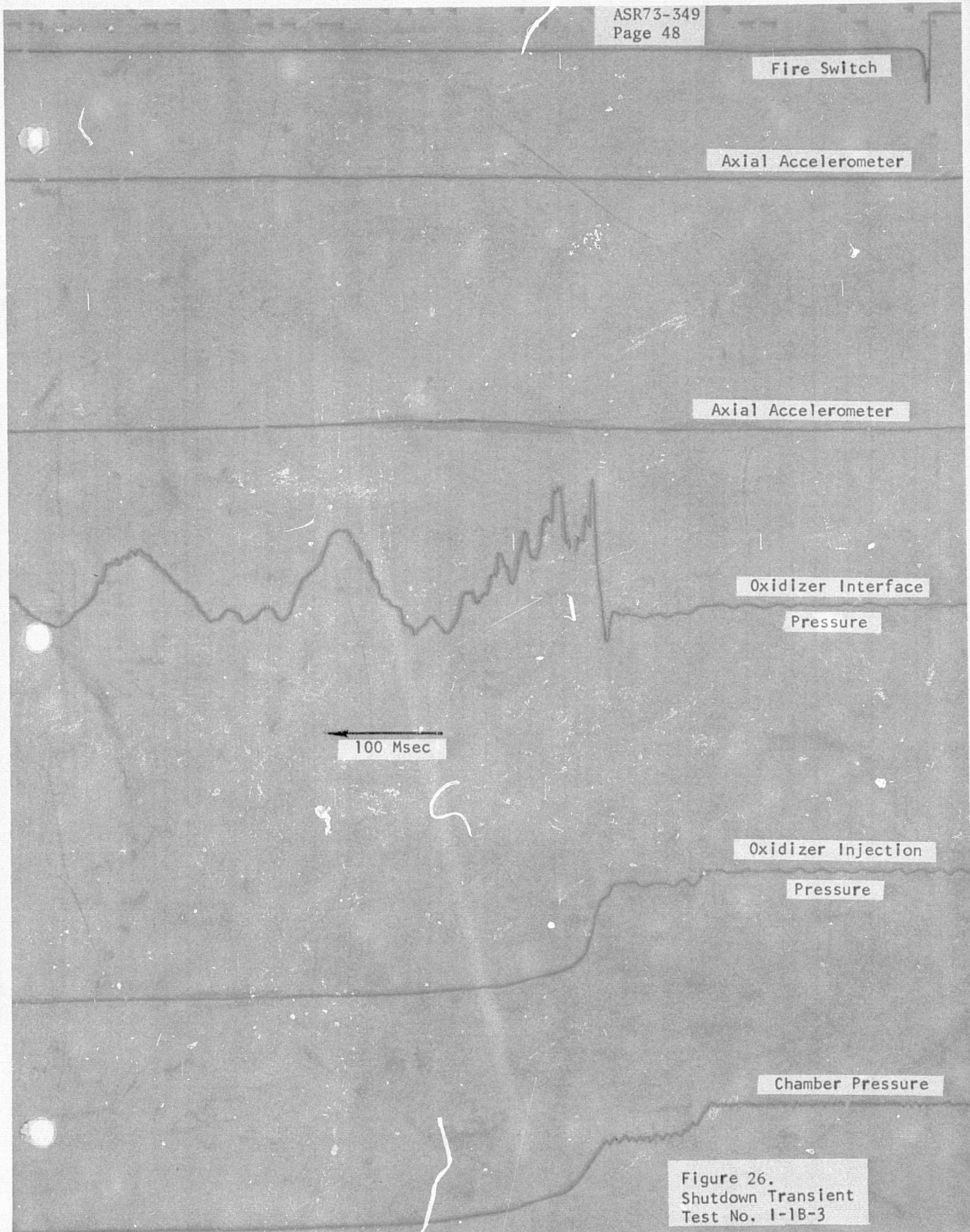

Figure 26.
Shutdown Transient
Test No. I-1B-3

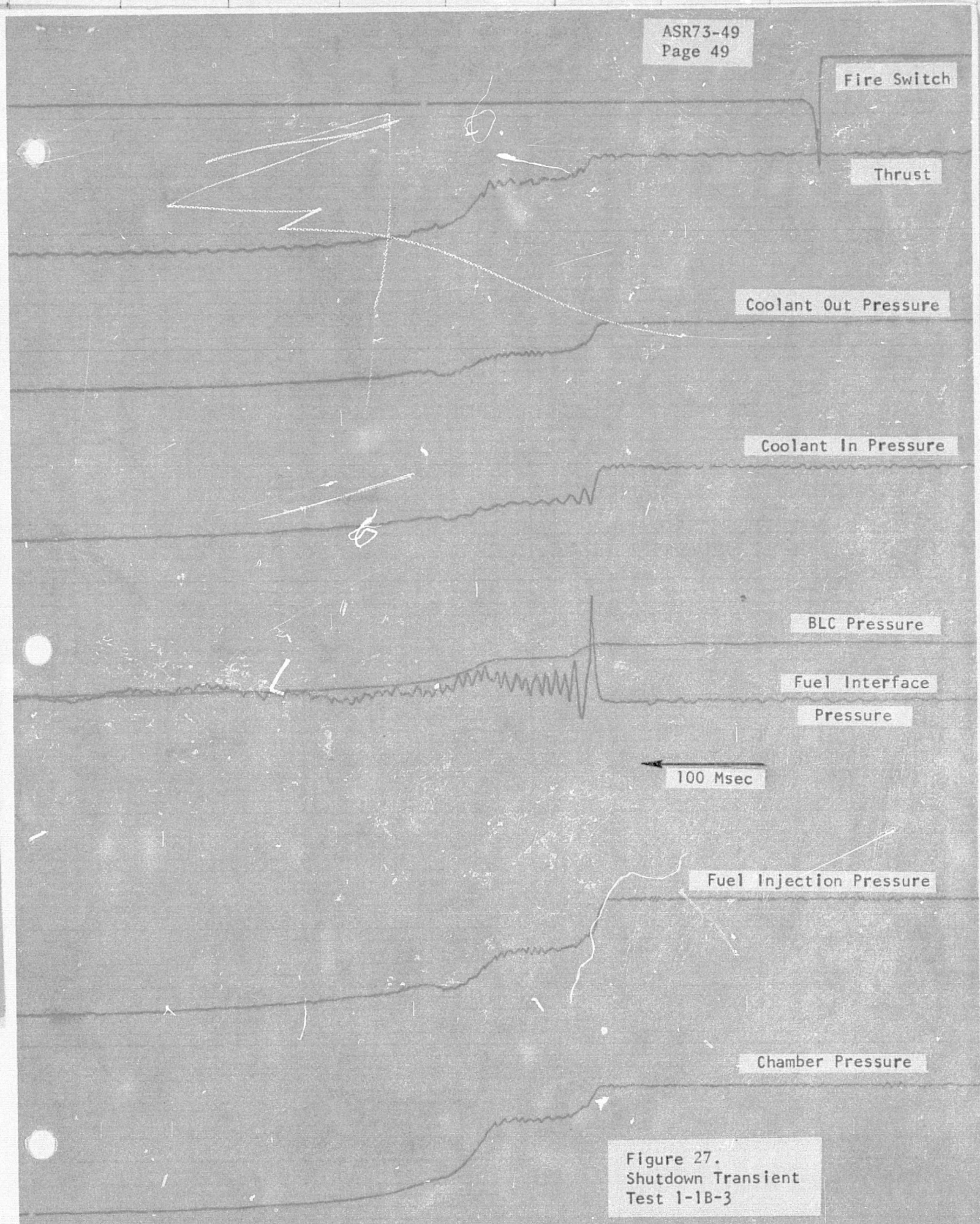

Figure 27.
Shutdown Transient
Test 1-1B-3

PERFORMANCE CHARACTERISTICS

Performance is summarized for all tests in Table 6 . The method of calculating performance from the test data is described in the Appendix. Performance is shown in Fig. 28 versus mixture ratio for the tests with unsaturated NTO and MMH using the L/D #1 injector at CTL-IV and WSTF. Performance on the tests at nominal conditions with 2 percent auxiliary film coolant at CTL-IV averaged approximately 310 seconds. A one percent improvement in injector performance is predicted with minimum development. Performance measured at WSTF was slightly over 308 seconds at nominal conditions. The deformed nozzle (as a result of the CTL-IV malfunction) may have resulted in a slight performance degradation at WSTF.

The WSTF data shown in this figure were taken on tests of 7 seconds duration (the 2-3 test sequence). Tests at WSTF indicated a trend of increasing performance with durations even beyond 10 seconds. Performance on a subsequent long duration test (2-5-50) is shown as a function of time in Fig. 29. The performance increase between data slices taken at 7 seconds and 30 seconds (the duration of the test) was greater than 1-1/2 seconds. Performance increases of 0.2-0.5 seconds between the 7 and 10 second data slices were typical for test series number 2. The reason for the performance variation with time at WSTF is not clear at this time. One long duration test with data was conducted at CTL-IV. Thermal data indicate failure of the supplemental film coolant ring began approximately 25-30 seconds into the test. Performance data from 5-30 seconds are also plotted in Fig. 29. It does not indicate a significant performance increase during this time. Also, performance measured on the shorter duration tests at CTL-IV were in good agreement with the data from this longer test as shown in Fig. 28.

As shown, the performance at nominal conditions agrees within 1/2 percent at the nominal conditions between the two test facilities. Longer duration tests at WSTF may result in nearly perfect agreement of specific impulse measurements between the facilities at a value of 310 seconds. Theoretical and measured performance and losses are shown in Table 7.

	1	2	3 CTL-IV TEST	4 SLICE SEC	5 $P_{c_{av}}$ PSIA	6 P_C Diff %	7 $P_{C_{NS}}$ PSIA	8 ΔP_F INJ PSI	9 ΔP_O INJ PSI	10 $\dot{W}_O$ lb/sec	11 Wo Diff %	12 $\dot{W}_F$ lb/sec
1		BYPASS COOLING										
2												
3			43	1.5	132.1	0.2	125.5	62.9	53.4	11.88	0.2	8.15
4			44	2.0	132.2	0.1	125.6	58.5	55.5	12.15	0.1	7.85
5			45	2.0	132.8	0.3	126.1	58.5	55.7	12.21	0.4	7.86
6			46	2.0	132.8	0.3	126.2	54.6	58.4	12.46	0.2	7.61
7			47	8.0	132.0	0.1	125.4	54.9	57.5	12.32	0.1	7.63
8			49	8.0	132.8	0.0	126.2	47.1	45.8	13.00	0.2	7.09
9			50	8.0	151.0	0.2	143.5	79.3	73.2	13.75	0.0	9.08
10			51	8.0	148.1	0.1	140.7	58.7	81.5	14.54	0.3	7.89
11			52	8.0	116.2	0.3	110.4	50.0	39.5	10.34	0.0	7.34
12			53	8.0	119.3	0.1	113.3	43.7	50.8	10.99	0.3	7.04
13			54	8.0	122.9	0.1	116.7	65.2	52.7	11.66	0.2	6.86
14			55	8.0	132.0	0.1	125.4	65.2	52.7	11.81	0.2	8.2
15			56	8.0	132.5	0.1	125.9	60.9	54.7	12.02	0.2	8.0
16			57	8.0	132.5	0.1	125.9	56.0	57.2	12.28	0.3	7.7
17			58	8.0	148.3	0.1	140.9	84.5	66.0	13.14	0.3	9.3
18												
19			REGENERATIVE COOLING									
20												
21			60	4.0	128.7	0.3	122.3	49.4	59.6	12.63	0.1	6.8
22			61	6.0	132.3	0.1	125.6	60.7	57.3	12.34	0.2	7.5
23			62	6.0	132.1	0.2	125.5	61.0	56.9	12.33	0.1	7.5
24			64	9.0	129.8	0.0	123.4	50.1	61.4	12.74	0.3	6.8
25			65	9.0	147.0	0.2	139.6	89.6	64.8	13.04	0.2	9.6
26			66	9.0	146.9	0.1	139.6	74.4	71.7	13.69	0.3	8.4
27			67	9.0	146.7	0.2	139.3	64.5	79.1	14.35	0.0	7.
28			68	9.0	115.7	0.3	109.9	53.8	39.1	10.28	0.3	7.
29			69	9.0	114.8	0.2	109.1	44.7	42.4	10.73	0.3	6.
30			70	9.0	114.5	0.1	108.8			11.18	0.2	6.
31			71	53.0	130.0	0.0	123.5	60.4	55.7	12.13	0.0	7.
32			71	8.0	130.7	0.1	124.1	58.6	56.7	12.23	0.2	7.
33			71	23.0	130.3	0.2	123.8	59.4	56.6	12.14	0.1	7.
34												
35												

FOLDOUT FRAME

TABLE 6. DEMONSTRATOR THRUST CHAMBER PERFORMANCE

12 $\dot{W}_F$ lb/sec	13 $\dot{W}_F$ Diff. %	14 O/F	15 $\dot{W}$ Total lb/sec	16 $\dot{W}_{BLC}$, % of WT	17 T_F^* J.OUT F	18 $T_{O_{INJ}}$ F	19 T_F^{**} Inlet F	20 F Pounds	21 F Diff %	22 P cell PSIA	23 F_{VAC} Pounds	24 VACU ϵ =
8.15	0.2	1.46	20.03	2.7			67	5048	0.1	0.54	5177	258
7.85	0.5	1.55	20.00	2.6			67	5070	0.5	0.53	5196	259
7.86	0.3	1.55	20.00	2.6			68	5096	0.2	0.51	5218	260
7.61	0.6	1.64	20.06	2.5			68	5088	0.1	0.51	5211	259
7.63	0.1	1.62	19.94	2.1			60	5034	0.1	0.59	5174	259
7.09	0.0	1.83	20.09	2.1				5064	0.1	0.81	5259	261
9.08	0.0	1.52	22.83	2.2			59	5926	0.2	0.63	5926	259
7.89	0.1	1.84	22.43	1.9			59	5699	0.0	0.62	5846	260
7.34	0.0	1.41	17.68	2.3			52	4428	0.2	1.37	*	*
7.04	0.1	1.56	18.03	2.1			54	4625	0.2	1.11	*	*
6.88	0.1	1.70	18.54	2.0				4951	0.1	0.98	*	*
8.24	0.1	1.43	20.06	2.3				4951	0.1	0.98	5186	258
8.01	0.2	1.50	20.03	2.2			53	4967	0.1	1.03	5213	260
7.71	0.1	1.59	20.00	2.1			51	4984	0.0	0.98	5218	261
9.31	0.2	1.41	22.45	1.8			57	5563	0.2	0.91	5780	257
6.80	0.3	1.856	19.43	2.5	189			4927	0.1	0.83	5126	263
7.52	0.5	1.643	19.87	2.6	183			5005	0.3	0.94	5229	263
7.52	0.3	1.638	19.85	2.6	183			5092	0.2	0.71	5260	264
6.81	0.1	1.862	19.58	2.4	211			4881	0.2	1.12	5149	263
9.08	0.0	1.436	22.12	2.8	178			5642	0.2	0.60	5784	26
8.41	0.1	1.628	22.10	2.6	193			5643	0.2	0.68	5805	26
7.79	0.0	1.842	22.14	2.4	197			5650	0.2	0.68	5813	26
7.22	0.1	1.423	17.50	2.8	187			4382	0.2	1.50	*4741	*27
6.56	0.2	1.635	17.30	2.6	190			4339	0.2	1.60	*4720	*27
6.13	0.2	1.825	17.31	2.4	197						*4723	*27
7.41	0.2	1.637	19.54	2.4	198			4515	0.2	2.58	5130	26
7.49	0.3	1.634	19.71	2.6				4986	0.2	0.08	5178	26
7.47	0.0	1.626	19.61	2.6				4852	0.2	1.30	5162	26
					* = T_{FINJ} for tests 60-71		** = T_{FINJ} for tests 43-58				*Nozzle Flow	

FOLDOUT FRAME 2

'ORMANCE

18	19	20	21	22	23	24	25	26		
UT T_{INJ} F	T_F^{**} inlet F	F Pounds	F Diff %	P cell PSIA	F_{VAC} Pounds	VACUUM $\epsilon = 9$	I_s, SEC $\epsilon = 72$	η_{ERE} %		
	67	5048	0.1	0.54	5177	258.8	306.8	96.8		
	67	5070	0.5	0.53	5196	259.8	307.8	96.6		
	68	5096	0.2	0.51	5218	260.1	308.1	96.6		
	68	5088	0.1	0.51	5211	259.8	307.4	96.0		
	60	5034	0.1	0.59	5174	259.4	307.2	96.2		
		5064	0.1	0.81	5259	261.6	309.5	96.4		
	59	5926	0.2	0.63	5926	259.6	307.7	96.0		
	59	5699	0.0	0.62	5846	260.7	308.2	95.8		
	52	4428	0.2	1.37	*	*	*	*		
	54	4625	0.2	1.11	*	*	*	*		
		4951	0.1	0.98	*	*	*	*		
		4951	0.1	0.98	5186	258.8	306.8	96.5		
	53	4967	0.1	1.03	5213	260.2	308.5	97.3		
	51	4984	0.0	0.98	5218	261.0	309.1	96.9		
	57	5563	0.2	0.91	5780	257.4	305.4	96.9		
		4927	0.1	0.83	5126	263.8	310.3	96.8		
		5005	0.3	0.94	5229	263.1	309.4	96.9		
		5092	0.2	0.71	5260	265.0	311.6	97.6		
		4881	0.2	1.12	5149	263.0	309.4	96.0		
		5642	0.2	0.60	5784	261.5	307.5	97.5		
		5643	0.2	0.68	5805	262.7	308.9	96.7		
		5650	0.2	0.68	5813	262.5	308.8	97.3		
		4382	0.2	1.50	*4741	*270.9	*318.4	*101.2		
		4339	0.2	1.60	*4720	*272.9	*321.0	*100.7		
					*4723	*272.9	*321.1	*100.0		
		4515	0.2	2.58	5130	262.6	308.7	96.9		
		4986	0.2	0.08	5178	262.7	308.9	96.8		
		4852	0.2	1.30	5162	263.2	309.5	97.0		

FINJ
sts

** = T_{FINJ} for tests 43-58

*Nozzle Flow Separation

PROJECT OF SHEET

ROCKETDYNE
A DIVISION OF NORTH AMERICAN AVIATION, INC.

CALCULATED BY
CHECKED
DATE

FOLDOUT FRAME 3

TABLE

	1	2	3	4	5	6	7	8	9	10	11	12	
			WSTF TEST	SLICE TIME, SEC	$P_{C_{AV}}$, PSIA	$P_{C_{DIFF}}$, %	$P_{C_{NS}}$, PSIA	ΔP_F INJ, PSI	ΔP_O INJ, PSI	$\dot{W}_O$, LB/SEC	$\dot{W}_{O_{DIFF}}$, %	$\dot{W}_F$, LB/SEC	$\dot{W}_{F_D}$
1			1-1A-1	1.7	127.0	2.1	120.6	50.1	48.6	10.89	0.8	7.77	0
2			1-1A-2	0									
3			1-1A-2A	1.7	133.4	2.5	126.7	46.7	55.1	11.61	0.2	7.66	0
4			1-1B-3	1.7	131.9	2.1	120.6	41.8	58.2	11.78	0.4	7.24	0
5			1-1B-4	4.7	130.3	1.7	123.8	45.3	59.0	11.71	0.7	7.23	0
6			1-1C-5	5.2	125.0								
7			1-1C-6	10.0	125.5								
8			1-2-1	10.0	123.1								
9			1-2-2	10.0	122.8								
10			1-2-3	10.0	122.7								
11			1-2-4	10.0	137.0								
12			1-2-5	10.0	137.0								
13			1-2-6	10.0	137.2								
14			1-2-7	10.0	110.1								
15			1-2-8	10.0	109.9			FUEL LEAKAGE INVALIDATED					
16			1-2-9	10.0	108.4			PERFORMANCE ON TESTS					
17			1-2-10	10.0	122.8			1-1C-5 THROUGH 1-4-5					
18			1-2-11	10.0	122.2								
19			1-2-12	10.0	122.6								
20			1-4-1	6.0	124.6								
21			1-4-2	6.0	126.6								
22			1-4-3	0									
23			1-4-3A	6.0	124.4								
24			1-4-4	6.0	123.3								
25			1-4-5	6.0	123.4								
26			2-1-1A	2.0	127.6	0.0	121.2	72.2	48.7	11.43	0.7	7.44	0
27			2-1-2	6.0	127.7	0.2	121.4	72.5	49.7	11.13	2.2	7.50	0
28			2-1-3	6.0	131.0	0.1	124.5	72.6	52.2	11.38	1.8	7.59	0
29			2-2-1	6.0	125.3	0.8	118.9	78.8	53.9	10.89	0.3	7.91	0
30			2-2-2	6.0	116.1	0.4	110.3	50.6	43.1	10.43	0.6	6.39	0
31			2-2-3	6.0	130.6	0.2	124.1	71.4	51.5	11.38	0.5	7.51	0
32			2-2-4	6.0	131.0	0.3	124.5	67.3	53.5	11.63	0.5	7.24	0
33			2-2-5	6.0	130.6	0.1	124.1	62.8	56.1	11.89	0.5	6.96	0
34			2-2-6	6.0	145.8	0.3	138.5	84.7	66.1	12.93	0.4	8.05	0
35			2-3-1	10.0	129.9	0.3	123.4	59.8	54.1	11.70	1.0	7.08	0

FOLDOUT [redacted]

TOR THRUST CHAMBER PERFORMANCE (cont'd)

15 $\dot{W}_{TOTAL}$, LB/SEC	16 W_{BLC}, % of WT	17 To_{INJ}, F	18 $T_{F_{INJ}}$, F	19 P_{CELL}, psia	20 F_{SITE}, Pounds	21 F_{VAC}, Pounds	22 F_{DIFF}, Percent	23 VACUUM I_S, Sec, $\varepsilon = 9$	24 VACUUM I_S, Sec, $\varepsilon = 72$	25 N_{ERE}, Percent	26 ΔP_{REGEN}	27	28
18.66	2.5	80.8	175.0	0.06	4761	4777	0.0	256.0	300.9	95.4	20.0		
	2.1												
19.27	2.1	80.2	178.8	0.08	4963	4984	0.0	258.6	304.0	95.5	19.3		
19.02	1.9	81.5	187.4	0.06	4961	4977	0.1	261.7	307.6	96.0	18.0		
18.66	2.0	82.9	206.9	0.06	4932	4948	0.0	261.2	307.1	95.9	16.1		
18.87	2.3	73.6	153.8	0.07	4807	4824	0.1	255.6	300.1	94.4	18.0		
18.63	2.4	74.0	190.6	0.07	4814	4831	0.0	259.3	304.4	96.1	18.1		
18.97	2.3	74.9	195.1	0.07	4928	4945	0.1	260.7	306.0	96.4	20.3		
19.99	2.3	80.1	180.4	0.07	4701	4718	0.1	236.0	277.0	87.2	19.2		
16.82	2.2	45.3	206.0	0.06	4365	4380	0.2	260.4	305.7	95.8	19.2		
18.90	2.3	80.7	201.0	0.07	4912	4928	0.1	260.8	306.1	96.4	18.6		
18.87	2.2	80.9	208.8	0.07	4923	4939	0.0	261.8	307.3	96.2	17.0		
18.85	2.1	81.0	212.8	0.07	4932	4949	0.0	262.5	308.1	96.0	16.3		
20.99	2.2	81.0	204.0	0.07	5503	5520	0.1	263.0	308.7	96.4	19.6		
18.97	2.2	74.8	195.3	0.08	4924	4943	0.2	260.5	306.3	95.7	17.3		

t'd)

19 P_{CELL}, psia	20 F_{SITE}, Pounds	21 F_{VAC}, Pounds	22 F_{DIFF}, Percent	23 VACUUM I_s, Sec $\varepsilon = 9$	24 VACUUM I_s, Sec $\varepsilon = 72$	25 N_{ERE}, Percent	26 ΔP_{REGEN}	27	28	29	30
0.06	4761	4777	0.0	256.0	300.9	95.4	20.0				
0.08	4963	4984	0.0	258.6	304.0	95.5	19.3				
0.06	4961	4977	0.1	261.7	307.6	96.0	18.0				
0.06	4932	4948	0.0	261.2	307.1	95.9	16.1				
0.07	4807	4824	0.1	255.6	300.1	94.4	18.0				
0.07	4814	4831	0.0	259.3	304.4	96.1	18.1				
0.07	4928	4945	0.1	260.7	306.0	96.4	20.3				
0.07	4701	4718	0.1	236.0	277.0	87.2	19.2				
0.06	4365	4380	0.2	260.4	305.7	95.8	19.2				
0.07	4912	4928	0.1	260.8	306.1	96.4	18.6				
0.07	4923	4939	0.0	261.8	307.3	96.2	17.0				
0.07	4932	4949	0.0	262.5	308.1	96.0	16.3				
0.07	5503	5520	0.1	263.0	308.7	96.4	19.6				
0.08	4924	4943	0.2	260.5	306.3	95.7	17.3				

PROJECT

SHEET OF

ROCKETDYNE
A DIVISION OF NORTH AMERICAN AVIATION, INC.

CALCULATED BY

CHECKED

DATE

FOLDOUT FRAME 3

TABLE

	1	2	3	4	5	6	7	8	9	10	11	12	1
			WSTF TEST	SLICE TIME, SEC	$P_{C_{AV}}$, PSIA	$P_{C_{DIFF}}$, %	$P_{C_{NS}}$, PSIA	P_F INJ, PSI	P_O INJ, PSI	$\dot{W}_O$, LB/SEC	$\dot{W}_{O_{DIFF}}$, %	$\dot{W}_F$, LB/SEC	$\dot{W}_{F_D}$
1			2-3-2	7.0	146.2	0.4	138.9	64.9	70.7	13.55	0.2	7.54	0
2			2-3-3	7.0	146.6	0.2	139.3	75.4	65.7	12.98	0.2	8.09	0
3			2-3-4	7.0	146.2	0.0	138.9	88.2	59.6	12.38	0.2	8.74	1
4			2-3-5	7.0	131.2	0.1	124.7	57.3	55.0	11.92	0.3	7.03	0
5			2-3-6	7.0	130.7	0.5	124.2	53.3	57.0	12.17	0.1	6.73	0
6			2-3-7	7.0	131.1	0.3	124.6	65.7	50.1	11.42	0.4	7.54	0
7			2-3-8	7.0	130.5	0.5	124.0	70.5	47.3	11.09	0.4	7.86	0
8			2-3-9	7.0	115.4	0.4	109.6	41.6	44.4	10.77	0.3	6.00	0
9			2-3-10	7.0	114.6	0.4	108.9	55.1	36.7	9.80	0.3	6.94	0
10			2-3-11	7.0	115.1	0.4	109.4	46.4	40.4	10.34	0.2	6.39	0
11			2-3-12	7.0	130.4	0.1	123.9	60.0	51.7	11.64	0.2	7.25	0
12			2-4-1	10.0	129.3	0.5	122.8	59.7	56.8	11.67	0.1	7.25	0
13			2-4-2	7.0	146.1	0.6	138.8	65.7	72.8	13.54	0.2	7.52	0
14			2-4-3	7.0	146.0	0.0	138.7	76.4	68.4	13.02	0.2	8.07	1
15			2-4-4	7.0	145.4	0.2	138.1	89.0	62.5	12.40	0.4	8.76	0
16			2-4-5	7.0	130.5	0.3	124.0	53.9	59.7	12.16	0.3	6.77	0
17			2-4-6	7.0	130.3	0.1	123.7	72.2	50.4	11.13	0.3	7.86	0
18			2-4-7	7.0	114.5	0.2	108.8	42.5	47.0	10.73	0.2	5.99	0
19			2-4-8	7.0	114.5	0.2	108.8	55.3	39.3	9.86	0.2	6.92	0
20			2-4-9	7.0	114.9	0.4	109.1	46.6	43.2	10.39	0.1	6.37	0
21			2-4-10	7.0	129.6	0.3	123.1	60.8	54.5	11.63	0.0	7.24	0
22			2-9-1	10.0	173.3	0.0	164.6	98.3	100.0	15.71	0.5	9.30	0
23			2-9-2	7.0	183.2	0.2	174.0	109.9	107.5	16.42	0.0	9.90	1
24			2-9-3	7.0	187.1	0.1	177.7	108.9	113.5	16.98	0.2	9.79	1
25			2-9-4	7.0	183.9	0.2	174.7	95.6	115.1	17.16	0.5	9.16	0
26			2-9-5	7.0	183.9	0.4	174.7	103.1	110.2	16.81	0.1	9.51	1
27			2-9-6	7.0	184.1	0.5	174.9	110.1	104.2	16.43	0.4	9.86	0
28			2-9-7	7.0	133.0	0.1	126.3	57.4	55.7	12.09	0.3	7.17	0
29			2-9-8	7.0	106.1	0.7	100.8	35.1	37.4	9.84	0.4	5.66	0
30			2-9-9	7.0	105.3	0.2	100.1	36.2	35.9	9.66	0.1	5.78	0
31			2-9-10	7.0	105.3	0.2	100.1	32.0	32.0	9.24	0.2	6.19	0
32			2-9-11	10.0	130.8	0.7	124.3	55.9	55.6	11.99	0.5	7.10	0
33													
34													
35													

FOLDOUT FRAME 1

THRUST CHAMBER PERFORMANCE (cont'd)

15 'AL' EC	16 $\dot{W}_{BLC}$, PERCENT OF WT.	17 $T_{O_{INJ}}$, F	18 $T_{F_{INJ}}$, F	19 P_{CELL}, PSIA	20 F_{SITE}, POUNDS	21 F_{VAC}, POUNDS	22 F_{DIFF}, %	23 VACUUM I_s, SEC $\varepsilon = 9$	24 $\varepsilon = 72$	25 η_{C^*} ERE', %	26 ΔP_{REG}	27	28
09	2.1	75.1	209.2	0.08	5518	5537	0.1	262.5	308.9	95.6	18.0		
08	2.2	75.4	199.3	0.07	5523	5541	0.1	262.9	309.1	96.4	19.0		
12	2.4	75.4	187.7	0.07	5495	5513	0.1	261.0	306.7	96.9	22.7		
95	2.2	75.5	210.9	0.07	4952	4969	0.2	262.3	308.5	96.0	15.9		
90	2.1	75.5	221.5	0.07	4941	4958	0.0	262.4	308.7	95.7	14.6		
95	2.3	75.5	197.2	0.07	4935	4952	0.1	261.3	307.2	96.5	17.2		
95	2.4	75.5	190.0	0.07	4908	4925	0.1	259.9	305.5	96.7	19.3		
77	2.1	75.5	220.8	0.07	4366	4382	0.1	261.3	307.4	95.7	12.0		
74	2.4	75.5	193.3	0.07	4314	4330	0.0	258.7	304.1	96.5	15.0		
72	2.2	75.5	208.4	0.07	4342	4358	0.1	260.6	331.4	95.9	13.8		
88	2.2	75.6	203.6	0.07	4919	4936	0.0	261.4	307.4	96.0	16.7		
92	2.2	84.9	205.9	0.07	4915	4932	0.0	260.7	306.5	95.8	18.2		
06	2.1	86.0	219.0	0.08	5528	5548	0.1	263.4	309.9	95.9	18.3		
08	2.2	86.2	208.8	0.08	5510	5528	0.1	262.2	308.3	96.1	19.8		
16	2.4	86.3	195.6	0.08	5465	5483	0.1	259.1	304.6	96.2	23.2		
94	2.1	86.3	223.1	0.07	4929	4946	0.0	261.1	307.3	95.3	15.4		
99	2.4	86.2	198.8	0.07	5455	5478	0.0	259.4	304.9	96.5	19.3		
72	2.1	86.1	228.0	0.07	4338	4353	0.1	260.4	306.4	95.4	12.6		
78	2.4	86.1	202.7	0.07	4319	4335	0.0	258.4	303.7	96.3	15.5		
75	2.2	86.1	216.9	0.07	5453	5492	0.0	260.2	305.9	95.7	13.9		
88	2.2	86.2	211.2	0.07	4905	4921	0.1	260.6	306.4	95.8	16.0		
01	2.1	84.2	190.5	0.09	6564	6585	0.0	263.3	309.7	92.6	26.4		
31	2.2	74.1	183.7	0.08	6929	6949	0.1	264.1	310.5		29.1		
77	2.1	74.8	189.6	0.11	7068	7095	0.0	265.1	311.8		29.5		
33	2.0	75.5	199.1	0.12	6945	6973	0.1	264.9	311.4		26.7		
31	2.1	75.8	193.1	0.11	6943	6970	0.0	264.9	311.6		29.1		
29	2.2	75.9	186.5	0.11	6929	6955	0.1	264.6	311.1		30.8		
26	2.1	75.8	193.3	0.07	5024	5040	0.1	261.7	307.8	95.7	17.2		
50	2.1	75.9	202.7	0.06	3994	4008	0.1	258.6	304.2	95.0	11.2		
44	2.1	76.3	197.9	0.06	3957	3973	0.1	257.3	302.6	94.7	13.6		
43	2.3	76.3	183.9	0.07	3946	3961	0.1	256.6	301.7	95.4	13.2		
09	2.1	76.4	193.5	0.07	4961	4977	0.1	260.8	306.7	95.4	16.5		

AME 2

FOLDOUT FR

(cont'd)

J'	19 P_{CELL}, PSIA	20 F_{SITE}, POUNDS	21 F_{VAC}, POUNDS	22 F_{DIFF}, %	23 VACUUM I_s, SEC $\varepsilon = 9$	24 VACUUM I_s, SEC $\varepsilon = 72$	25 η_{C^*ERE}, %	26 ΔP_{REG}	27	28	29	30
2	0.08	5518	5537	0.1	262.5	308.9	95.6	18.0				
3	0.07	5523	5541	0.1	262.9	309.1	96.4	19.0				
7	0.07	5495	5513	0.1	261.0	306.7	96.9	22.7				
9	0.07	4952	4969	0.2	262.3	308.5	96.0	15.9				
5	0.07	4941	4958	0.0	262.4	308.7	95.7	14.6				
2	0.07	4935	4952	0.1	261.3	307.2	96.5	17.2				
0	0.07	4908	4925	0.1	259.9	305.5	96.7	19.3				
8	0.07	4366	4382	0.1	261.3	307.4	95.7	12.0				
3	0.07	4314	4330	0.0	258.7	304.1	96.5	15.0				
4	0.07	4342	4358	0.1	260.6	331.4	95.9	13.8				
6	0.07	4919	4936	0.0	261.4	307.4	96.0	16.7				
9	0.07	4915	4932	0.0	260.7	306.5	95.8	18.2				
0	0.08	5528	5548	0.1	263.4	309.9	95.9	18.3				
8	0.08	5510	5528	0.1	262.2	308.3	96.1	19.8				
6	0.08	5465	5483	0.1	259.1	304.6	96.2	23.2				
1	0.07	4929	4946	0.0	261.1	307.3	95.3	15.4				
8	0.07	5455	5478	0.0	259.4	304.9	96.5	19.3				
0	0.07	4338	4353	0.1	260.4	306.4	95.4	12.6				
7	0.07	4319	4335	0.0	258.4	303.7	96.3	15.5				
9	0.07	5453	5492	0.0	260.2	305.9	95.7	13.9				
2	0.07	4905	4921	0.1	260.6	306.4	95.8	16.0				
5	0.09	6564	6585	0.0	263.3	309.7	92.6	26.4				
7	0.08	6929	6949	0.1	264.1	310.5		29.1				
5	0.11	7068	7095	0.0	265.1	311.8		29.5				
1	0.12	6945	6973	0.1	264.9	311.4		26.7				
1	0.11	6943	6970	0.0	264.9	311.6		29.1				
5	0.11	6929	6955	0.1	264.6	311.1		30.8				
3	0.07	5024	5040	0.1	261.7	307.8	95.7	17.2				
7	0.06	3994	4008	0.1	258.6	304.2	95.0	11.2				
9	0.06	3957	3973	0.1	257.3	302.6	94.7	13.6				
9	0.07	3946	3961	0.1	256.6	301.7	95.4	13.2				
5	0.07	4961	4977	0.1	260.8	306.7	95.4	16.5				

PROJECT

SHEET OF

ROCKETDYNE
A DIVISION OF NORTH AMERICAN AVIATION, INC.

CALCULATED BY

CHECKED

DATE

FOLDOUT FRAME 3

TABLE

	1	2	3	4	5	6	7	8	9	10	11	12	13
			WSTF TEST	SLICE TIME, SEC	$P_{C_{AV}}$, PSIA	$P_{C_{DIFF}}$, %	$P_{C_{NS}}$, PSIA	P_F INJ, PSI	P_o INJ, PSI	$\dot{W}_o$, LB/SEC	$\dot{W}_{o_{DIFF}}$, %	$\dot{W}_F$, LB/SEC	$\dot{W}_{F_{DI}}$ %
1			2-5-1	10.0	182.6	0.3	173.5	106.6	108.3	16.34	0.6	9.88	0.
2			2-5-2	7.0	187.9	0.3	178.5	107.4	113.1	16.85	0.5	9.95	0.
3			2-5-3	7.0	184.5	0.5	175.3	100.7	110.4	16.70	0.5	9.59	0.
4			2-5-4	7.0	183.9	0.4	174.7	93.7	114.4	17.03	0.5	9.26	0.
5			2-5-5	7.0	184.6	0.2	175.4	106.5	104.8	16.36	0.6	9.90	0.
6			2-5-6	7.0	149.5	0.0	142.1	69.8	69.4	13.39	0.5	8.06	0.
7			2-5-7	7.0	148.6	0.2	141.1	60.3	75.4	13.96	0.5	7.50	0.
8			2-5-8	7.0	149.3	0.2	141.8	80.2	62.4	12.76	0.4	8.65	0.
9			2-5-9	7.0	133.0	0.1	126.3	54.1	55.0	12.04	0.3	7.15	0.
10			2-5-10	7.0	133.5	0.1	126.8	63.7	49.5	11.45	0.2	7.75	0.
11			2-5-11	7.0	132.5	0.1	125.9	47.4	60.0	12.55	0.5	6.69	0.
12			2-5-12	7.0	106.3	0.8	101.0	32.7	37.2	9.96	0.2	5.58	0.
13			2-5-13	7.0	106.4	0.8	101.0	40.5	32.5	9.28	0.2	6.21	0.
14			2-5-14	7.0	105.8	0.8	100.5	34.3	35.8	9.68	0.2	5.76	0.
15			2-5-15	7.0	132.2	0.5	125.5	32.7	37.2	11.95	0.3	7.12	0.
16			2-5-15	10.0	131.5	0.7	124.9	53.4	53.9	11.93	0.3	7.10	0.
17			2-5-15	15.0	130.6	0.1	124.1	53.7	54.9	11.91	0.3	7.06	0.
18			2-5-15	30.0	128.9	0.4	122.4	53.3	55.6	11.83	0.3	6.96	0.
19													
20													
21													
22													
23													
24													
25													
26													
27													
28													
29													
30													
31													
32													
33													
34													
35													

FOLDOUT FRAME /

NSTRATOR THRUST CHAMBER PERFORMANCE (cont'd)

14	15	16	17	18	19	20	21	22	23	24	25	26	27
°F	$\dot{W}_{TOTAL}$, LB/SEC	$\dot{W}_{BLC}$, PERCENT OF WT.	$T_{o\ INJ}$, F	$T_{F_{INJ}}$, F	P_{CELL}, PSIA	F_{SITE}, POUNDS	F_{VAC}, POUNDS	F_{DIFF}, %	VACUUM I_s, SEC $\varepsilon = 9$	VACUUM I_s, SEC $\varepsilon = 72$	η_{C^*ERE}, %	ΔP_{REG}	
65	26.23	2.3	82.7	184.9	0.11	6954	6981	0.1	266.2	312.8	96.8	28.5	
69	26.80	2.3	82.7	188.9	0.12	7106	7134	0.0	266.2	312.7	96.2	29.2	
74	26.29	2.2	82.7	192.8	0.12	696.3	6991	0.0	265.9	312.3	96.1	27.3	
84	26.29	2.2	82.7	199.9	0.12	6949	6978	0.0	265.4	311.4	96.0	26.1	
65	26.26	2.3	82.7	188.3	0.12	6966	6994	0.0	266.3	312.9	96.3	30.2	
66	21.45	2.3	82.6	193.2	0.08	5653	5673	0.1	264.5	310.7	96.1	21.6	
86	21.46	2.1	82.7	206.3	0.08	5626	5648	0.0	2632	308.7	95.7	19.6	
48	21.40	2.4	82.7	180.9	0.19	5637	5655	0.1	264.2	310.4	96.6	23.5	
69	19.19	2.2	82.6	198.7	0.07	5034	5051	0.1	263.3	309.3	95.8	17.3	
48	19.20	2.4	82.6	183.8	0.07	5037	5054	0.1	263.2	309.2	96.4	19.6	
88	19.24	2.1	82.6	211.0	0.08	5026	5045	0.2	262.2	307.4	95.6	15.7	
79	15.54	2.1	82.5	215.0	0.06	4033	4047	0.2	260.5	305.9	95.3	11.7	
49	15.49	2.4	82.6	193.3	0.06	4025	4040	0.2	260.9	306.6	95.9	13.7	
68	15.44	2.2	82.5	205.8	0.06	4003	4018	0.0	260.3	305.8	95.3	12.4	
68	19.07	2.2	82.5	199.4	0.07	5003	5020	0.1	263.2	309.2	95.8	16.6	
68	19.03	2.2	82.4	200.9	0.07	4996	5012	0.0	263.4	309.4	95.9	15.9	
69	18.97	2.2	82.3	202.9	0.07	4983	5000	0.0	263.6	309.6	96.0	15.5	
70	18.79	2.2	81.8	209.1	0.08	4951	5969	0.1	264.5	310.7	96.3	15.2	

t'd)

19	20	21	22	23	24	25	26	27	28	29	30
P_{CELL}, PSIA	F_{SITE}, POUNDS	F_{VAC}, POUNDS	F_{DIFF}, %	VACUUM I_s, SEC $\varepsilon = 9$	VACUUM I_s, SEC $\varepsilon = 72$	η_{C^*ERE}, %	ΔP_{REG}				
0.11	6954	6981	0.1	266.2	312.8	96.8	28.5				
0.12	7106	7134	0.0	266.2	312.7	96.2	29.2				
0.12	696.3	6991	0.0	265.9	312.3	96.1	27.3				
0.12	6949	6978	0.0	265.4	311.4	96.0	26.1				
0.12	6966	6994	0.0	266.3	312.9	96.3	30.2				
0.08	5653	5673	0.1	264.5	310.7	96.1	21.6				
0.08	5626	5648	0.0	2632	308.7	95.7	19.6				
0.19	5637	5655	0.1	264.2	310.4	96.6	23.5				
0.07	5034	5051	0.1	263.3	309.3	95.8	17.3				
0.07	5037	5054	0.1	263.2	309.2	96.4	19.6				
0.08	5026	5045	0.2	262.2	307.4	95.6	15.7				
0.06	4033	4047	0.2	260.5	305.9	95.3	11.7				
0.06	4025	4040	0.2	260.9	306.6	95.9	13.7				
0.06	4003	4018	0.0	260.3	305.8	95.3	12.4				
0.07	5003	5020	0.1	263.2	309.2	95.8	16.6				
0.07	4996	5012	0.0	263.4	309.4	95.9	15.9				
0.07	4983	5000	0.0	263.6	309.6	96.0	15.5				
0.08	4951	5969	0.1	264.5	310.7	96.3	15.2				

PROJECT

SHEET OF

ROCKETDYNE
A DIVISION OF NORTH AMERICAN AVIATION, INC.

CALCULATED BY
CHECKED
DATE

FOLDOUT FRAME 3

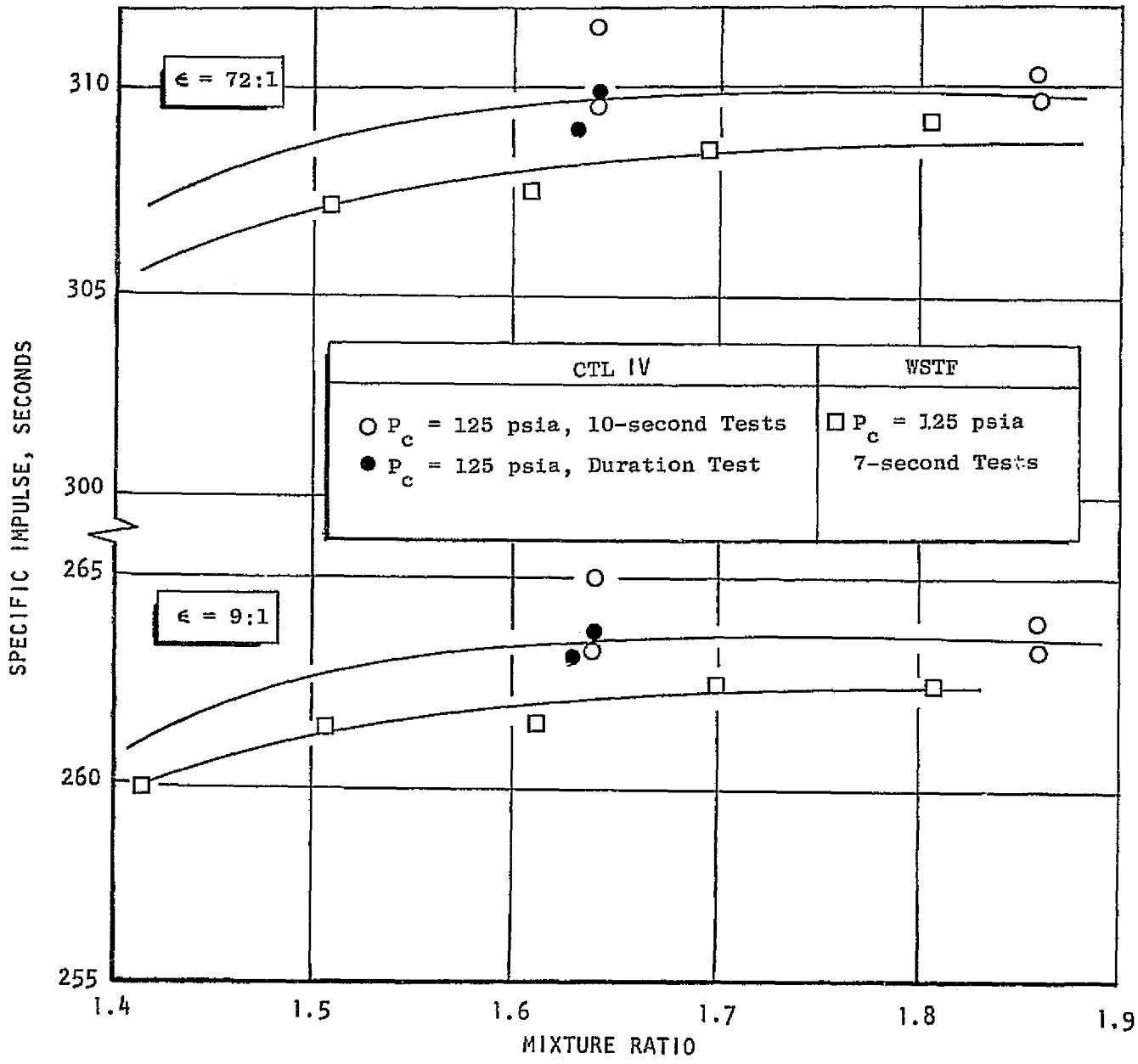

Figure 28. Comparison of Performance Measured at CTL-IV and WSTF

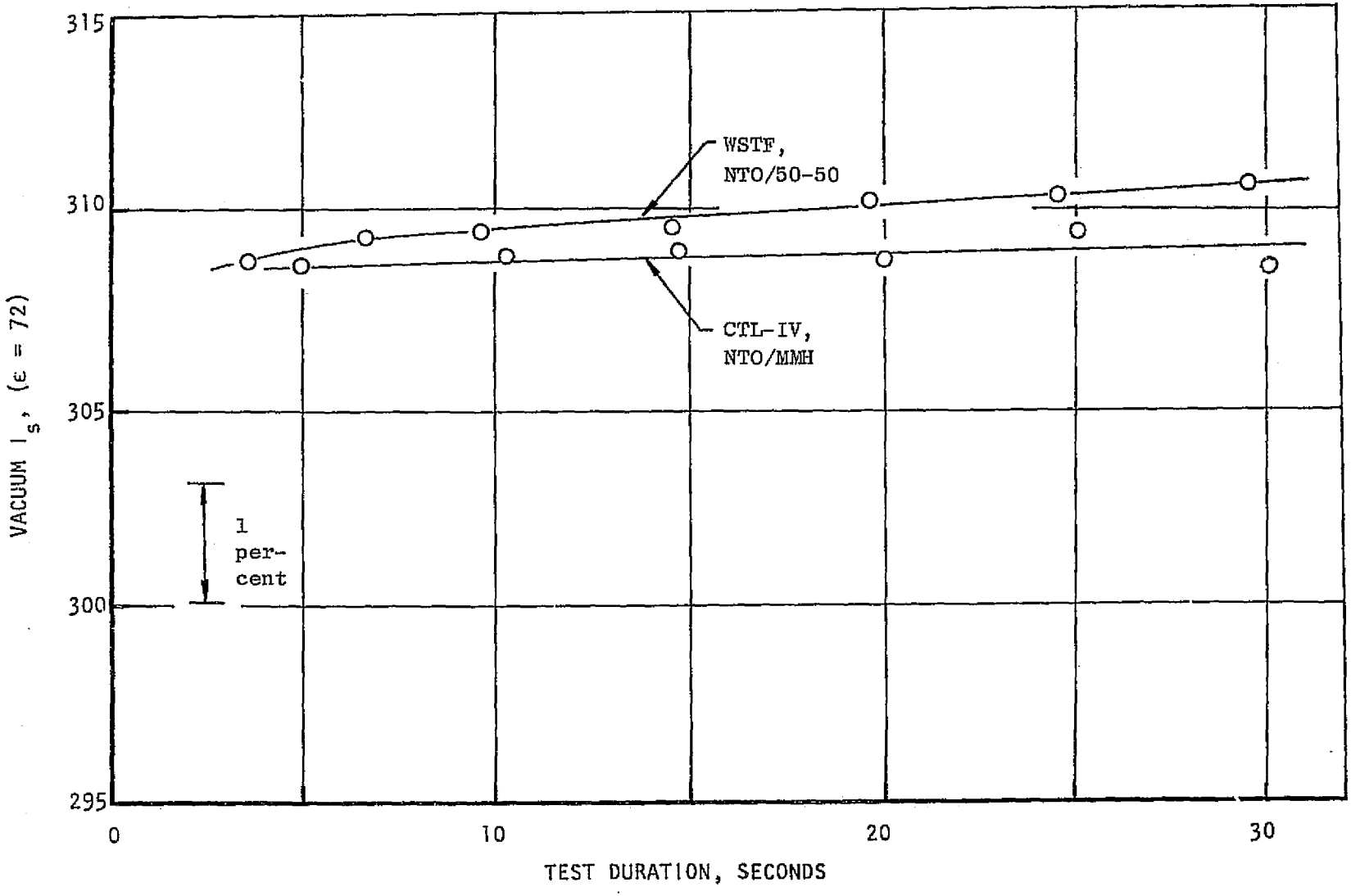

Figure 29. Performance Variation During Longer Duration Tests

TABLE 7

OME SPECIFIC IMPULSE SUMMARY

	FLIGHT SYSTEM AT ϵ = 72	TEST SYSTEM AT ϵ = 72	TEST SYSTEM AT ϵ = 9
ODK SPECIFIC IMPULSE, SEC	332.6	332.6	302.4
DIVERGENCE EFFICIENCY	0.985	0.985	0.915
COMBUSTION EFFICIENCY	0.974	0.965*	0.965*
REGEN HEATING EFFICIENCY	1.006	1.005	1.005
IMPURITY FACTOR	0.998	0.998	0.998
DRAG LOSS, SEC	-6.5	-6.5	-3.0
STRATIFICATION LOSS, SEC	-1.0	-1.0	-1.5
DELIVERED SPECIFIC IMPULSE, SEC	312.9	309.6	263.3

* L/D #1 INJECTOR BASED ON SOLID WALL CHAMBER TESTS

The variation of performance with chamber pressure and mixture ratio measured at WSTF over the ranges for which the demonstrated was designed is shown in Fig. 30 for unsaturated propellants and approximately 2 percent film cooling. An increase in performance of approximately 1 second occurs at the upper end of the nominal operating range of the OME (P_c = 140 psia, o/f = 1.8), compared to performance at nominal conditions. Performance decreases by approximately 3 seconds operating at a chamber pressure of 110 psi and a mixture ratio of 1.45. Performance data measured at CTL-IV at off-design chamber pressures did not show the trend. Low pressure data was involved due to nozzle separation. High pressure data indicated a slight pressure loss.

Performance with NTO/MMH and the L/D #1 injector without film coolant was determined at WSTF during test sequence 2-1. During these tests, a facility oxidizer leak occurred at the start of each test and decayed during the test. This leak decreased performance to an unknown extent and is probably responsible for erratic performance on the first few tests of the series. The data also appear questionable when compared to subsequent tests with film coolant in which the performance was as high or higher than the tests without film coolant.

Performance with helium saturated propellants is shown in Fig. 31 and 32 . A performance penalty of approximately 1 second results under nominal operating conditions. The shape of the measured performance curve at 140 psia chamber pressure and 225 psia saturation pressure appears to be more sensitive to mixture ratio compared to the rest of the data. However, the point at nominal mixture ratio is consistent with all other data.

Operating at a chamber pressure of 175 psia would increase the performance by about 4 seconds. An OME derivative used for a Space Tug application would operate at a chamber pressure of approximately 240 psia and would have a significantly higher area ratio. The 100 psia test conditions simulate the effect of vehicle pressurization system failure. A performance loss of over 1 percent occurs under these conditions relative to performance at the design point.

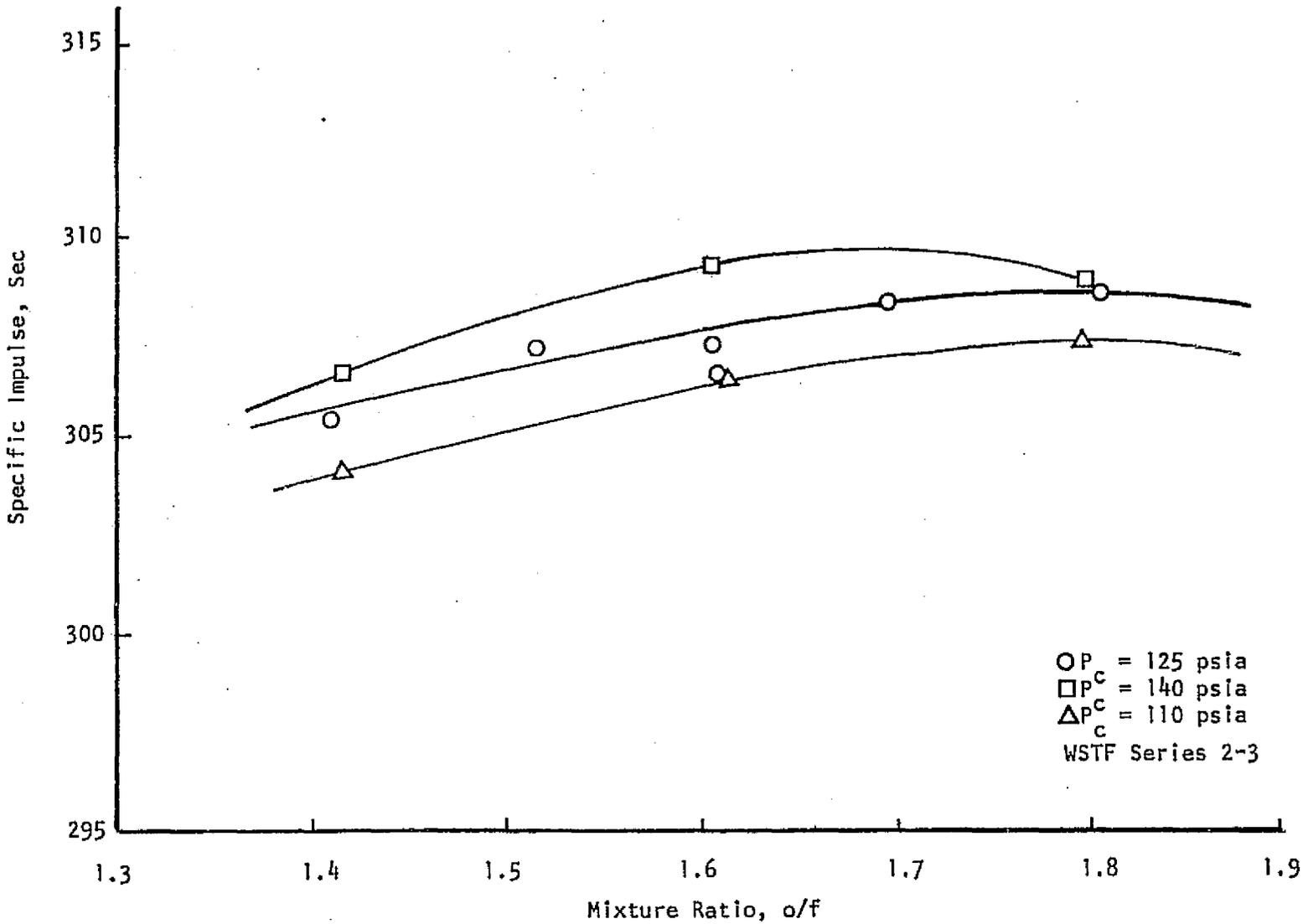

Figure 30. OME Engine Performance - Unsaturated Propellants (NTO/MMH)

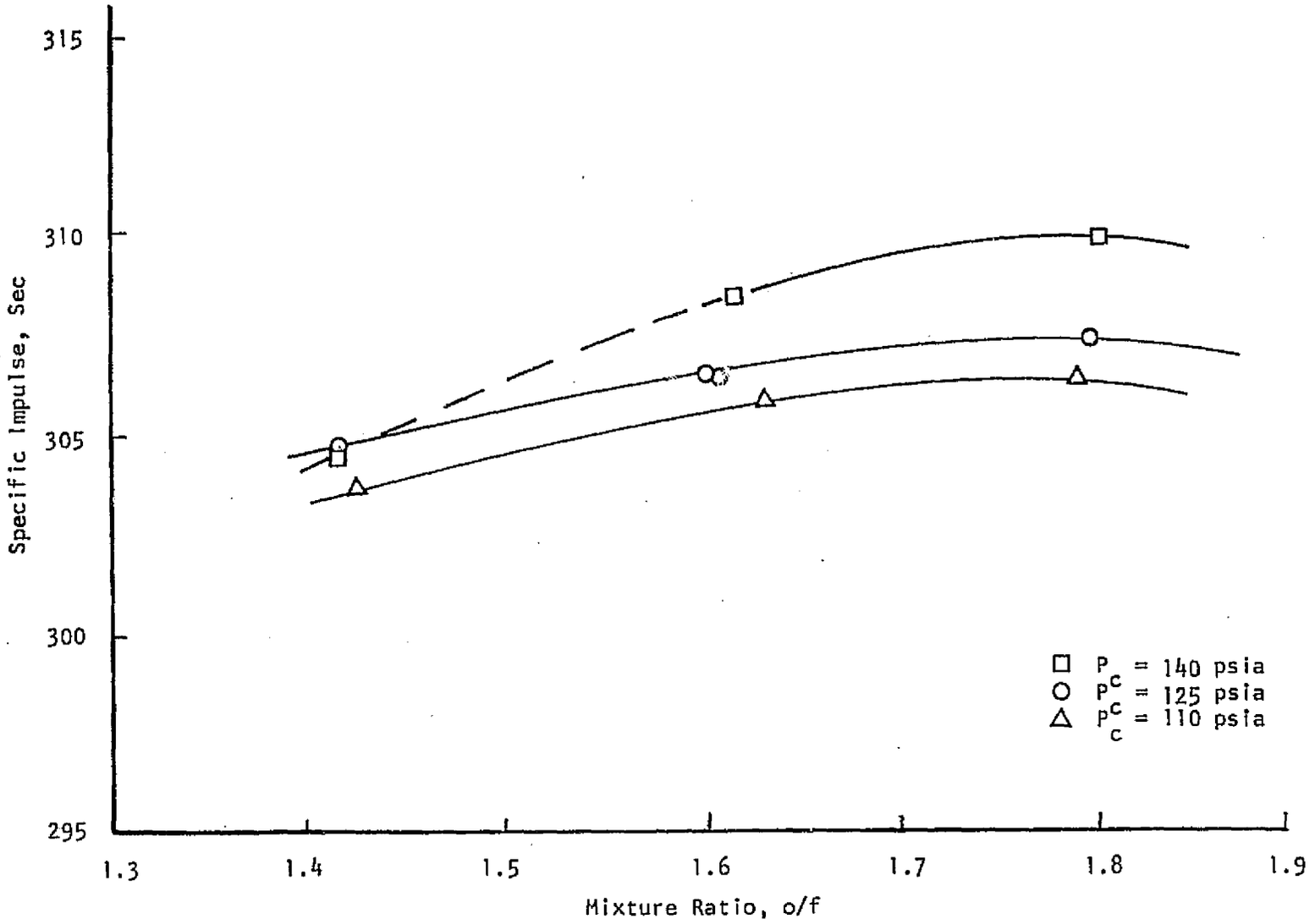

Figure 31. OME Engine Performance - Saturated Propellants
Tests 2-4-1 through 10 (MMH Fuel)
Helium Saturation - 225 psia

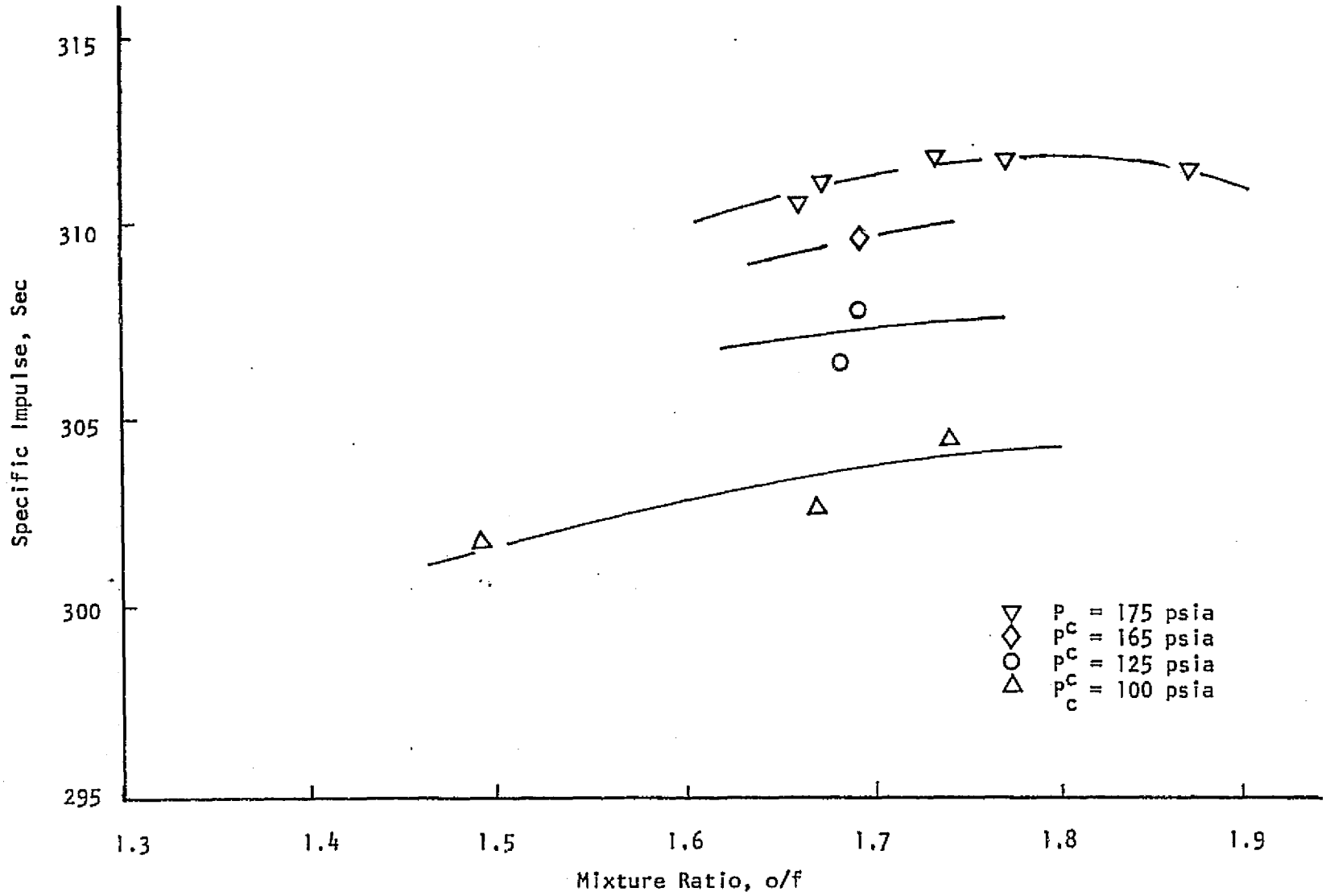

Figure 32. OME Performance - Saturated Propellants (NTO/MMH)
Helium Saturation - 165 psia

The performance of NTO with helium saturated 50-50 fuel and the #1 like-doublet injector is shown in Fig. 33. The nominal mixture ratio for this propellant combination is 1.60 for equal tank volumes. At this mixture ratio and a chamber pressure of 125 psia, a performance level of approximately 310 seconds was measured. These tests were of 7 seconds duration. The performance was shown in Fig. 29 for the 30 second duration test (2-5-1) as a function of time.

Operating at a high mixture ratio with this propellant combination results in a performance loss (rather than a performance gain as was the case with NTO/MMH). It was predicted analytically and shown in Fig. 49, 66, and 67 of the Data Dump for Task I and II that both ODK and delivered Is for NTO/MMH peaks at a higher value of o/f than for NTO/50-50. Figure 58 and 59 of the same reference indicate NTO/50-50 performance to be 2.2 seconds higher than NTO/MMH at 1.6 and 1.65 o/f, respectively. A gain of approximately 1 second in performance occurs at a chamber pressure of 140 psia. Performance sensitivity to chamber pressures is approximately the same as with the NTO/MMH combination, as shown in Fig. 34 which summarizes the WSTF data.

The L/D #2 injector was tested at WSTF during Series 1. Fuel leakage rendered most of the data unusable. The remaining data are questionable because of a possible oxidizer leak in the facility and the short durations (in view of the transient performance measured on longer duration tests) of these tests. The results indicate performance equal to or lower than the L/D #1 injector. Previous comparisons of these injectors during a company sponsored program at Rocketdyne indicated slightly higher performance for the L/D #2 injector.

THERMAL DATA

Thermal data taken during the tests at both facilities consisted of fuel bulk temperature rise, regenerative chamber back wall temperatures, and radiation cooled nozzle temperatures. These data, together with the data generated during the heated tube tests under this contract, were used to provide an indication of the safety margin at which the thrust chamber and nozzle were operating.

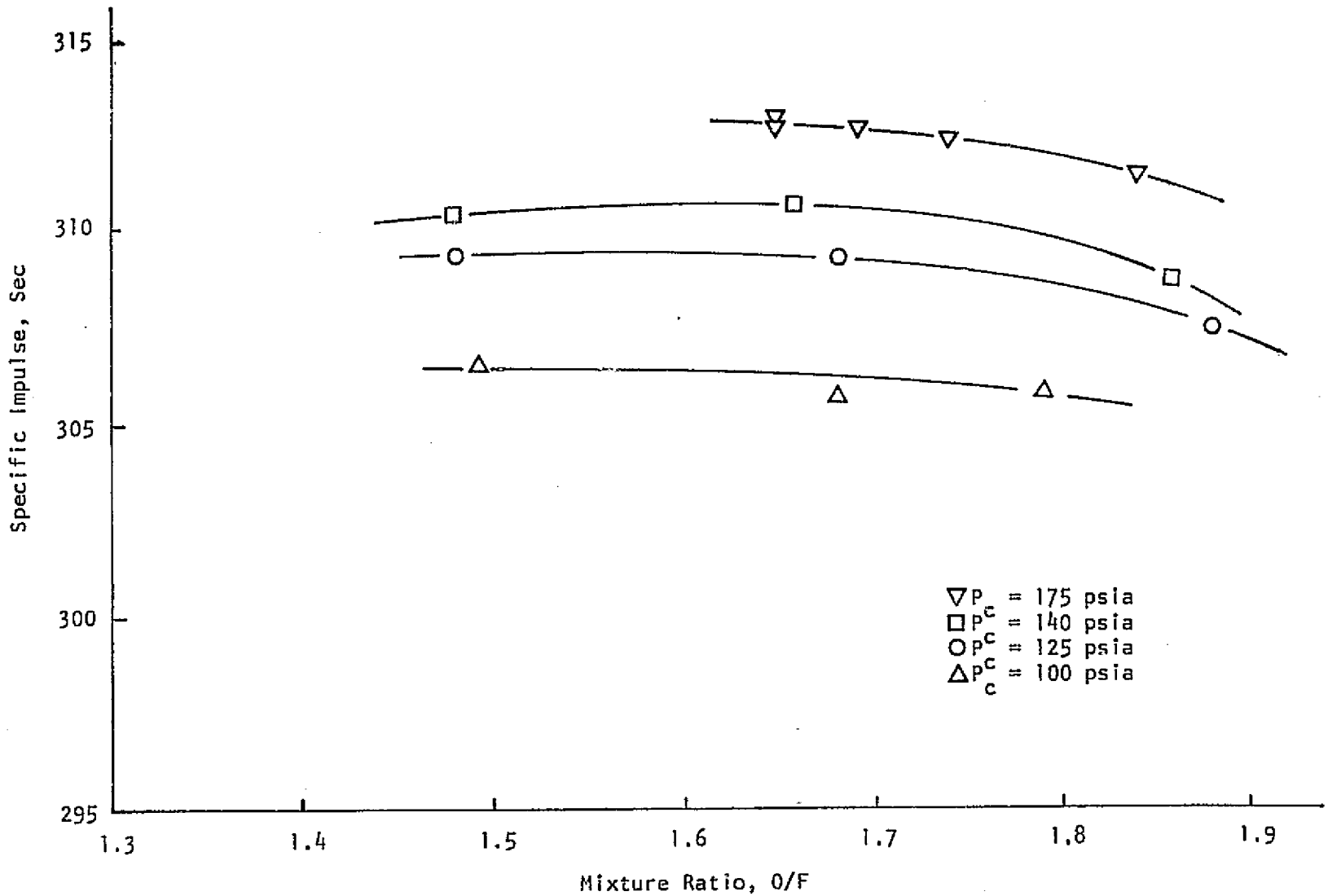

Figure 33. OME Performance - Saturated Propellants (NTO/50-50)
Helium Saturation - 165 psia

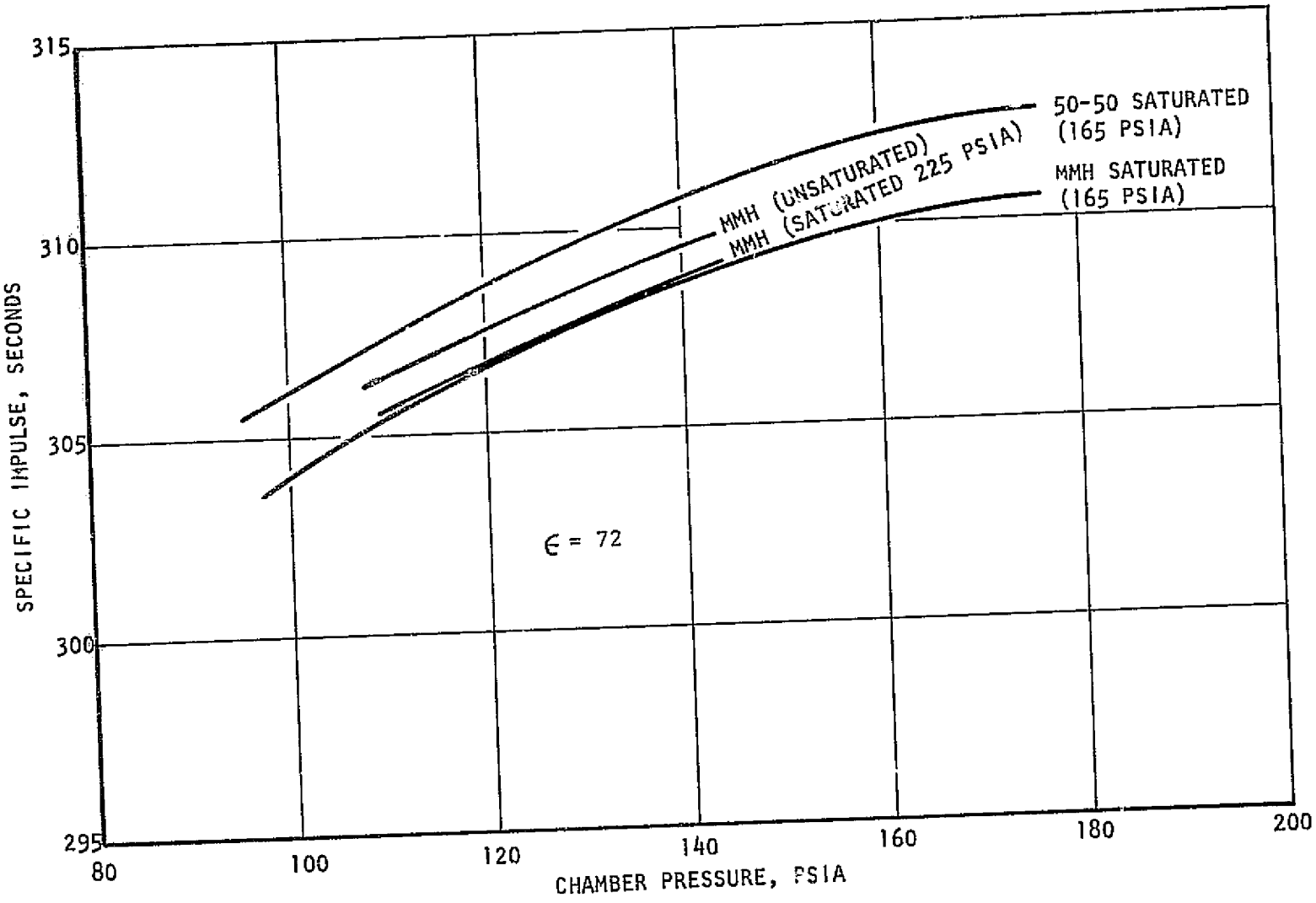

Figure 34. Summary of OME Performance Measured at WSTF

Bulk Temperature Rise and Heat Load

Coolant inlet and outlet temperatures, ΔT's, and the heat load are tabulated in Table 8. The operating conditions are shown in this table. Fuel inlet and outlet temperatures were each measured in three locations. Three bulk temperature rises were calculated based on the three outlet temperature thermocouples. The inlet temperature thermocouple TFB-6 was used as the reference temperature for all three ΔT's because of its proximity to the inlet and general agreement with the fuel flowmeter temperature thermocouple. Temperature rises calculated in this manner generally agree with each other within 5 percent for the bypass cooled tests at CTL-IV and within 10 percent for the regeneratively cooled tests at the same facility with ΔT_3 generally exhibiting the lowest value and ΔT_2 the highest.

The three coolant temperature rise measurements taken at WSTF generally agreed within 5 percent except for the last half of the last test series, 2-5 (NTO/50-50), on which ΔT_1 and ΔT_3 generally agreed within 6 F, while ΔT_2 was about 15 F higher. The data fit for these latter tests was improved by basing ΔQ on ΔT_1 and ΔT_3 only for these cases.

The response of the coolant bulk temperature at the outlet for a typical test at CTL-IV is shown in Fig. 35. Two of the three outlet temperatures have reached steady state conditions in approximately 5 seconds, while the third required almost 9 seconds to reach steady state. However, even the slow responding measurement reached approximately 96 percent of steady state value in 5 seconds. Only one long duration test with recorded outlet temperatures was run at CTL-IV. This was the last of a series and started with an unusually high bulk outlet temperature probably indicating hot outlet and injector manifolds. The result was a cooling transient of approximately 10 seconds, shown in Fig. 36. The coolant temperature then remained constant until 30-35 seconds, when an abrupt rise indicated failure of the BLC ring. Typical average outlet bulk temperature transients measured at WSTF are shown in Fig. 37. Most tests at WSTF were approximately 6 to 10 seconds duration. The bulk temperature response time for these tests appears to be approximately

TABLE

	1	2 CTL-IV TEST NO.	3 NOMINAL DURATION (SEC)	4 P_c (PSIA)	5 MR o/F	6 $\dot{W}_c=\dot{W}_F$ (lb/sec)	7 JACKET ΔP (PSI)	8 OUTLET TFB-1 (F)	9 OUTLET TFB-2 (F)	10 OUTLET TFB-3 (F)	11 INLET TFB-4 (F)	12 INLET TFB-5 (F)	13 INL TFB (F
1													
2		DUMP COOLED											
3													
4		47	10	125	1.61	7.48	15.6	179	190	187	58	59	58
5		48	10	126	1.74	7.25	16.2	197	203	199	67	68	69
6		49	10	126	1.83	7.25	16.0	192	198	195	61	61	63
7		50	10	143	1.52	7.27	15.4	199	206	202	61	62	63
8		51	10	141	1.85	7.37	15.8	204	212	206	61	62	63
9		52	10	110	1.41	7.35	15.5	195	199	199	79	85	81
10		53	10	113	1.56	7.35	15.6	195	201	199	72	79	78
11		54	10	117	1.70	7.37	16.2	196	202	201	73	77	76
12		55	10	125	1.44	7.21	15.4	192	197	195	68	71	68
13		56	10	125	1.50	7.35	15.4	198	202	200	69	71	69
14		57	10	126	1.59	7.32	15.6	198	202	199	68	70	67
15		58	10	141	1.40	7.25	16.7	192	197	194	63	62	62
16		59	1	~127	~1.5								
17													
18		REGENERATIVELY COOLED											
19													
20		60	5	122	1.86	6.80	12.9	180	194	189	54	54	56
21		61	7	126	1.64	7.52	15.8	183	190	183	58	57	96
22		62	7	126	1.64	7.52	15.6	187	191	184	56	56	60
23		**63	30										
24		64	10	124	1.86	6.84	11.9	212	224	211	63	61	70
25		65	10	140	1.44	9.08	21.0	180	182	178	61	61	70
26		66	10	140	1.63	8.41	18.1	191	198	193	64	64	7
27		67	10	140	1.84	7.79	15.5	211	214	198	65	63	7
28		68	10	111	1.44	7.22	15.9	200	193	187	70	69	7
29		69	10	110	1.66	6.56	15.9	211	211	199	67	66	7
30		70	10	109	1.86	6.13	15.9	234	240	216	69	68	7
31		7	10	130	1.63	7.28	14.1	202	202	191	64	64	7
		71	185	130	1.63	7.27	14.5	208	194	187	63	62	7
33		71	185	130	1.64	7.32	14.6	239	212	198	73	73	7
34		71	185	124	1.61	7.36	13.9	219	224	211	62	60	7
35													

FORM R 79-Y-3 Notes: Tests 37-46 and 59 too short for thermal data. No data on test 63. All data slices taken near e
Test 71 sliced at 10, 25, 55, and 175 sec.

T CHAMBER THERMAL DATA

16	17	18	19	20	21	22	23	24	25	26	27	28	29
					REGENERATIVELY COOLED CHAMBER BACKWALL TEMPERATURES								
ΔT_3 (F)	$\overline{\Delta T}$ (F)	ΔQ (BTU/SEC)	T8 (F) TOP	T9 (F)	T10 (F)	T11 (F)	T12 (F) TOP	T13 (F)	T14 (F) TOP	T15 (F)	T16 (F) TOP	T17 (F)	
128	127	674	189	195	183	188	150	150	159	159	103	100	
131	131	674	203	213	198	206	169	162	175	172	119	117	
134	133	685	197	205	191	195	162	156	164	165	111	109	
140	141	728	203	208	196	202	165	158	167	168	111	109	
144	145	759	206	213	199	206	170	161	170	171	113	111	
114	116	605	197	200	194	210	177	165	183	175	125	127	
120	122	637	198	202	197	212	177	165	180	175	125	126	
124	125	654	200	204	198	212	177	164	178	174	124	125	
124	126	645	197	199	215	204	170	176	171	183	116	123	
129	130	678	200	203	198	207	173	161	173	172	119	118	
129	131	681	201	204	198	210	172	161	172	171	115	115	
132	132	679	194	196	191	198	163	153	163	164	108	107	
135	134	652	196	203	188	194	155	151	166	163	105	90	
126	133	710	190	195	182	188	161	149	161	159	107	101	
128	135	721	193	194	180	187	171	146	160	158	108	98	
150	163	792	212	222	205	210	178	164	174	171	118	114	
117	121	780	177	192	169	177	154	140	147	147	100	97	
129	134	800	190	195	171	195	169	148	160	157	111	107	
135	151	835	206	209	186	202	184	158	171	166	118	111	
118	131	672	196	199	181	198	183	156	169	165	122	119	
133	145	675	205	212	194	211	192	165	175	170	125	121	
148	172	749	222	227	203	218	204	171	186	178	134	127	
127	134	707	200	208	189	203	183	156	168	165	120	115	
125	134	706	202	202	188	196	176	154	167	163	116	112	
125	140	733	213	206	199	208	194	167	177	173	130	143	
151	164	857	201	209	193	199	171	157	164	166	112	114	

19	20	21	22	23	24	25	26	27	28	29	30
		REGENERATIVELY COOLED CHAMBER BACKWALL TEMPERATURES									
T8 (F) TOP	T9 (F)	T10 (F)	T11 (F)	T12 (F) TOP	T13 (F)	T14 (F) TOP	T15 (F)	T16 (F) TOP	T17 (F)		
189	195	183	188	150	150	159	159	103	100		
203	213	198	206	169	162	175	172	119	117		
197	205	191	195	162	156	164	165	111	109		
203	208	196	202	165	158	167	168	111	109		
206	213	199	206	170	161	170	171	113	111		
197	200	194	210	177	165	183	175	125	127		
198	202	197	212	177	165	180	175	125	126		
200	204	198	212	177	164	178	174	124	125		
197	199	215	204	170	176	171	183	116	123		
200	203	198	207	173	161	173	172	119	118		
201	204	198	210	172	161	172	171	115	115		
194	196	191	198	163	153	163	164	108	107		
196	203	188	194	155	151	166	163	105	90		
190	195	182	188	161	149	161	159	107	101		
193	194	180	187	171	146	160	158	108	98		
212	222	205	210	178	164	174	171	118	114		
177	192	169	177	154	140	147	147	100	97		
190	195	171	195	169	148	160	157	111	107		
206	209	186	202	184	158	171	166	118	111		
196	199	181	198	183	156	169	165	122	119		
205	212	194	211	192	165	175	170	125	121		
222	227	203	218	204	171	186	178	134	127		
200	208	189	203	183	156	168	165	120	115		
202	202	188	196	176	154	167	163	116	112		
213	206	199	208	194	167	177	173	130	143		
201	209	193	198	171	157	164	166	112	114		

PROJECT OF SHEET

ROCKETDYNE
A DIVISION OF NORTH AMERICAN AVIATION, INC.

CALCULATED BY
CHECKED
DATE

FOUR BRAVE

	1	2	3	4	5	6	7	8	9	10	11	12	13
		WSTF TEST NO.	NOMINAL DUR, SECONDS	$P_{C'}$ PSIA	MR O/F	$\dot{W}_e$ LB/SEC	OUTLET TPB-1 F	OUTLET TPB-2 F	OUTLET TPB-3 F	INLET TPB-5 F	ΔT_1 F	ΔT_2 F	ΔT_3 F
1	NTO/MMH	- NO BLC											
2		2-1-1A	2.1	121.2	1.54	7.44	151	148	162	40	117	108	12
3		2-1-2	6.1	121.4	1.48	7.50	190	189	196	41	149	147	15
4		2-1-3	6.1	124.5	1.50	7.59	193	192	199	43	150	149	15
5		2-1-1	6.1	118.9	1.54	7.91	180	179	183	41	139	137	14
6		2-2-2	6.1	110.3	1.63	6.39	206	203	209	46	160	157	16
7		2-2-3	6.1	124.1	1.51	7.51	203	200	200	47	156	153	15
8		2-2-4	6.1	124.5	1.61	7.25	210	208	208	47	164	161	16
9		2-2-5	6.1	124.1	1.71	6.96	215	209	214	44	171	165	16
10		2-2-6	6.6	138.5	1.61	8.05	207	202	202	43	164	159	15
11	NTO/MMH	UNSATURATED											
12		2-3-1	10.0	124.4	1.61	7.08	197	195	193	74	123	121	11
13		2-3-2	7.0	138.9	1.80	7.54	209	211	206	75	135	136	13
14		2-3-3	7.0	139.3	1.61	8.09	199	201	198	75	124	126	12
15		2-3-4	7.0	128.9	1.42	8.74	189	189	185	75	113	113	11
16		2-3-5	7.0	124.7	1.70	7.03	209	212	211	75	134	136	13
17		2-3-6	7.0	124.2	1.81	6.73	220	222	222	75	145	146	14
18		2-3-7	7.0	124.6	1.61	7.54	197	200	195	75	122	124	12
19		2-3-8	7.0	124.0	1.41	7.86	190	193	188	75	115	118	11
20		2-3-9	7.0	109.6	1.80	6.00	210	227	217	75	144	152	14
21		2-3-10	7.0	108.9	1.41	6.94	192	197	190	75	117	122	11
22		2-3-11	7.0	109.4	1.62	6.39	207	214	204	75	132	139	13
23		2-3-12	7.0	123.0	1.61	7.25	203	208	200	75	128	133	12
24	NTO/MMH	SATURATED											
25		2-4-1	10.0	122.8	1.61	7.25	206	207	204	84	122	123	12
26		2-4-2	7.0	138.8	1.80	7.62	219	220	217	84	134	136	13
27		2-4-3	7.0	126.7	1.61	8.07	200	210	207	84	125	126	12
28		2-4-4	7.0	128.1	1.42	8.76	196	197	193	84	112	113	11
29		2-4-5	7.0	124.0	1.80	6.77	223	225	221	84	139	141	13
30		2-4-6	7.0	123.7	1.42	7.86	198	202	196	84	114	118	11
31		2-4-7	7.0	108.8	1.79	6.09	228	233	224	84	143	148	14
32		2-4-8	7.0	108.8	1.43	6.92	202	207	199	84	118	123	11
33		2-4-9	7.0	109.1	1.63	6.37	217	221	213	84	133	137	12
34		2-4-10	7.0	123.1	1.61	7.24	211	214	208	84	127	130	12
35													

DEMONSTRATOR THRUST CHAMBER THERMAL DATA (cont'd)

14	15	16	17	18	19	20	21	22	23	24	25	26	27
$\overline{\Delta T}_1$ F	ΔQ BTU/SEC	T_8 F	T_9 F	T_{10} F	T_{11} F	T_{12} F	T_{13} F	T_{14} F	T_{15} F	T_{16} F	T_{17} F		
116	610	126	125	117	133	93	88	113	112	56	56		
150	800	180	192	173	186	141	136	146	146	92	90		
152	817	182	194	173	191	144	136	148	146	93	92		
139	781	167	186	165	185	132	130	138	137	82	82		
160	725	201	222	185	250	158	146	158	153	102	100		
155	824	189	202	176	217	150	140	149	146	96	94		
162	832	197	203	182	227	156	144	153	150	99	97		
168	832	205	215	184	236	160	146	156	152	100	99		
161	920	191	200	174	229	151	139	148	145	4	2		
121	608	201	201	190	201	166	158	165	160	116	112		
134	718	206	212	198	206	170	165	168	165	118	116		
124	712	199	201	190	198	165	160	162	159	115	113		
112	696	190	187	179	198	157	151	155	152	110	107		
135	676	209	209	198	203	173	166	168	165	120	117		
146	699	216	217	206	210	180	172	173	169	123	120		
122	654	199	197	188	195	164	158	162	160	115	113		
115	641	192	191	182	189	157	153	158	156	112	110		
145	629	218	220	210	216	180	174	174	170	124	122		
118	583	195	190	186	191	160	156	160	158	114	112		
133	605	206	206	198	203	168	165	167	165	119	117		
129	663	203	203	193	198	168	162	165	162	116	115		
121	625	208	208	198	204	174	169	167	169	120	119		
134	718	224	217	209	218	185	178	174	174	127	125		
124	712	209	206	197	205	173	168	167	167	122	120		
111	692	197	193	186	193	163	159	160	160	116	115		
139	668	221	218	210	217	185	179	174	174	127	126		
114	640	200	196	190	195	166	161	162	163	119	116		
144	612	223	224	216	219	187	182	175	177	129	127		
119	583	203	200	195	197	169	164	164	166	119	117		
133	601	216	213	206	209	178	174	172	172	123	120		
127	654	212	208	200	205	177	170	169	171	123	122		

FOLDOUT FRAME 2

19	20	21	22	23	24	25	26	27	28	29	30
T_{11} F	T_{12} F	T_{13} F	T_{14} F	T_{15} F	T_{16} F	T_{17} F					
133	93	88	113	112	56	56					
186	141	136	146	146	92	90					
191	144	136	148	146	93	92					
185	132	130	138	137	82	82					
250	158	146	158	153	102	100					
217	150	140	149	146	96	94					
227	156	144	153	150	99	97					
236	160	146	156	152	100	99					
229	151	139	148	145	4	2					
201	166	158	165	160	116	112					
206	170	165	168	165	118	116					
198	165	160	162	159	115	113					
198	157	151	155	152	110	107					
203	173	166	168	165	120	117					
210	180	172	173	169	123	120					
195	164	158	162	160	115	113					
189	157	153	158	156	112	110					
216	180	174	174	170	124	122					
191	160	156	160	158	114	112					
203	168	165	167	165	119	117					
198	168	162	165	162	116	115					
204	174	169	167	169	120	119					
218	185	178	174	174	127	125					
205	173	168	167	167	122	120					
193	163	159	160	160	116	115					
217	185	179	174	174	127	126					
195	166	161	162	163	119	116					
219	187	182	175	177	129	127					
197	169	164	164	166	119	117					
209	178	174	172	172	123	120					
205	177	170	169	171	123	122					

PROJECT OF SHEET

ROCKETDYNE
A DIVISION OF NORTH AMERICAN AVIATION, INC.

CALCULATED BY
CHECKED
DATE

TABLE 8. D

	1	2	3	4	5	6	7	8	9	10	11	12	13
		WSTF TEST NO.	NOMINAL DUR, SECONDS	$P_{C'}$ PSIA	MR O/F	$\dot{W}_c$ LB/SEC	OUTLET TFB-1 F	OUTLET TFB-2 F	OUTLET TFB-3 F	INLET TFB-5 F	ΔT_1 F	ΔT_2 F	ΔT_3 F
1	NTO/MMH	SATURATED (CONTINUED)											
2		2-9-1	10.0	164.6	1.69	9.30	191	189	195	64	127	114	13
3		2-9-2	7.0	174.0	1.66	9.90	184	187	181	58	125	128	12
4		2-9-3	7.0	177.7	1.73	9.79	190	192	187	59	130	133	12
5		2-9-4	7.0	174.7	1.87	9.16	201	200	196	58	143	142	13
6		2-9-5	7.0	174.7	1.77	9.51	194	195	189	57	137	138	13
7		2-9-6	7.0	174.9	1.67	9.86	188	189	183	57	131	132	12
8		2-9-7	7.0	126.3	1.69	7.17	194	195	190	57	137	138	13
9		2-9-8	7.0	100.8	1.741	5.66	203	206	199	58	145	149	14
10		2-9-9	7.0	100.1	1.67	5.78	197	203	194	58	139	145	13
11		2-9-10	7.0	100.1	1.49	6.19	184	186	181	58	126	129	12
12		2-9-11	10.0	124.3	1.69	7.10	192	199	189	57	135	142	13
13	NTO/50-50	SATURATED											
14		2-5-1	10.0	173.5	1.65	9.88	186	188	181	52	133	135	12
15		2-5-2	7.0	178.5	1.69	9.95	191	189	186	55	136	134	13
16		2-5-3	7.0	175.3	1.74	9.59	194	195	189	54	140	141	13
17		2-5-4	7.0	174.7	1.84	9.26	201	203	196	53	148	150	14
18		2-5-5	7.0	175.4	1.65	9.90	190	191	184	53	137	138	13
19		2-5-6	7.0	142.1	1.66	8.06	195	196	189	53	142	143	13
20		2-5-7	7.0	141.1	1.86	7.50	208	208	202	53	155	155	14
21		2-5-8	7.0	141.8	1.48	8.65	180	185	177	53	127	132	12
22		2-5-9	7.0	126.3	1.69	7.15	198	204	194	53	145	151	14
23		2-5-10	7.0	126.8	1.48	7.75	183	188	180	53	130	135	12
24		2-5-11	7.0	125.9	1.88	6.69	210	218	205	53	157	165	15
25		2-5-12	7.0	101.0	1.79	5.58	214	224	206	53	161	171	15
26		2-5-13	7.0	101.0	1.49	6.21	191	203	186	53	138	150	13
27		2-5-14	7.0	100.5	1.68	5.76	203	216	198	53	150	163	14
28		2-5-15	7.0	125.5	1.68	7.12	197	207	193	53	144	154	14
29		2-5-15	10.0	124.9	1.68	7.10	198	210	194	53	145	157	14
30		2-5-15	15.0	124.1	1.69	7.06	201	212	1.96	53	148	159	1
31		2-5-15	30.0	122.4	1.70	6.96	205	216	206	52	153	164	1
32													
33													
34													
35													

FOLDOUT FRAME /

ATOR THRUST CHAMBER THERMAL DATA (cont'd)

14	15	16	17	18	19	20	21	22	23	24	25	26	27
ΣT_1 F	ΔQ BTU/SEC	T_8 F	T_9 F	T_{10} F	T_{11} F	T_{12} F	T_{13} F	T_{14} F	T_{15} F	T_{16} F	T_{17} F		
124	818	195	189	179	190	160	152	156	154	105	106		
125	881	196	185	176	190	159	146	152	150	100	101		
131	907	204	189	181	201	164	149	15[illegible]	152	104	102		
141	916	214	195	190	209	172	157	158	157	107	105		
136	916	209	170	183	201	165	151	155	153	105	101		
129	905	201	183	177	193	159	146	151	149	101	99		
136	677	198	193	186	192	160	153	158	158	105	105		
145	583	209	205	197	201	166	162	164	165	109	107		
140	574	203	201	193	196	162	158	161	161	107	105		
126	554	192	186	181	185	184	149	156	154	101	99		
136	687	198	193	186	192	160	153	159	158	105	105		
132	929	197	182	178	187	156	145	152	151	94	96		
134	947	208	183	183	197	163	147	154	153	98	99		
139	946	211	188	185	200	164	149	156	154	100	99		
147	966	218	194	193	209	169	152	160	158	102	101		
135	951	207	182	179	196	160	144	151	150	96	96		
140	803	205	189	185	195	161	149	156	156	100	97		
153	816	218	203	198	206	170	158	165	164	107	105		
128	785	186	173	170	174	147	140	148	148	92	91		
146	740	200	194	187	185	159	153	159	160	102	100		
131	724	186	175	169	172	149	144	149	151	94	93		
158	746	216	210	200	197	169	162	167	168	108	107		
162	641	214	214	207	187	168	165	165	167	96	94		
140	618	194	195	177	169	154	151	156	157	99	99		
152	623	203	207	196	179	161	159	162	164	102	100		
146	738	200	197	185	187	159	153	159	160	101	100		
148	745	201	198	185	181	159	153	160	160	102	101		
150	751	204	199	191	179	160	155	160	161	104	103		
157	774	210	201	195	178	163	156	161	161	104	104		

FOLDOUT FRAME 2

19 T_{11} F	20 T_{12} F	21 T_{13} F	22 T_{14} F	23 T_{15} F	24 T_{16} F	25 T_{17} F	26	27	28	29	30
190	160	152	156	154	105	106					
190	159	146	152	150	100	101					
201	164	149	153	152	104	102					
209	172	157	158	157	107	105					
201	165	151	155	153	105	101					
193	159	146	151	149	101	99					
192	160	153	158	158	105	105					
201	166	162	164	165	109	107					
196	162	158	161	161	107	105					
185	184	149	156	154	101	99					
192	160	153	159	158	105	105					
187	156	145	152	151	94	96					
197	163	147	154	153	98	99					
200	164	149	156	154	100	99					
209	169	152	160	158	102	101					
196	160	144	151	150	96	96					
195	161	149	156	156	100	97					
206	170	158	165	164	107	105					
174	147	140	148	148	92	91					
185	159	153	159	160	102	100					
172	149	144	149	151	94	93					
197	169	162	167	168	108	107					
187	168	165	165	167	96	94					
169	154	151	156	157	99	99					
179	161	159	162	164	102	100					
187	159	153	159	160	101	100					
181	159	153	160	160	102	101					
179	160	155	160	161	104	103					
178	163	156	161	161	104	104					

PROJECT OF
SHEET

ROCKETDYNE
A DIVISION OF NORTH AMERICAN AVIATION, INC.

CALCULATED BY
CHECKED
DATE

FOLDOUT FRAME 3

FIGURE 35

COOLANT OUTLET BULK TEMPERATURE RESPONSE FOR THE OME THRUST CHAMBER

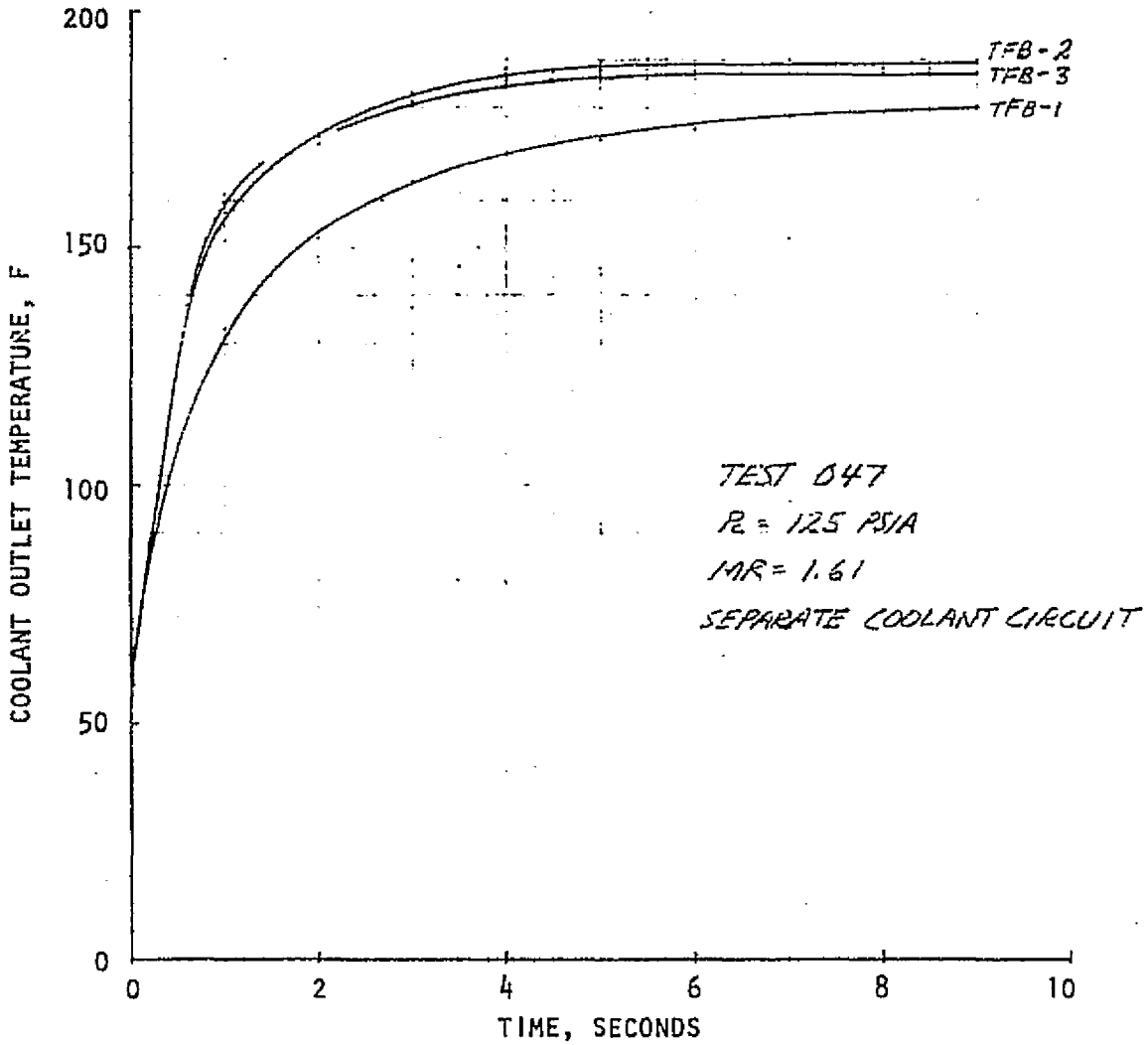

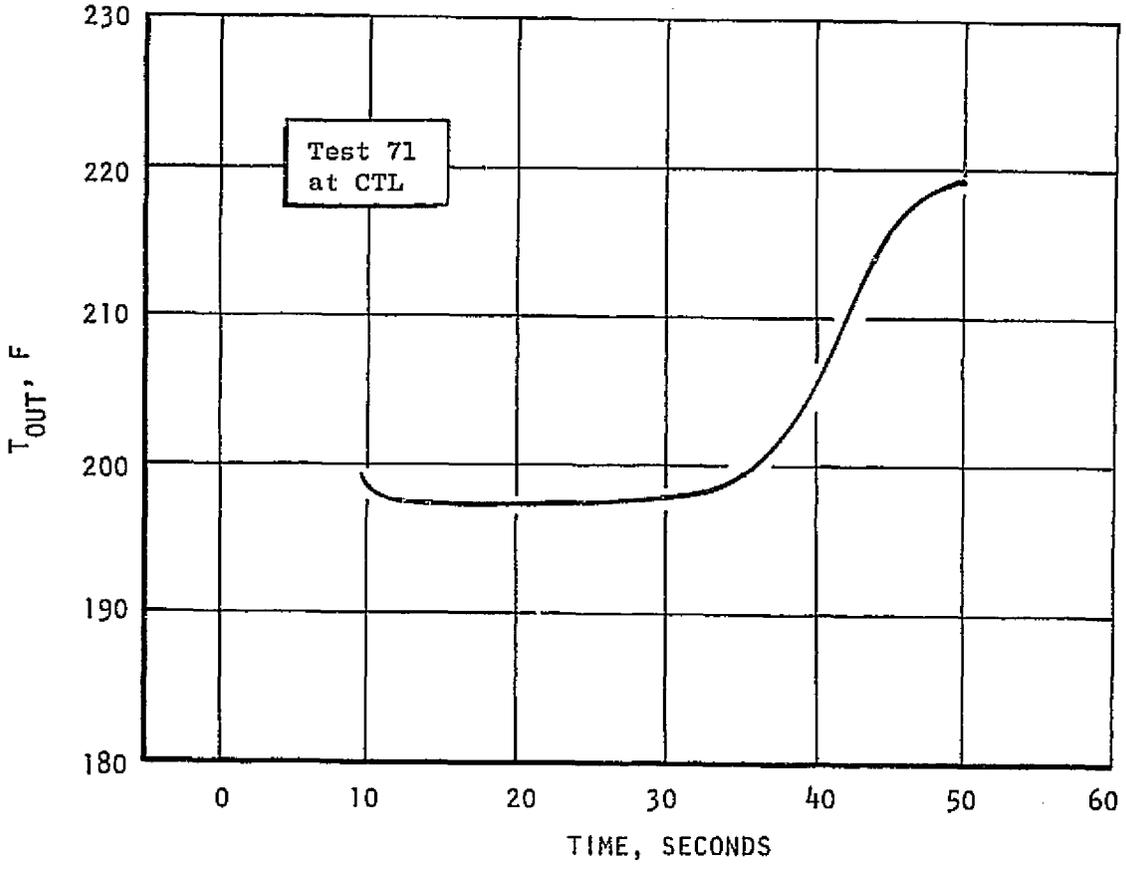

Figure 36. Coolant Outlet Bulk Temperature

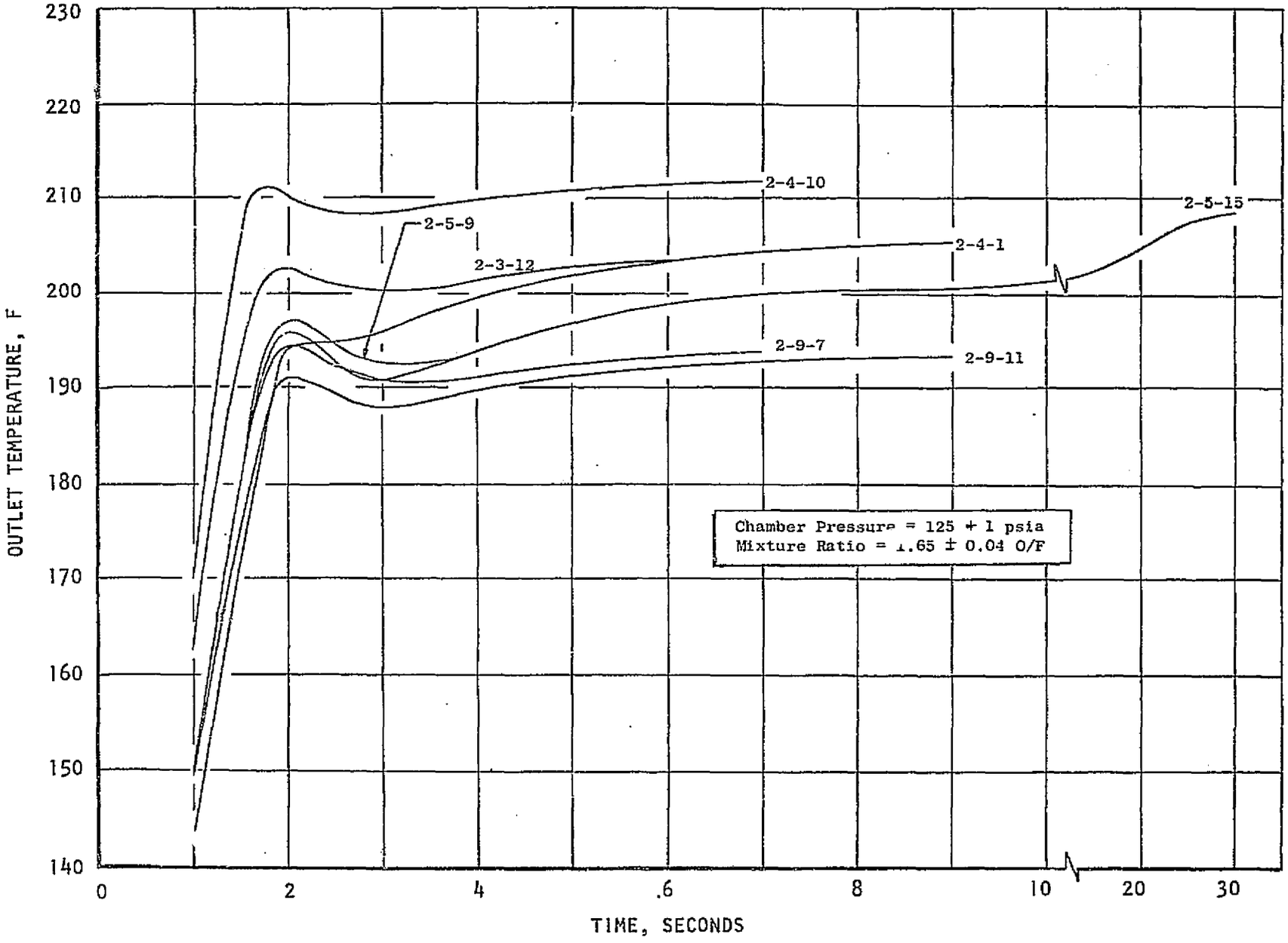

Figure 37. Outlet Bulk Temperature Transient at WSTF

6 seconds. One test was of 30-seconds duration. The temperature transient for this test, also plotted in Fig. 37, indicates a similar transient for the first 7-10 seconds; but subsequently, this temperature continues to rise gradually, so that the heat load measured at 7 seconds is approximately 4 percent less than the heat load at 30 seconds. Thus, the heat loads reported based on WSTF data may be four to five percent below the steady state value. A significant part of the transient at both facilities may be due to the massive exit manifold which would not be present on the flight chamber. A flight type exit manifold is incorporated into the integrated chamber, which is to be tested soon.

The average values of the ΔT's were multiplied by the fuel flowrate through the jacket and the specific heat of the fuel to determine the heat absorbed by the fuel. In Fig. 38 the heat loads are plotted versus chamber pressure for the bypass cooled tests at CTL-IV with coded symbols to denote mixture ratio ranges. These data follow the predicted variation with P_c to the 0.8 power. However, the measured absolute values of the heat load were approximately 10 percent lower than the predicted values which were based on heat sink chamber test data. The effect of mixture ratio could not be distinguished except at the lowest mixture ratio conditions (o/f = 1.4 - 1.44).

The similar plot is presented in Fig. 39 of the regeneratively cooled test data. Both the predicted and experimental values are higher for this case because of the reduced effectiveness of the heated boundary layer coolant. The experimental data in this case was 15 percent to 20 percent lower than the predicted heat loads. The ranges shown represent the three bulk temperature rise measurements made for each test. In spite of the increased data scatter, a more definitive trend of heat load with mixture ratio can be detected in the results of the regeneratively cooled tests.

The heat load versus chamber pressure measured at WSTF for NTO/MMH propellants is shown in Fig. 40. No effect on heat load results from saturating the propellants. The mixture ratio trends are generally in the same direction,

C-2

FIGURE 38

CME CHAMBER INTEGRATED HEAT LOAD
SEPARATE COOLANT CIRCUIT

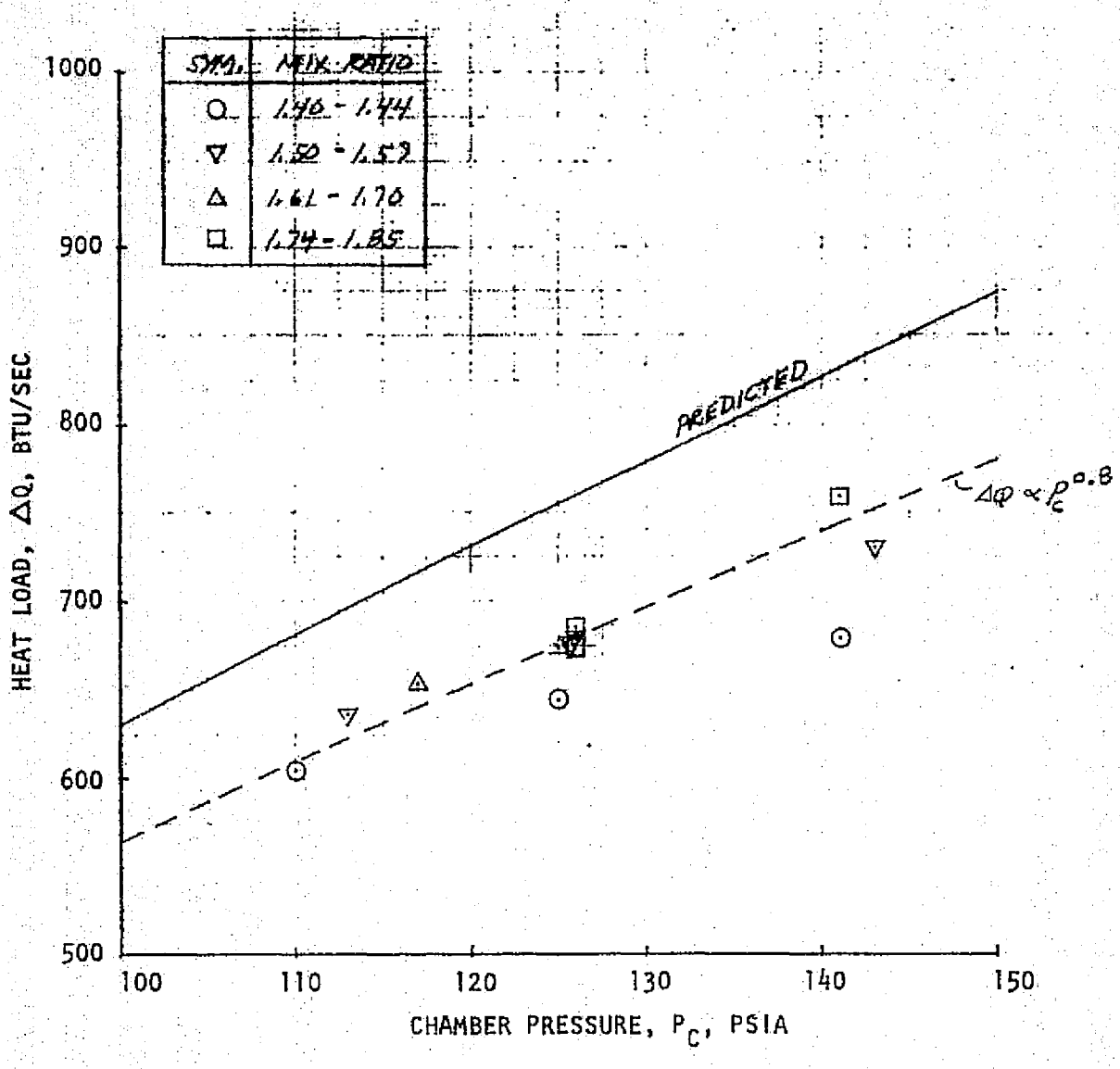

FIGURE 39

OME CHAMBER INTEGRATED HEAT LOAD REGENERATIVE COOLANT CIRCUIT

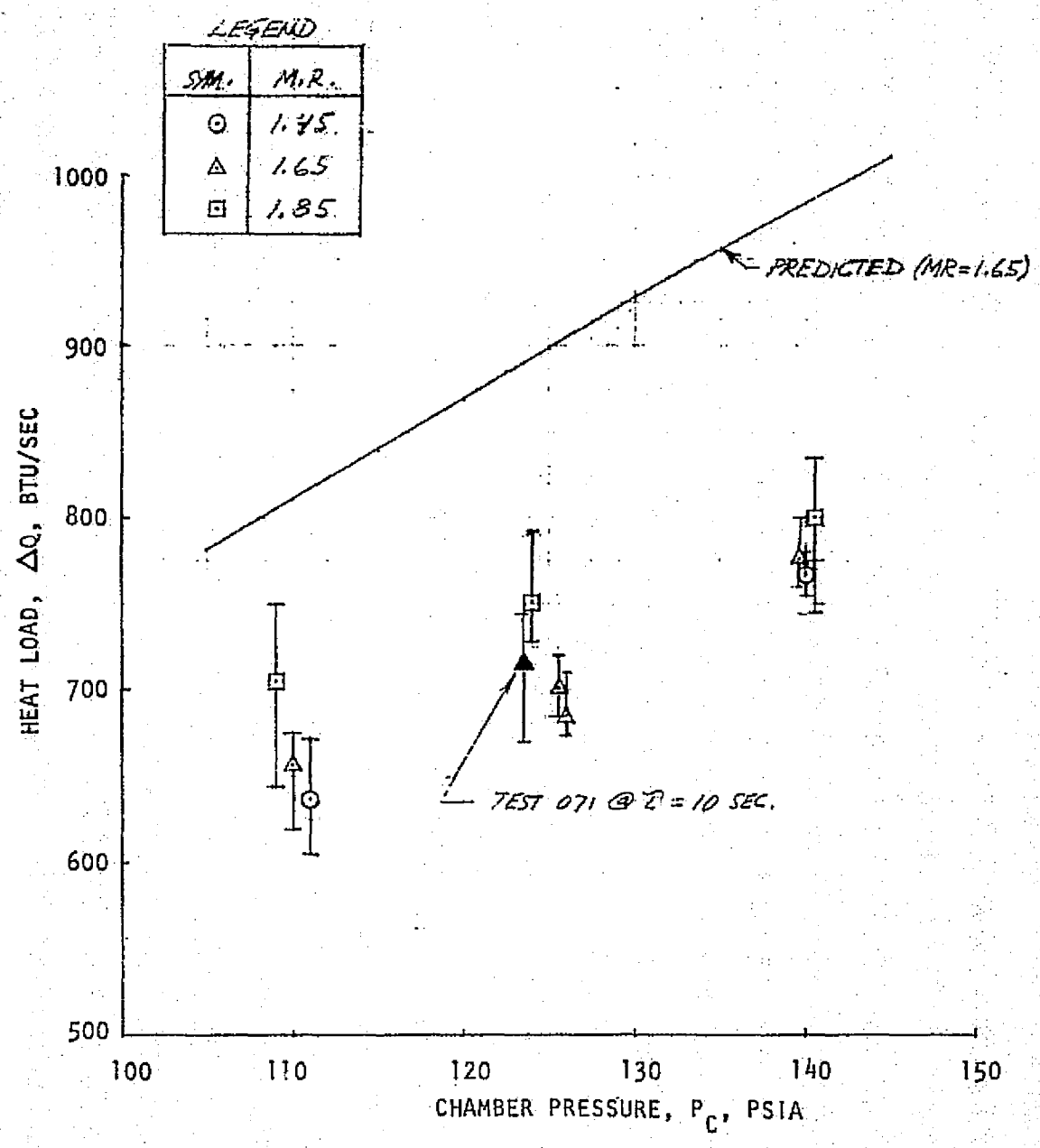

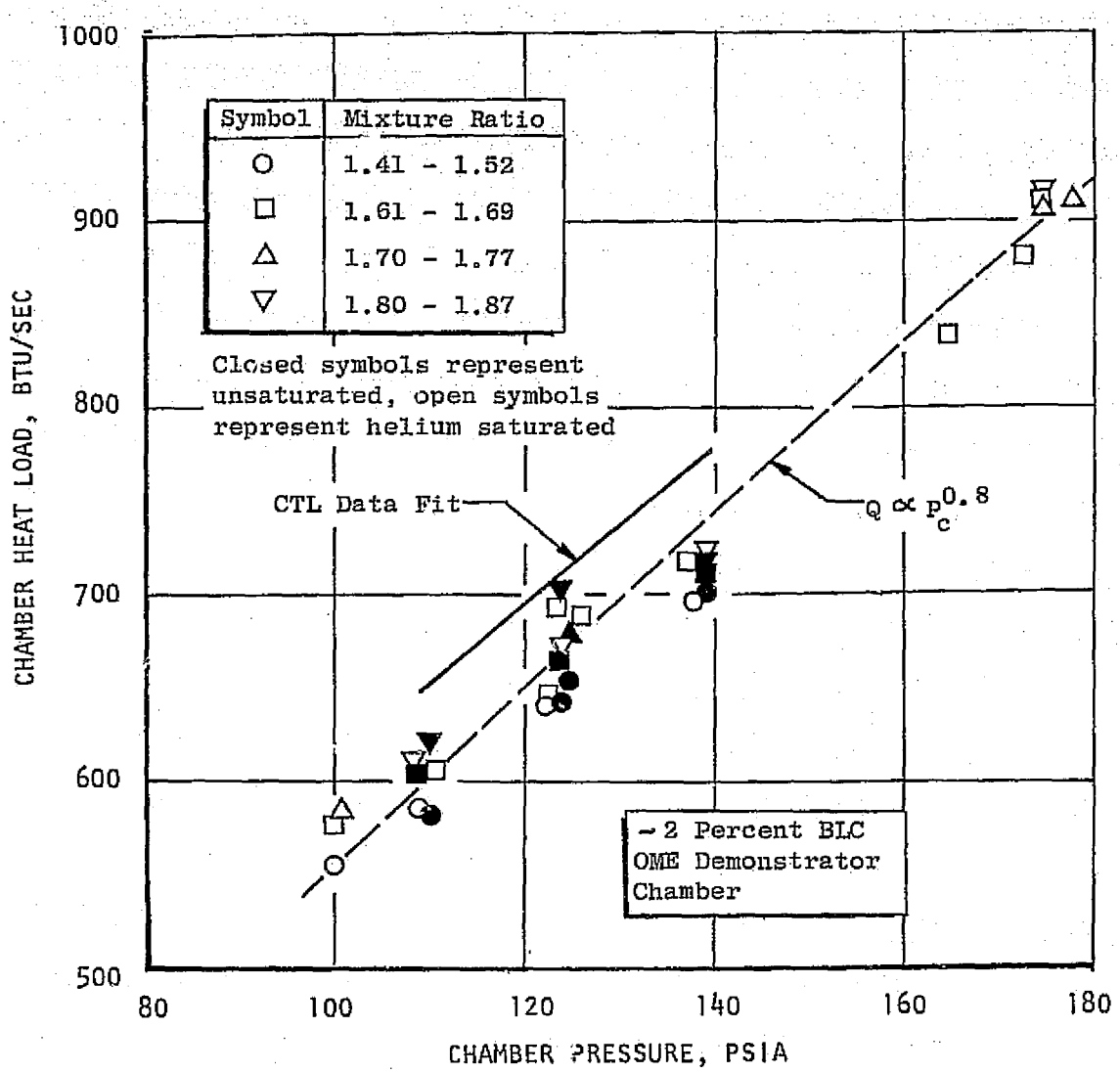

Figure 40. Heat Load Variation With Chamber Pressure for NTO/MMH at WSTF

although less pronounced, than the data taken at CTL-IV. The mixture ratio trend does not appear quite as clear at the nominal chamber pressure as at other points. However, it should be noticed that the entire data spread at nominal chamber pressure is approximately plus or minus 5 percent, which may obscure any trends due to mixture ratio. The data indicates that the heat load is proportional to the 0.8 power of chamber pressure, as predicted. The best fit curve through the CTL-IV data is also plotted in Fig. 40. The CTL-IV curve is approximately 5 percent higher than the WSTF curve, which is within the scatter of the data at both facilities. The first tests of each series seem to be particularly slow in responding and gave data which were lower than that of comparable tests later in the series. For this reason, data from first tests are not included in the plots.

Data from the test series conducted without auxiliary film coolant are plotted in Fig. 41. A line following the 0.8 power of Pc is passed through the nominal data points and shows fairly good agreement with the limited amount of data. The trend of increasing heat load and increasing mixture ratio is present, but barely perceptive, as analytically predicted. The curve from the data of Fig. 40 (with film coolant) is reproduced here and indicates that the inclusion of approximately 2 percent film coolant reduces the heat load by 20 percent, which is also in agreement with the theoretical prediction.

The heat load measured at WSTF with the NTO/50-50 propellant combination is shown in Fig. 42. The data again follows the 0.8 power of P_c relationship. The slight dependence of heat load on mixture ratio is seen with this propellant combination as it was also with NTO/MMH. The data implies an increase of approximately 6 percent in heat load with 50-50 as compared to MMH.

The heat load curves for all conditions are summarized in Fig. 43. Table 9 lists experimental safety factors. No useful thermal data were obtained with L/D #2 injector because of the brief duration of some of the tests and the facility and engine leakage which occurred on the longer tests.

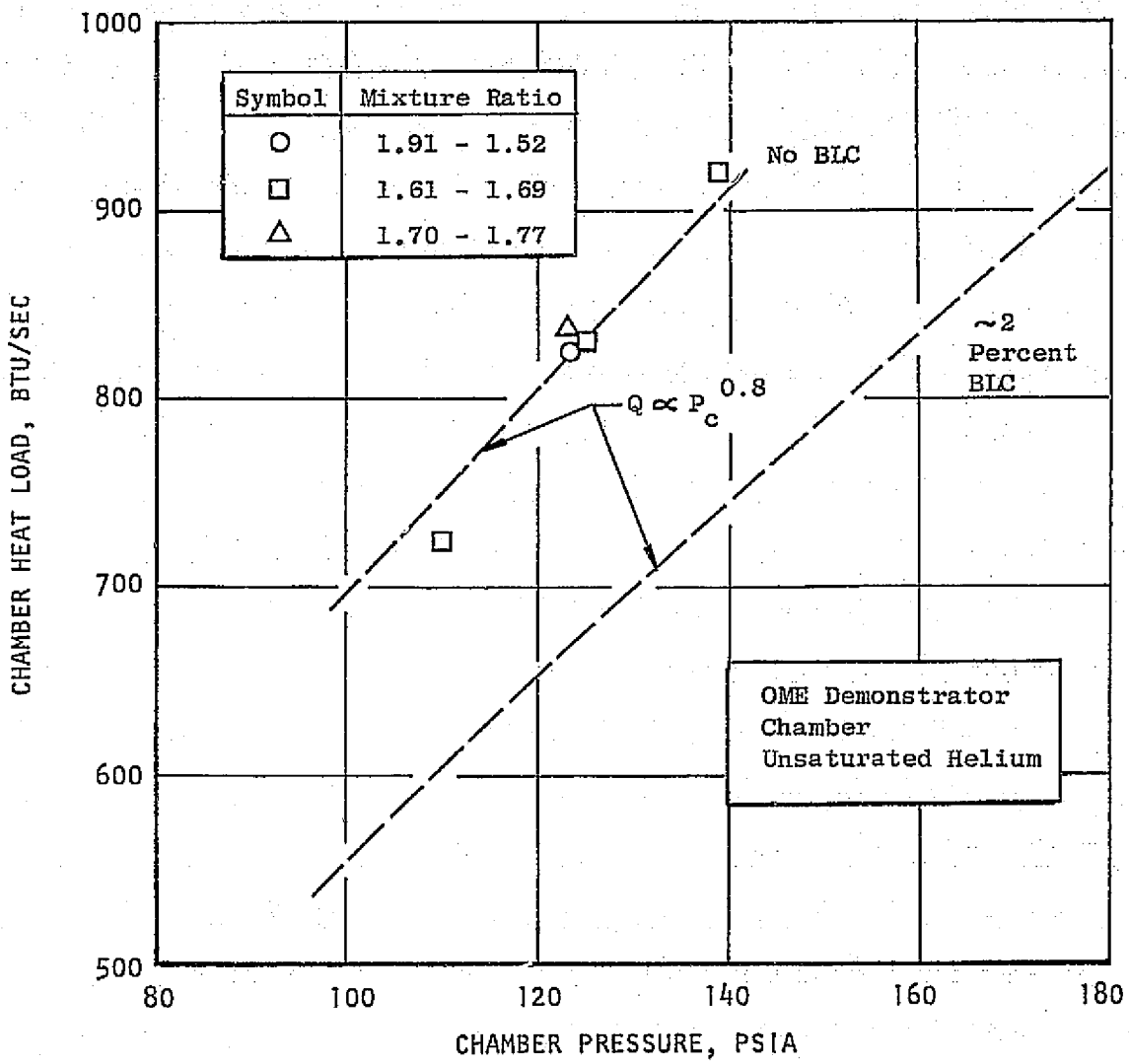

Figure 41. Effect of Film Coolant on Heat Load

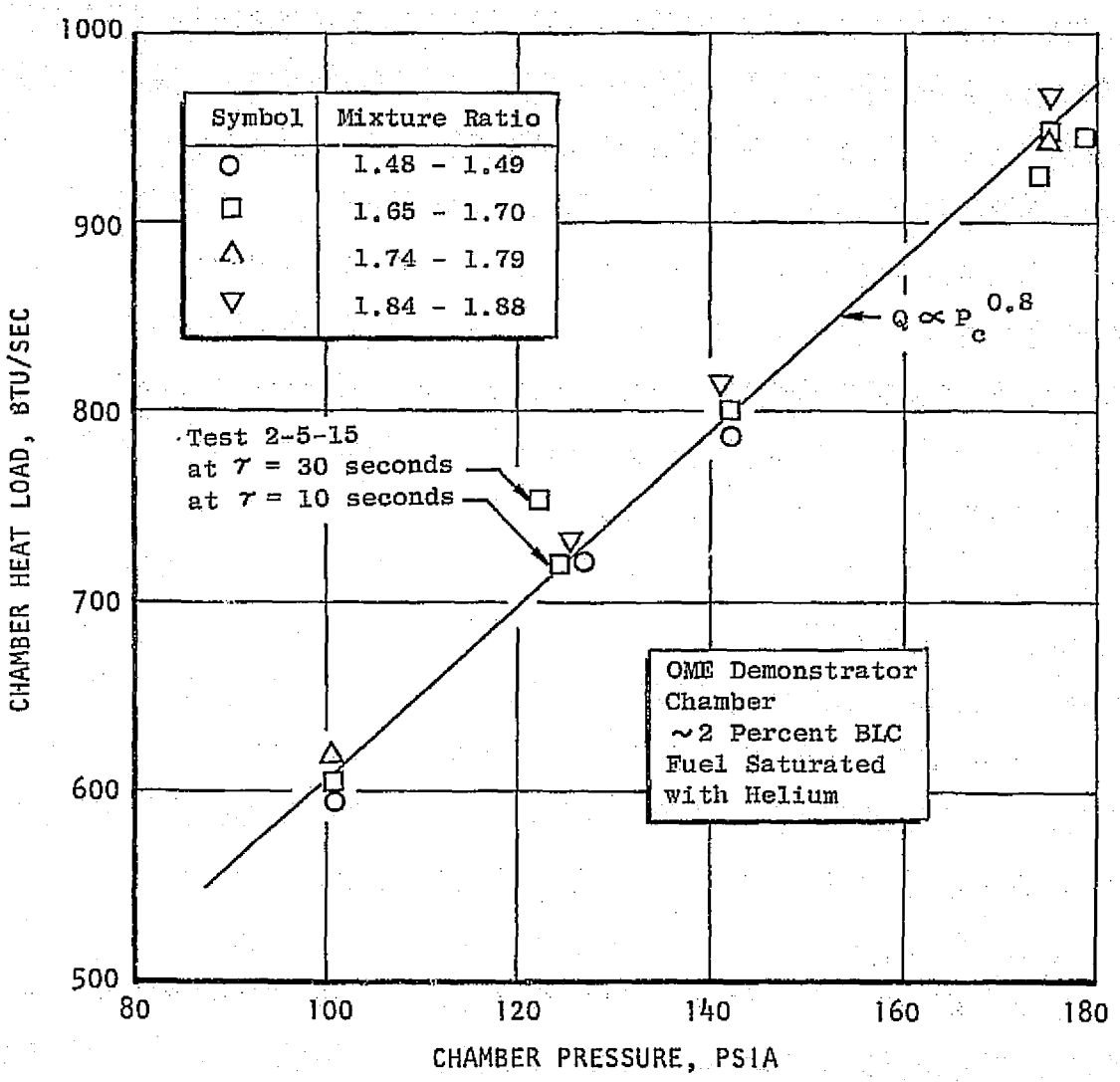

Figure 42. Heat Load Variation With Chamber Pressure for NTO/50-50

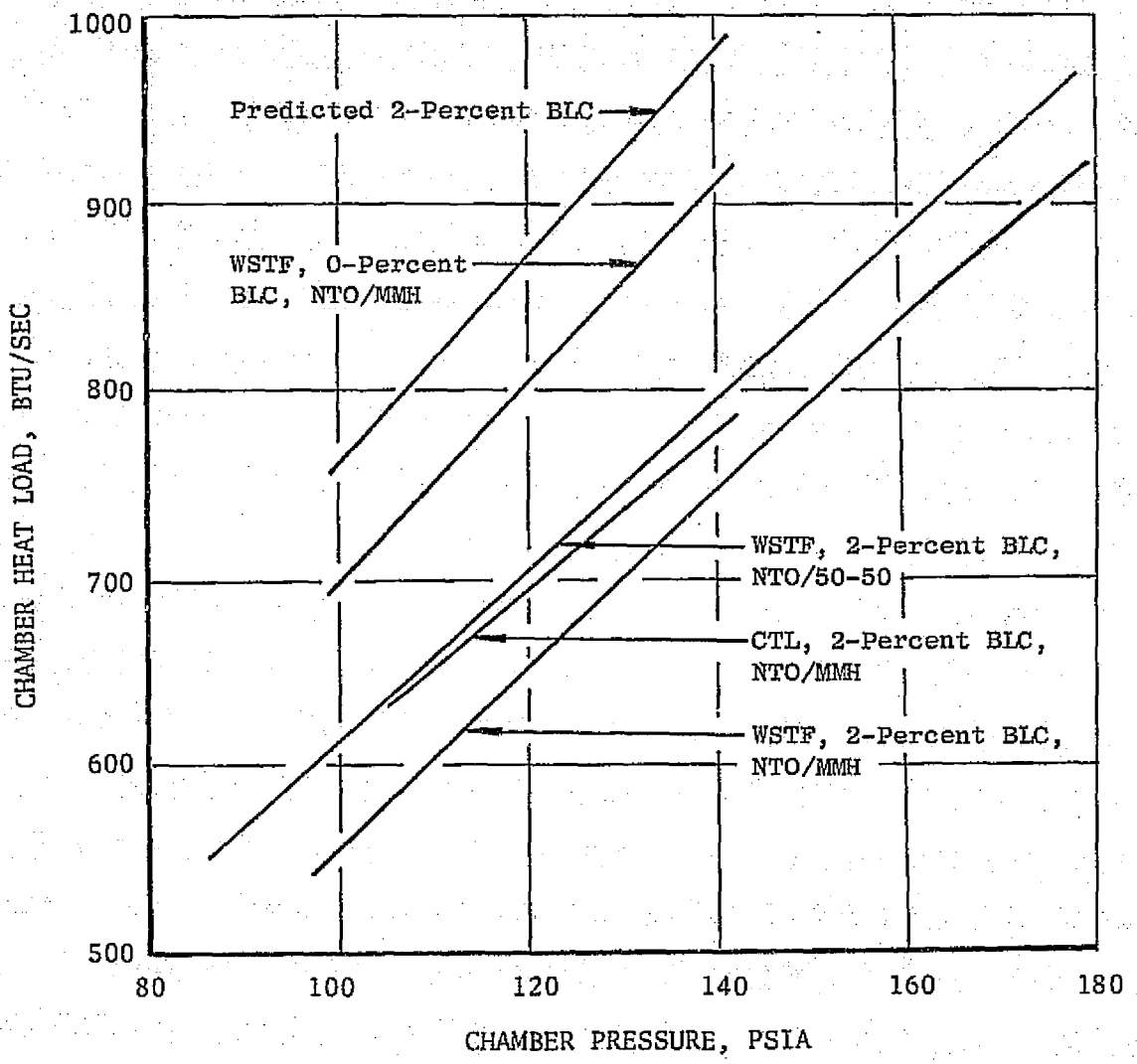

Figure 43. Summary of Demonstrator Heat Load Data

Table 9. Thermal Safety Factors Based on Experimental Data

Propellant	Safety Factor (1-D) Nominal	Off-Design**
NTO/MMH with 2% BLC	3.5	2.8
NTO/MMH with no BLC	2.0	1.4
NTO/50-50 with 2% BLC	3.0	2.2

* P_c = 125 psia; $T_{bulk\ in}$ = 70F; o/f = 1.65 (MMH), 1.60 (50-50); Fuel Injector ΔP = 45 psi

** P_c = 120 psia; $T_{bulk\ in}$ = 100F; o/f = 1.84 (MMH), 1.79 (50-50); Fuel Injector ΔP = 36 psi

Back Wall Temperatures

Back wall temperatures were measured on the thrust chamber to indicate steady state values during operation and also values at the start of each test. Steady state values are significant in that the OME is required to operate at maximum back wall temperature of less than 600F. The starting temperature of the back wall indicated values to which the back wall could be safely heated by soakback or other external heat inputs prior to start.

Backwall temperatures for a start from ambient conditions; i.e., the first test series, are shown in Fig. 44 and 45 for typical tests conducted at CTL-IV and WSTF, respectively. As would be expected, the response is more rapid in the higher heat flux regions. The throat responds in about 3 sec; the injector end in about 5 sec; and the nozzle region in about 8 sec. The multiple curves for each region indicate data taken at the various circumferential locations. Back wall temperatures on a hot start test at CTL-IV are shown in Fig. 46. Circumferential variations in the initial temperatures of over 50 degrees were sometimes noted as a result of the horizontal orientation of the engine, variations in soakback, and possibly local blowback in the altitude cell. The injector end, typically, experienced the hot-test prestart temperatures. On the most extreme case, the starting temperature was over 400F. No abnormalities were exhibited during the start transient on these tests.

Typical hot start back wall temperature transients recorded at WSTF are shown in Fig. 47. Hot start transients generally did not exhibit as high a starting temperature at the injector end as was recorded at CTL-IV. This is probably due to the differences in procedures between tests at the two facilities. At WSTF the engine was purged between tests. The ability of the thrust chamber to start without purges between firings was demonstrated at CTL-IV by purging only after a test series was completed. Heat from soakback and blowback resulted in high temperatures after shutdown on these tests.

FIGURE 44

BACK WALL TEMPERATURE RESPONSE FOR
THE OME THRUST CHAMBER

COLD START

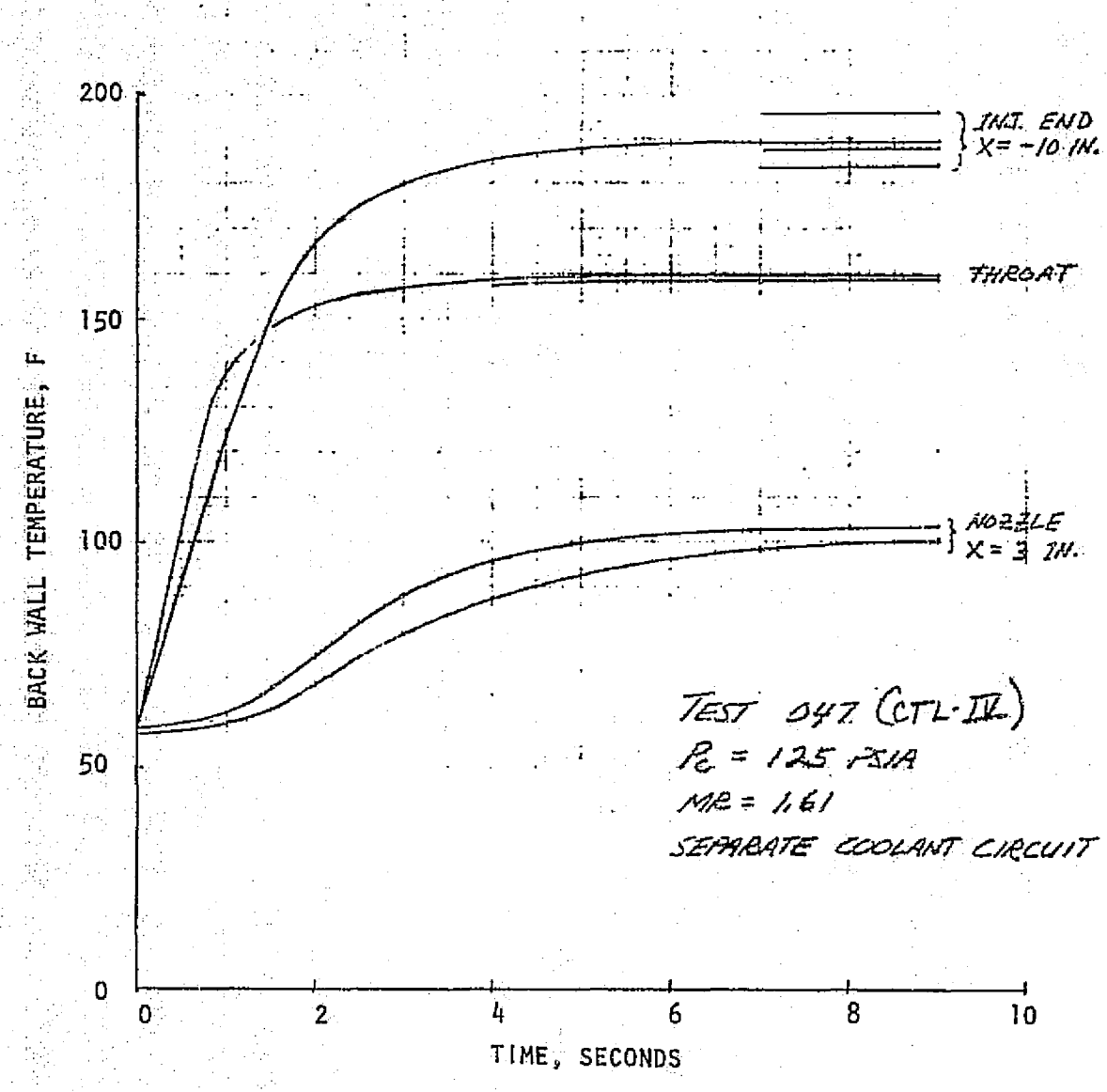

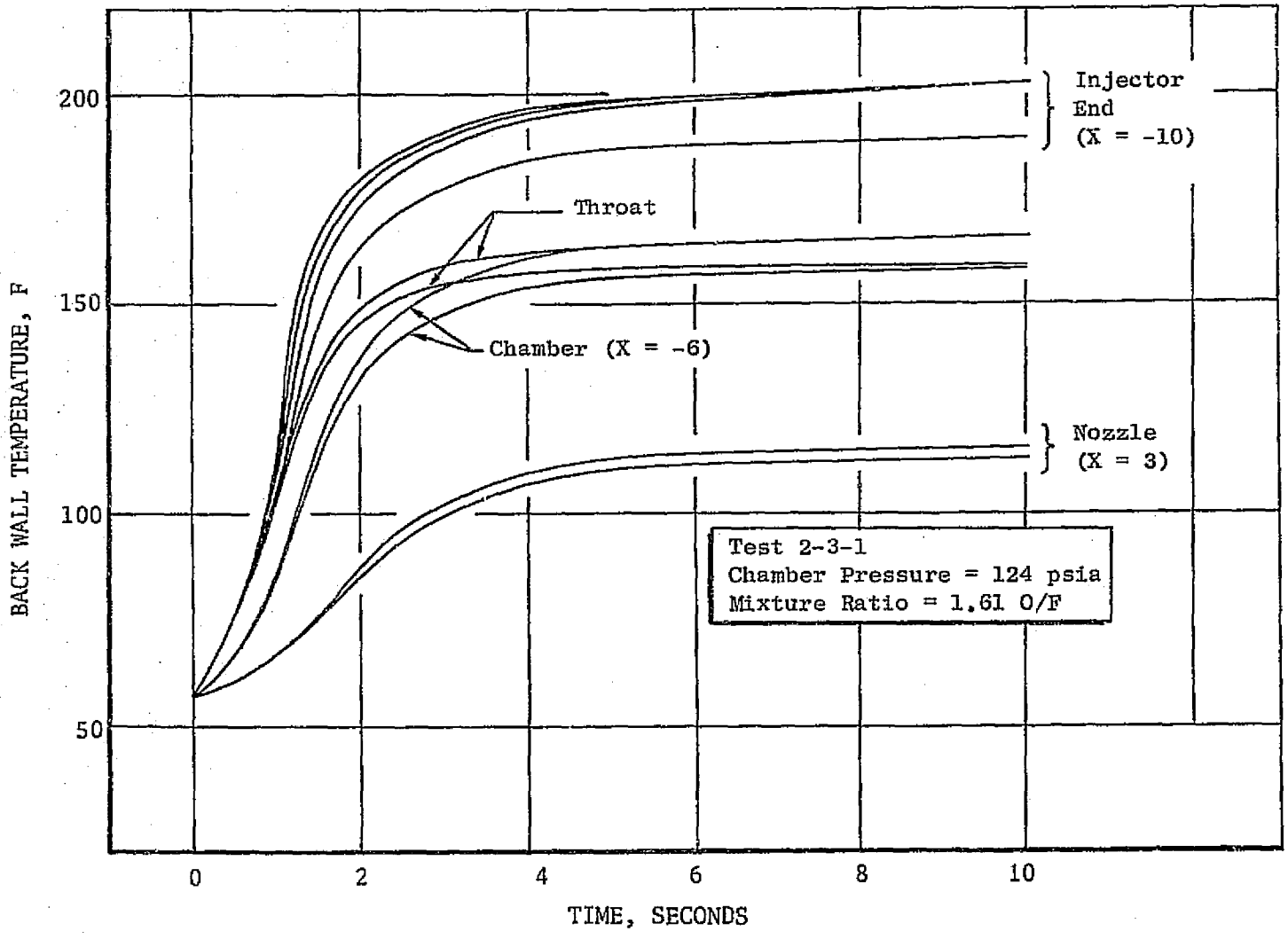

Figure 45. Typical Cold Start Transients at WSTF

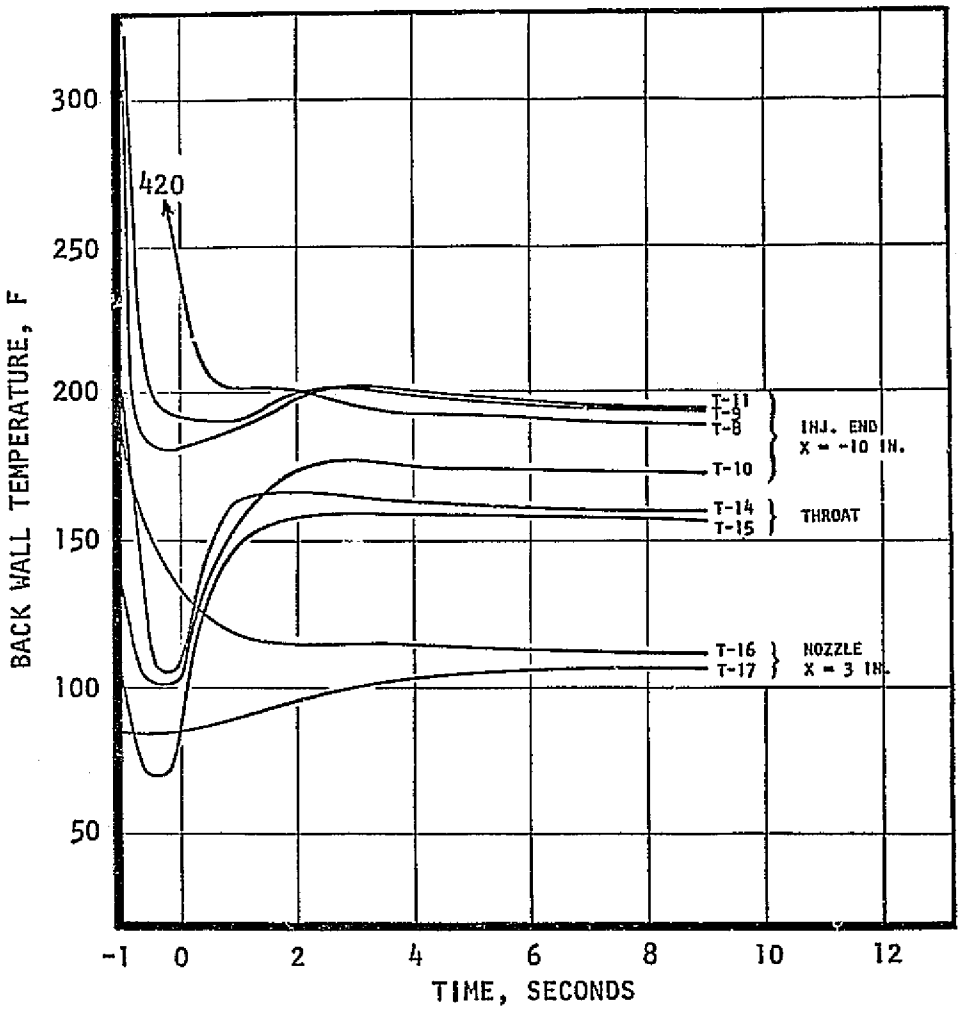

HOT START
TEST 66 (CTL-IV)

Figure 46. Regeneratively Cooled T/C Backwall Temperature Response

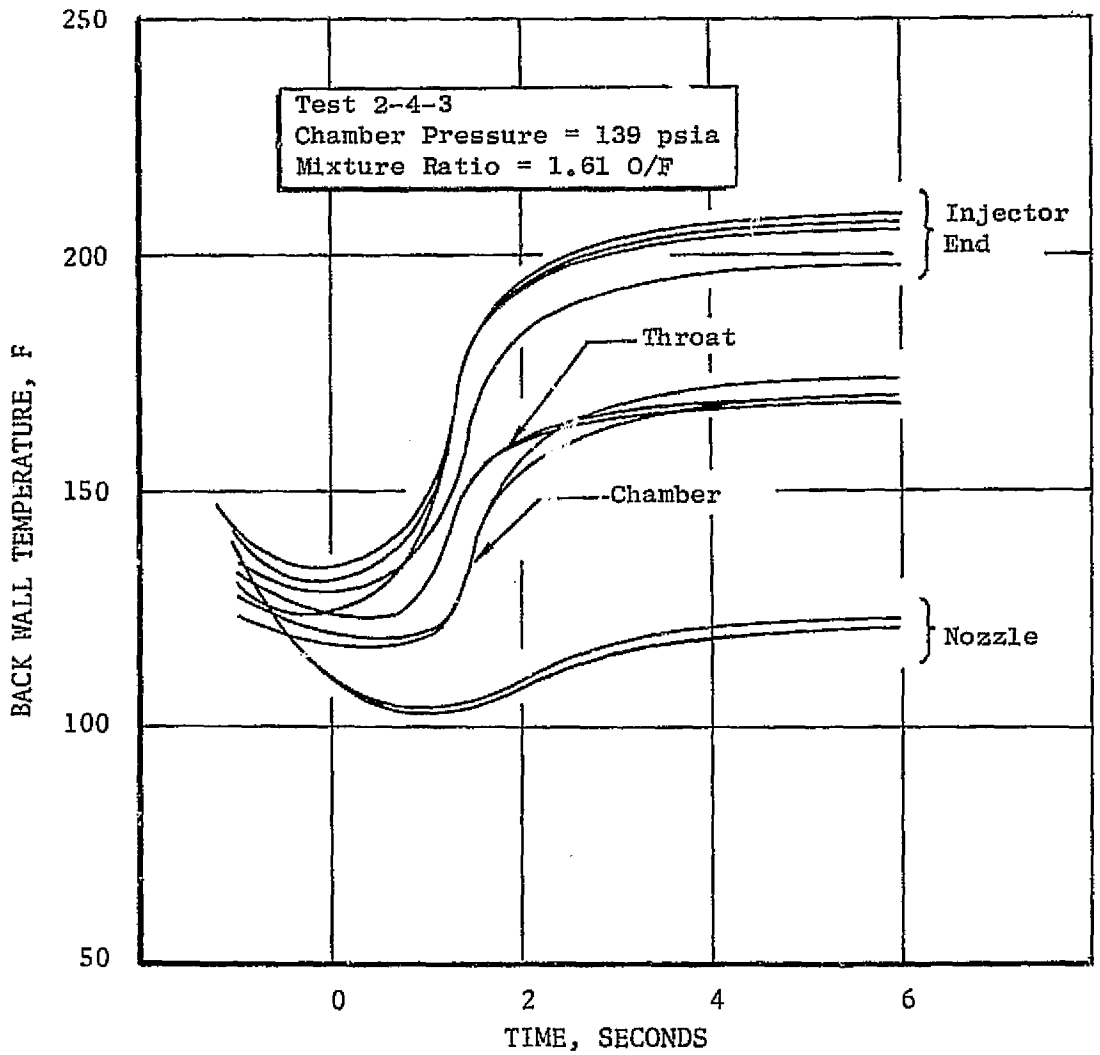

Figure 47. Typical WSTF Hot Start Backwall Temperature Transient

Steady state back wall temperatures are shown in Table 9. Steady state values of injector-end back wall temperatures are analyticcaly 30F above coolant outlet temperatures and may be used as indications of circumferential uniformity of the heat load. Injector-end back wall temperature data recorded at CTL-IV generally had a circumferential variation of less than 15 degrees (less than 10F excluding T10, which consistently ran low). Agreement between the temperature measurements made at the throat located 180 degrees apart was generally within 5F. Agreement was within 10F for opposing thermocouples in the nozzle region. At all locations the thermocouples located at the top of the chamber tended to read hotter than those located at the bottom of the chamber. The top thermocouples generally started at a higher temperature on hot start tests than the bottom thermocouples. However, the steady state temperature relationship between top and bottom measurements indicated hotter top measurements for cold start tests as well as hot start tests. Temperature measurements at the injector end generally exhibited the same trends at WSTF as the CTL-IV data. T-10 was the generally lowest reading location and the largest variation between injector end temperatures T-8, T-9, and T-11 was generally less than 6F for test series 2-3 (NTO/MMH unsaturated) and 2-4 (NTO/MMH saturated). Backwall temperatures measured at the throat and nozzle regions (2 at each location: T-14, T-15, and T-16, T-17, respectively) generally agreed within 2F at each location.

Experimental steady state back wall temperature measurements at nominal operating conditions are compared with the analytically predicted outer profile in Fig. 48. Since the actual heat load was experimentally determined to be about 25 percent lower than predicted, the analytical back wall temperature profile was based on a heat flux profile which was 25 percent below the originally predicted profile.

In the combustion zone the measured temperatures are about 15-20F lower than predicted outer surface values. The temperatures are however, above the predicted bulk temperature which they must be in actuality. In the nozzle region (x = 3.0 in.) the measured temperature also appears approximately 10F lower than predicted although the fact that the measurement was made near the region of the step change in channel width tends to complicate the results.

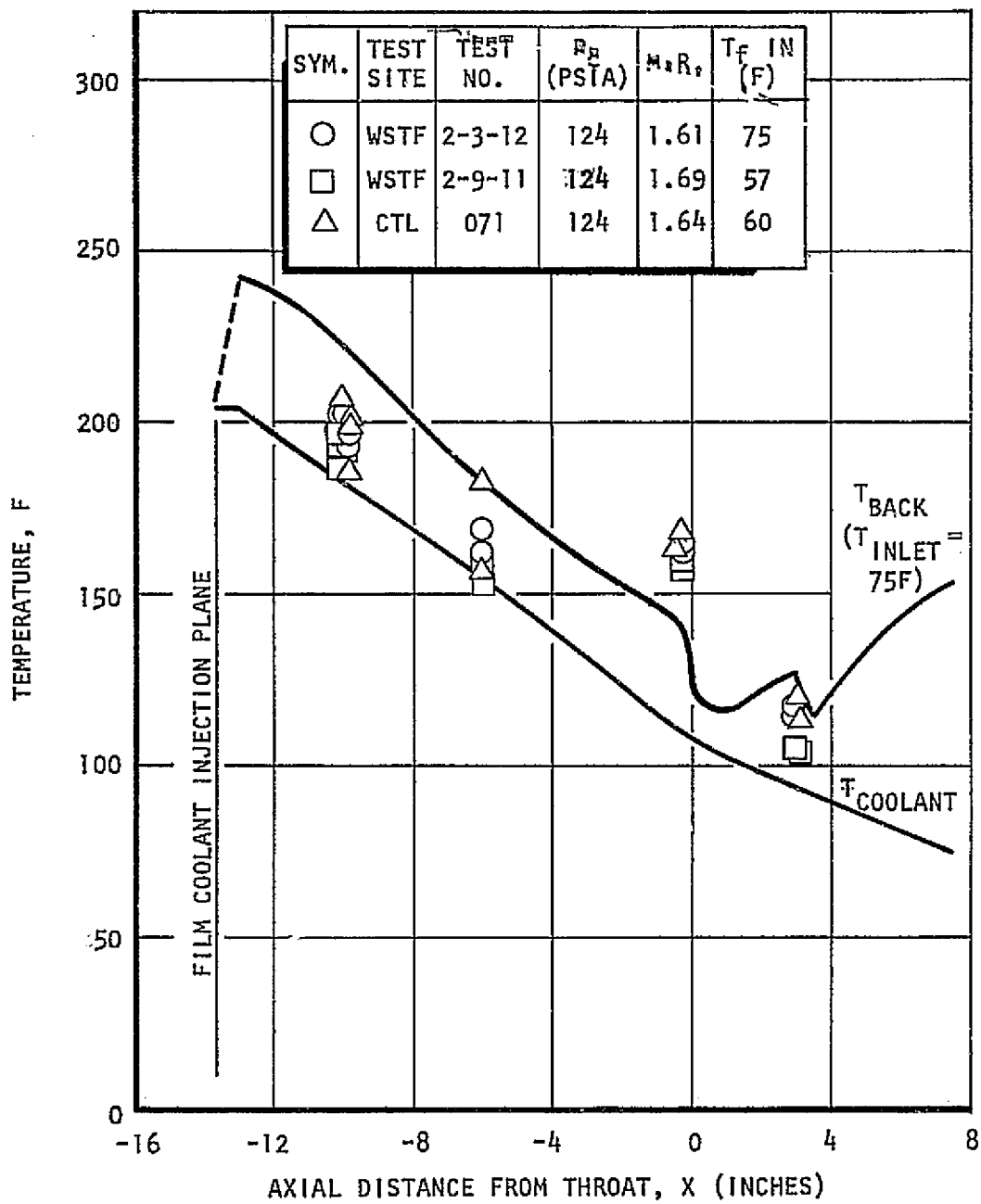

Figure 48. Back Wall Temperature Profile for the OME Demonstrator (Nominal Conditions)

Longitudinal conduction would tend to smooth the temperature profile in this region thereby making measured and predicted results in better agreement for the 75F inlet temperature case.

In the throat region the measured temperatures are about 20F higher than predicted. An analysis was conducted to determine if a higher throat heat flux could account for this discrepancy. An increase in heat flux of 40 percent resulted in a one degree increase in the outer surface temperature (confirming the original analysis that back wall temperature is relatively insensitive to heat flux level.) In order to achieve back wall temperatures similar to those measured the projected heat flux level would have been considerably in excess of burn-out conditions. Post test inspection of the OME demonstrator, however, did not indicate any discoloration due to overheating anywhere in the chamber.

The effect of longitudinal conduction was also determined to have a negligible (<1F) effect on outer surface temperature at the throat. The items most strongly affecting the outer surface temperature are bulk temperature and the coolant film coefficient in that order. The required increase in bulk temperature at the throat would indicate a nozzle heat load about 60 percent higher than predicted. This is in contradiction to the regeneratively cooled nozzle data and radiation nozzle results where the low nozzle temperatures indicate a lower than predicted heat flux level.

It appears at this time that the most likely reason for the higher throat outer surface temperature is a discrepancy in the coolant film coefficient distribution around the channel. The effect of the throat region curvature on a forced convection nucleate boiling liquid is not clearly understood. A degradation of the film coefficient along the outer wall (convex side of curved section) is possible. Further investigation in this area is needed to better predict back wall temperature. Assuming, however, that the inner wall (concave side of curved section) conditions are unaffected (i.e., T_{wg} is correct) the life of the throat region is actually increased due to a decreased temperature differential between inner and outer surfaces.

A predicted outer surface temperature profile (also based on measured heat load) for off-design conditions is compared with experimental results in Fig. 49. The comparative results are similar to those noted for nominal operating conditions. The back wall temperatures are, of course, somewhat higher due to increased coolant bulk temperature resulting from the higher mixture ratio.

Radiation Nozzle

The radiation cooled nozzle requires approximately 15 sec to reach near equilibrium conditions. Only two tests were conducted at CTL-IV exceeding that duration. None of the nozzle thermocouples functioned on the 185 sec duration test (last test at CTL-IV). On the 30 sec duration test (test 063) the digital data system failed so that only two temperature traces were available from the strip charts. These data plotted in Fig. 50 indicate a slightly more rapid transient than predicted and a steady state value of approximately 1900F which is approximately 400 degrees lower than predicted with fairly good agreement between the two measurements. Data taken at WSTF on the 30 sec duration test (Fig. 51) indicate nozzle temperatures even lower than measured at CTL-IV. Three of the four temperature readings at $\epsilon = 8.7$ are in excellent agreement. The TC 27 measurement is probably in error because other thermocouple data in the same circumferential location (T9, T23) indicate slightly higher than average temperatures. The maximum variation in steady state temperatures at the exit of the nozzle was 100F.

Transient data from the shorter (10 sec) duration tests at WSTF were also lower than the data taken at CTL-IV at a comparable times. Although it is analytically difficult to justify these temperatures as low as those recorded at WSTF it should be noted that visual comparisons of the radiation cooled nozzles during the tests based on motion pictures indicated a dull glow at CTL-IV while none was evident at WSTF. Hopefully, future longer duration tests with the more extensively instrumented integrated thrust chamber will clarify the data. Little difference in the temperature transients was noted between tests with MMH and tests with 50-50 as shown in Fig. 52.

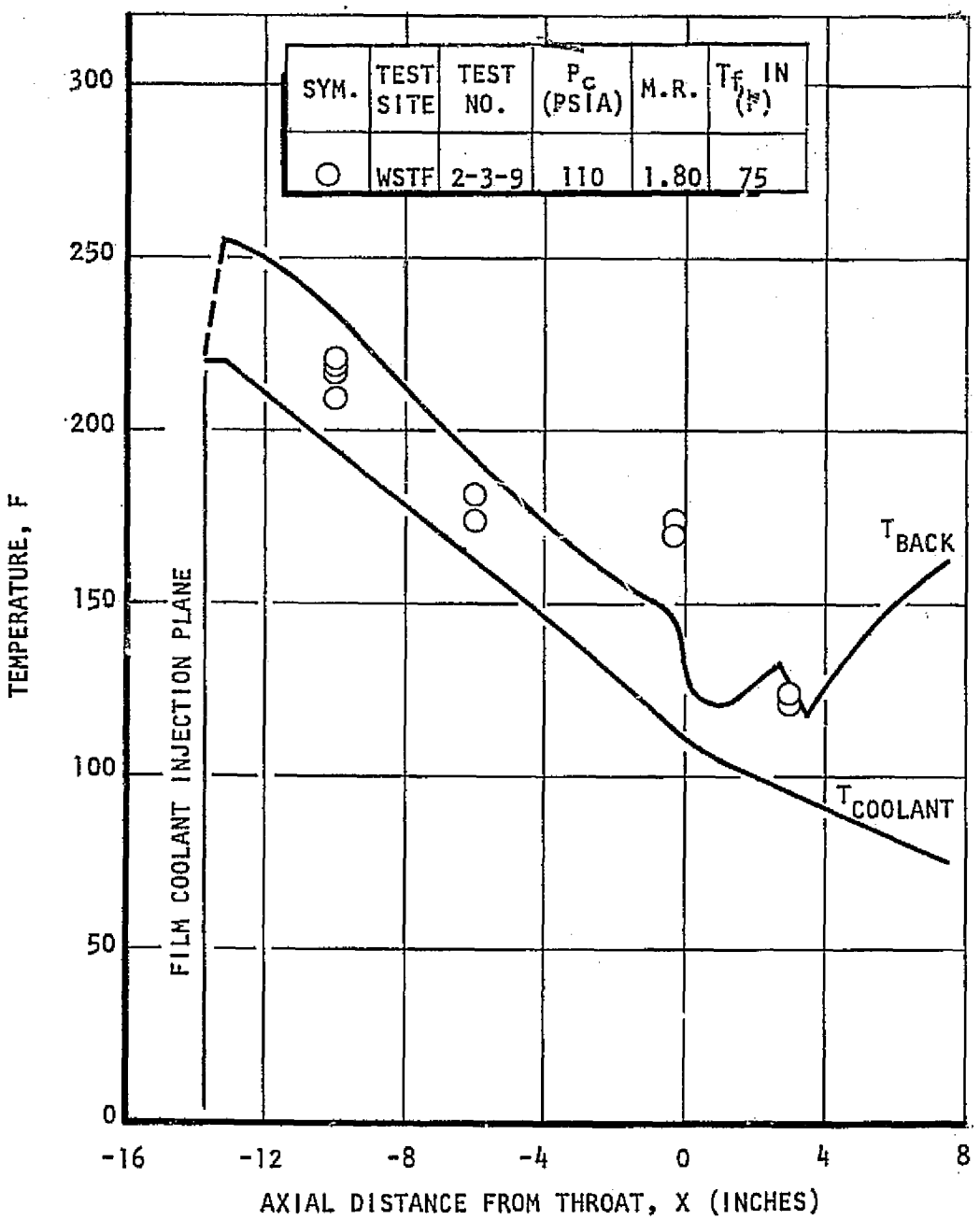

Figure 49. Back Wall Temperature Profile for the OME Demonstrator (Off-Design)

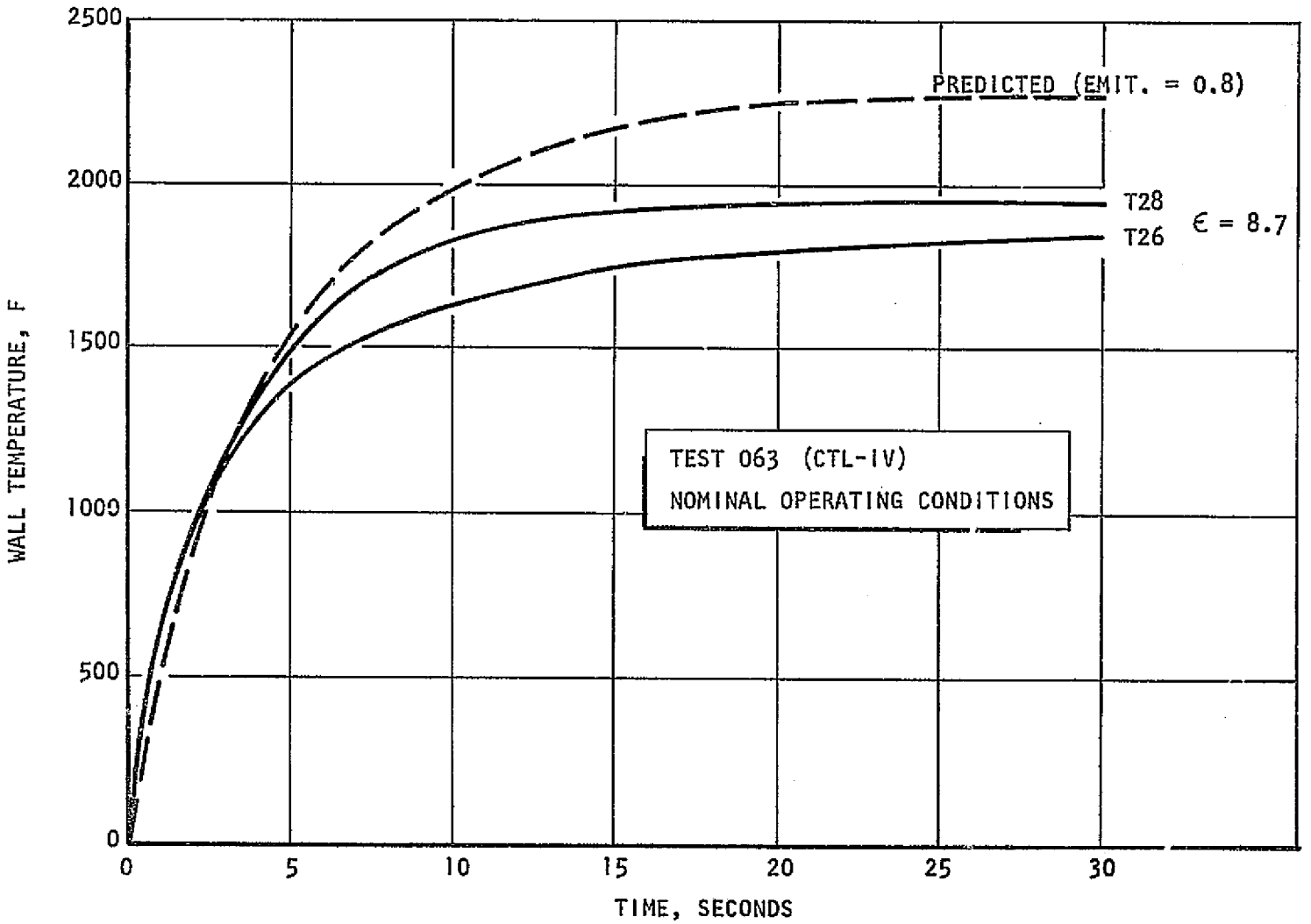

Figure 50. Radiation Cooled Nozzle Temperature Response

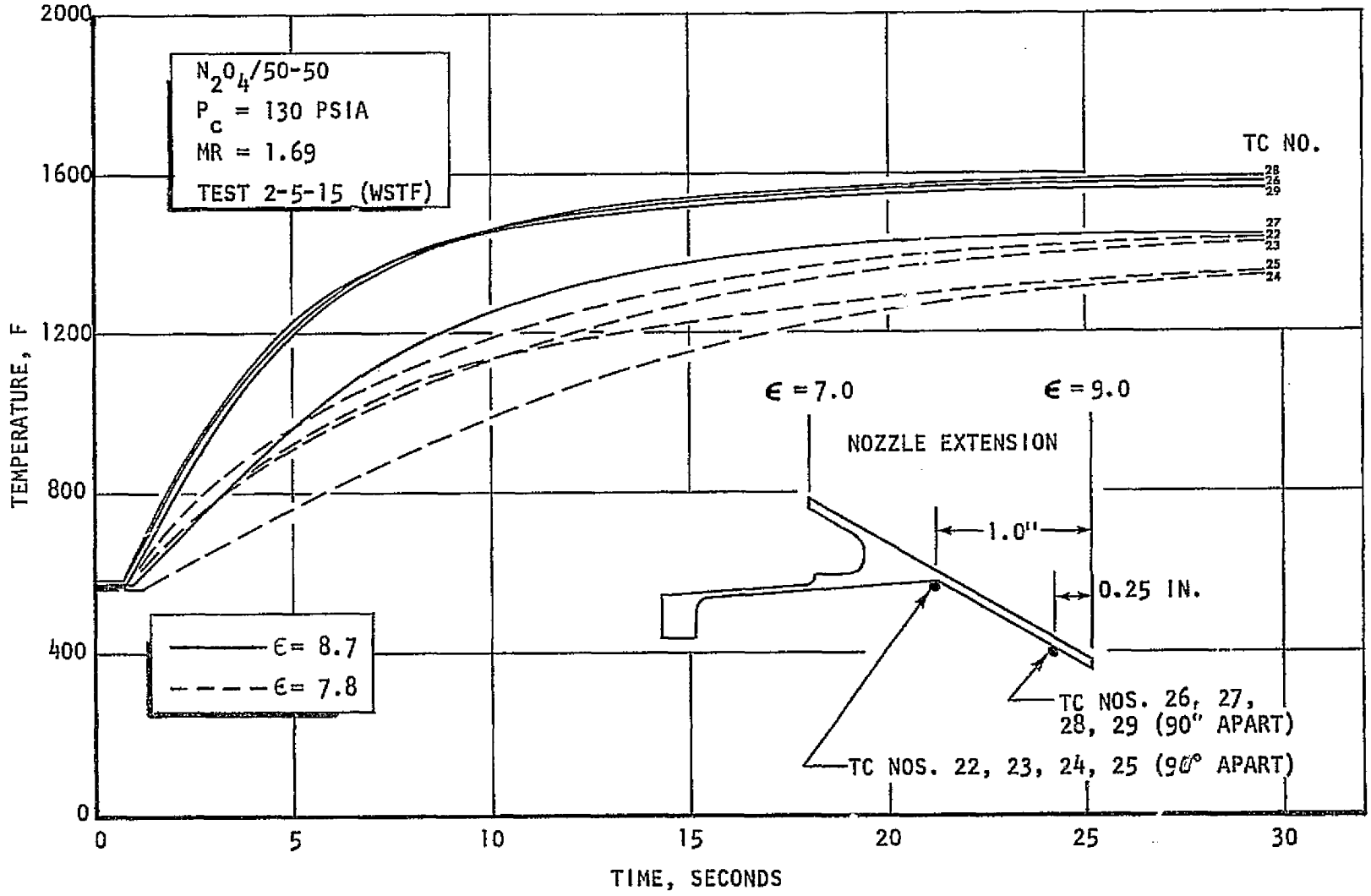

Figure 51. Radiation Cooled Nozzle Temperature Transients

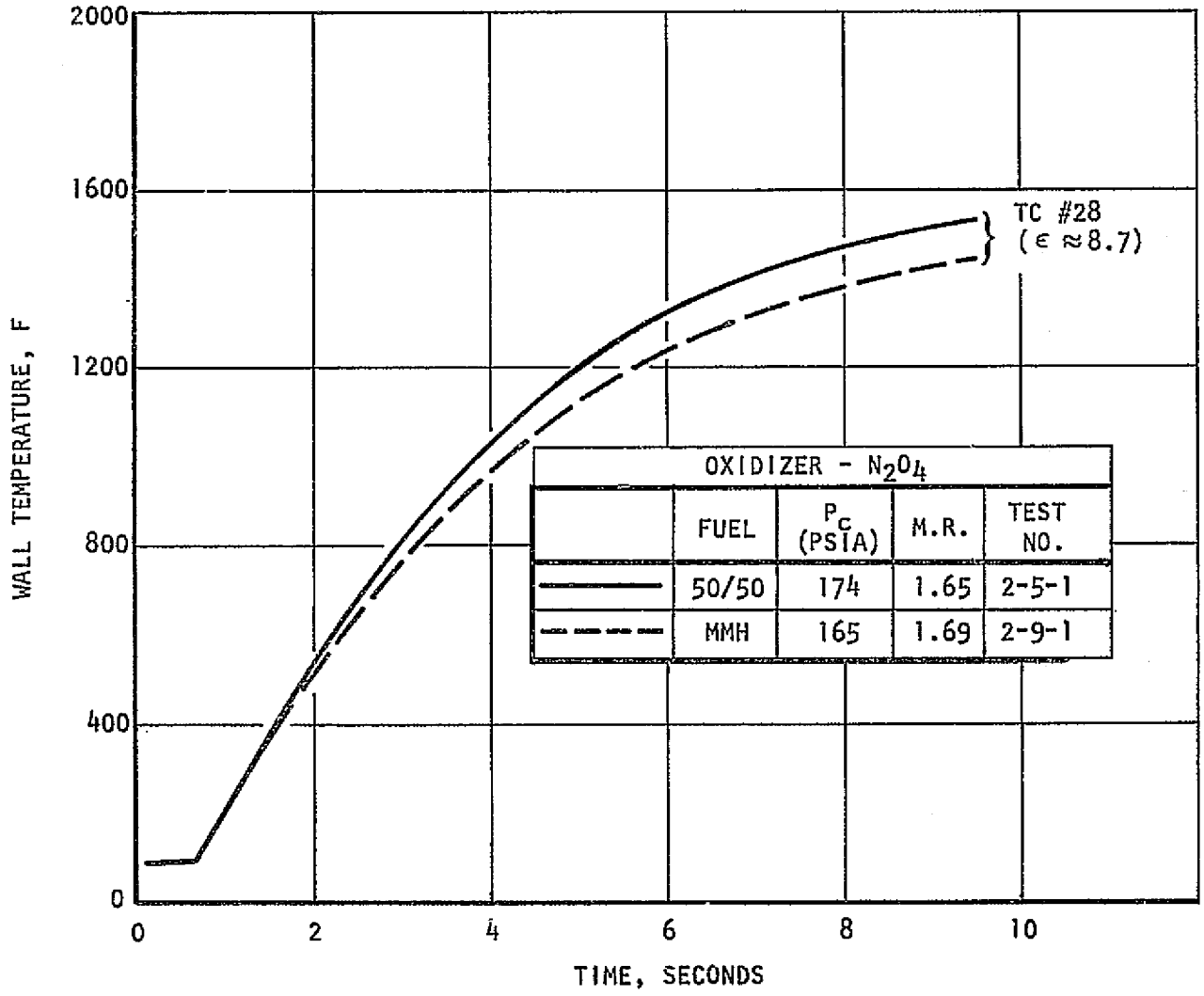

Figure 52. Effect of Fuel on Radiation Cooled Nozzle Temperature

Coolant Jacket ΔP

The regenerative jacket pressure drop versus flowrate is shown in Fig. 53. Inlet and outlet pressures were measured at the same locations in the manifolds at both facilities, and were therefore comparable with the predicted pressure drop which did not include manifold losses. The pressure drops for the regeneratively cooled tests at CTL-IV are seen to be approximately 1-2 psi below the predicted values, while data taken at WSTF was approximately 1-2 psi above the predicted value.

Pressure drops calculated by subtracting the fuel injection pressure from the regenerative coolant jacket inlet pressure are shown in Fig. 54. This ΔP includes the jacket exit manifold and crossover passage pressure drops. A much better consistency between these data from the two facilities is apparent implying that a discrepancy exists between the coolant jacket exit pressures. The ΔP from the coolant jacket exit to the fuel injector was examined and found to be low (generally < 2 psi) and sometimes negative based on WSTF data compared to 3-6 psi based on CTL-IV data. The CTL-IV data, therefore, appears more credible. However, at each facility, the ΔP values were obtained by subtracting absolute pressure measurements (~ 200 psia) so that such variations are within instrumentation accuracies. More precise pressure drop data should be obtained by using a differential pressure transducer or by low pressure flow calibration tests.

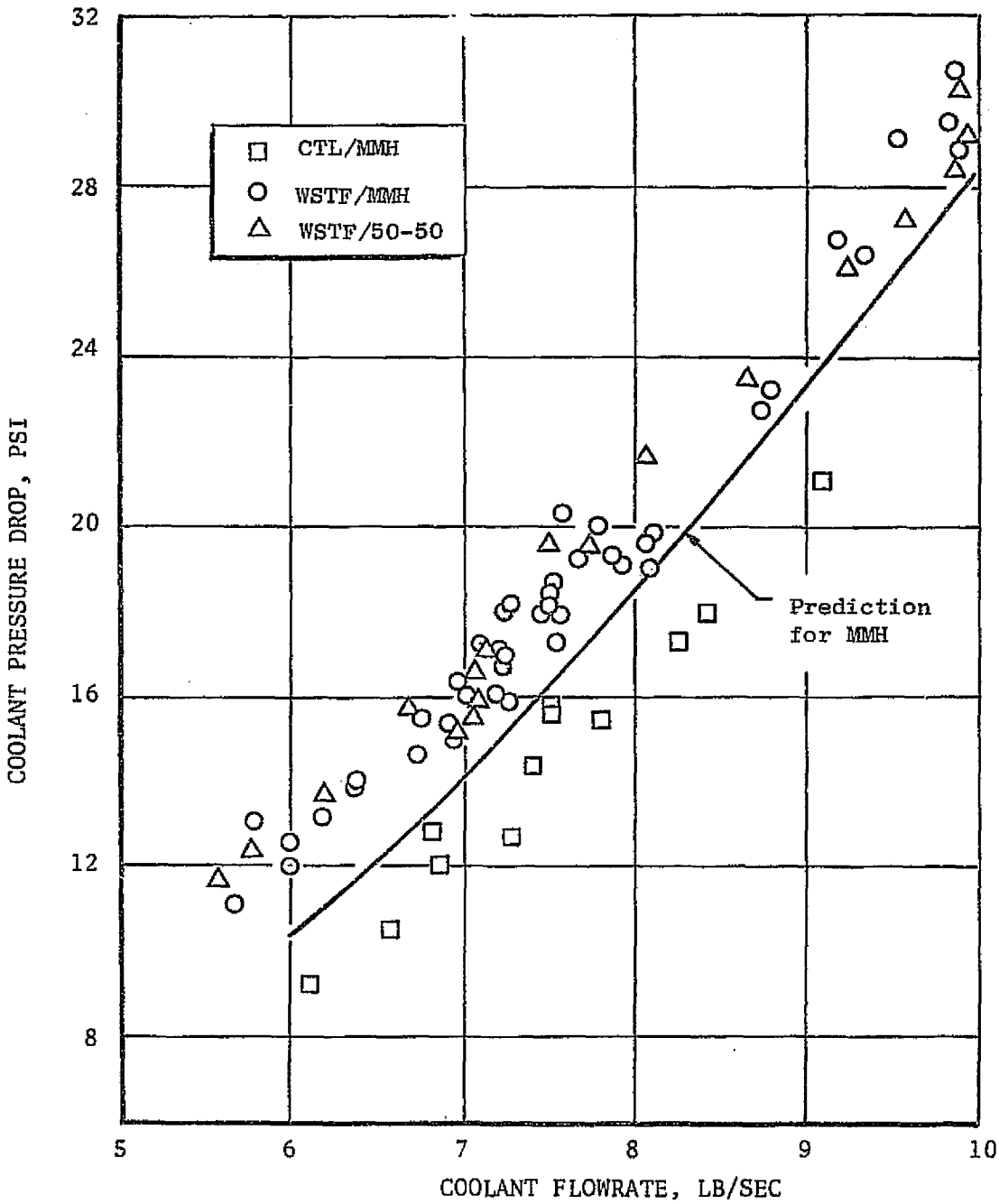

Figure 53 . Coolant Jacket Pressure Drops

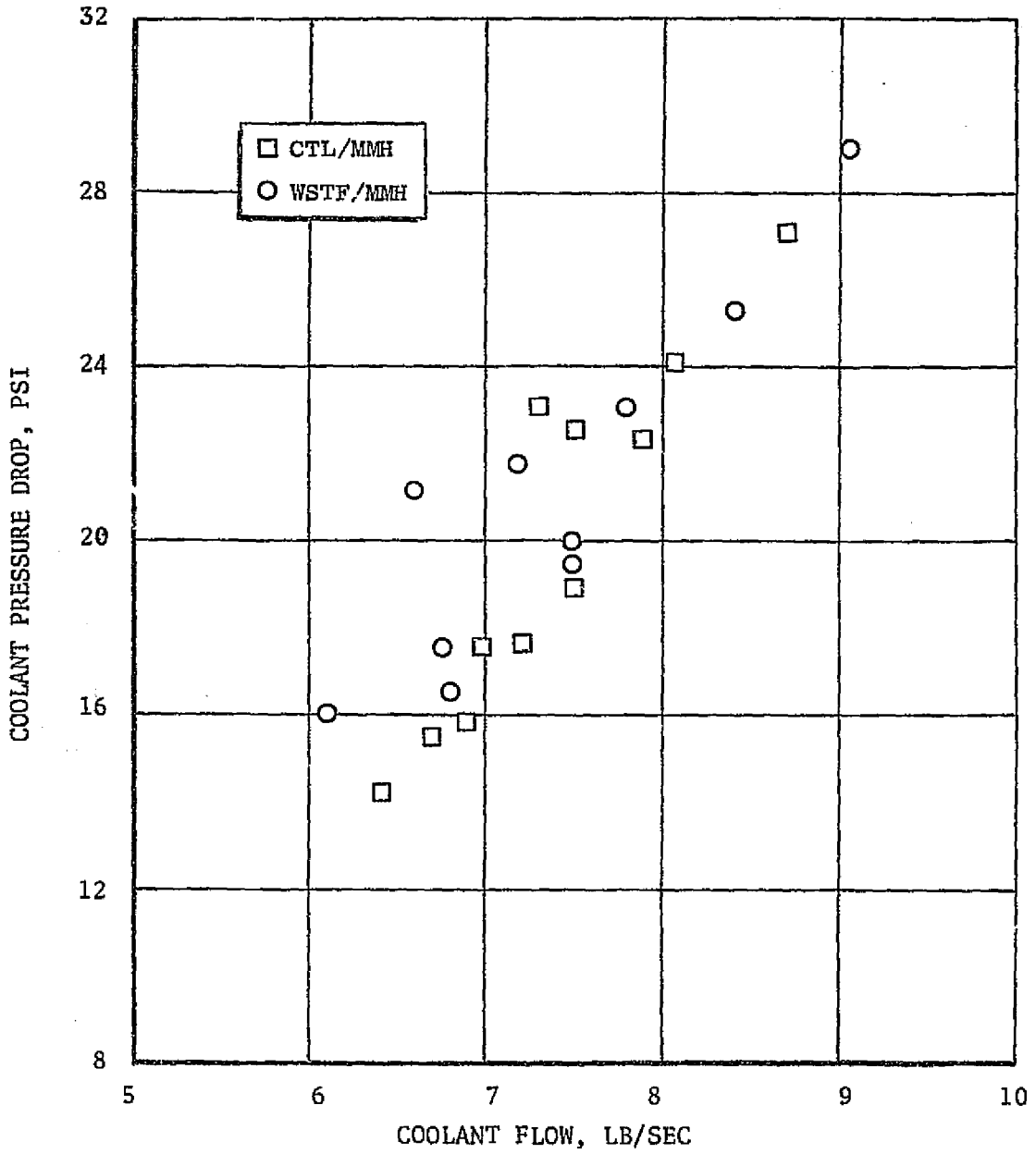

Figure 54. Pressure Drop Between Coolant Jacket Inlet and Fuel Injector

CONCLUSIONS

Sufficient data has been generated by these test series to warrant conclusions concerning the performance, thermal, and stability characteristics of the Rocketdyne designed OME regeneratively cooled thrust chamber.

SAFETY

The thrust chamber is capable of operating safely not only over the design ranges of chamber pressure and mixture ratio, but also at off design conditions such as those encountered during a vehicle pressurization system failure or for an application requiring high chamber pressure such as the storable Space Tug engine. The thrust chamber can start and operate safely with either a fuel or an oxidizer lead. Oxidizer rich shut downs, possibly including a fuel depletion sequence, can be tolerated. The thrust chamber can restart safely without purges between firings. Safe operation was demonstrated with helium saturation of the propellants and with helium bubbles in the oxidizer system. Helium bubbles in the fuel were not run but data is being generated during heated tube experiments under Task IX.

PERFORMANCE

Measured performance data implies that the engine tested would achieve a vacuum specific impulse of 310 seconds with a high (72:1) nozzle typical of OME applications. Further injector development would be expected to improve the specific impulse by at least 3 seconds.

HEAT TRANSFER

Heat loads were substantially lower than the predicted values implying higher safety factors or the ability to improve performance by reducing boundary layer coolant or increasing the combustor length. Low nozzle temperatures imply that the radiation cooled nozzle attach point could be moved closer to the throat reducing the thrust chamber weight and further reducing the heat load of the regenerative coolant. As an

alternative, the low regenerative heat loads and nozzle temperatures suggest the possibility of increasing the regeneratively cooled nozzle area ratio slightly and replacing the coated Columbium radiation cooled nozzle with a more reliable uncoated nozzle of L605 which can operate at temperatures up to 1900F. Back wall temperatures during or after operation at any point on the regenerative thrust chamber do not exceed 450F and may actually be considerably lower.

STABILITY

No incidents of combustion instability occured on the 112 tests over the complete range of chamber pressures and mixture ratios. Although bomb tests would be required for verification, this implies a very stable injector/thrust chamber combination.

FABRICATION

The feasibility of the electroforming fabrication technique was demonstrated not only by the above safe operating record but also by the demonstrated ability to repair the thrust chamber using the same method when it was damaged by a facility malfunction.

RECOMMENDED FURTHER EFFORT

The completed program was addressed to the areas requiring most immediate resolution or verification. Other areas which should now be investigated and areas which were uncovered by the completed test program are as follows.

The injector-end manifold, film coolant ring, and injector manifold were designed to provide the extreme flexibility required for the first regeneratively cooled hardware. This entailed some compromise in the thermal and pressure transient characteristics compared to a flight type chamber. Now that the acoustic cavity configuration appears to be adequate (although not necessarily optimum), and the film coolant flowrate is defined, a chamber and injector assembly should be tested which closely simulate flight configuration at the injector end. The chamber should be more extensively instrumented to better define the thermal conditions circumferentially and axially on the chamber. This configuration should be tested over the entire design range of chamber pressure and mixture ratios as well as at the high and low off-design conditions to which the demonstration chamber was subjected. Various on and off time duty cycles should be tested at altitude without purging between tests to simulate hot and cold start and restarts. Various duration oxidizer and fuel leads should be programmed to demonstrate flexibility. Long duration tests should be conducted to determine final steady state performance and heat transfer values.

A high area ratio heat sink nozzle ($\epsilon = 72$) is available and should be tested with thermocouple instrumentation to verify nozzle heat transfer rates and to obtain a direct measurement of performance with a high area ratio nozzle.

Regenerative thrust chamber life was analytically determined to be limited by the number of cycles (1500) rather than by operating time. The cyclic strains are thermally induced and can be simulated with relatively short duration tests. The OME requirement of 1000 cycles should be demonstrated by the integrated chamber after other tests have been conducted. Altitude tests are preferable, although representative results could probably be obtained with sea level tests. Analyses would have to be made, in the latter case, to assure that the separation point would not become the critical life location.

Extreme adverse operating conditions should be imposed on the chamber to determine its capabilities. These include helium bubbles in the fuel, fuel depletion shutdown, and plugged channel operation. Since these conditions could result in chamber damage, the tests should be the final ones attempted or should use the demonstrator hardware.

APPENDIX

OME PERFORMANCE DATA REDUCTION

Measurement	Symbol	Units
1. Thrust	F	lb
2. Injector end chamber pressure	P_c	psia
3. Oxidizer flowrate	$\dot{W}_o$	lb/sec
4. Total fuel flowrate	$\dot{W}_F$	lb/sec
5. Fuel injection manifold temperature	T_F	F
6. Ambient pressure (exit)	P_a	psia
7. Throat area	A_t	in^2
8. Expansion area ratio	ϵ	
9. Oxidizer injection pressure	P_{OI}	psia
10. Fuel injection pressure	P_{FI}	psia
11. BLC orifice downstream pressure	P_{BLC}	psia
12. BLC orifice diameter	D	in.
13. Fuel specific gravity	ρ_F	

PROCEDURE

1. Compute boundary layer flowrate ($\dot{W}_{BLC}$)

$$\dot{W}_{BLC} = 2.9 \times D^2 \times \sqrt{\rho_F \times (P_{FI} - P_{BLC})}$$

2. Compute total propellant flowrate ($\dot{W}_T$)

$$\dot{W}_T = \dot{W}_o + \dot{W}_F$$

3. Compute boundary layer coolant fraction (BLC)

$$BLC = \frac{\dot{W}_{BLC}}{\dot{W}_T}$$

4. Compute mixture ratio (MR)

$$MR = \frac{\dot{W}_o}{\dot{W}_F}$$

5. Compute nozzle stagnation pressure (P_{NS})

$$P_{NS} = 0.95 \times P_c$$

6. Compute characteristic velocity (C*)

$$C^* = \frac{32.174 \times P_{NS} \times A_t}{\dot{W}_T}$$

7. Compute site thrust coefficient ($C_{F\ SITE}$)

$$C_{F\ SITE} = \frac{F}{P_{NS}\ A_t}$$

8. Compute vacuum thrust coefficient ($C_{F\ VAC}$)

$$C_{F\ VAC} = C_{F\ SITE} + \frac{\epsilon\ P_a}{P_{NS}}$$

9. Compute expected vacuum thrust coefficient (C_{FVE})

$$C_{FVE} = 1.360 \times [1 + 0.06 \times BLC] + [(MR - 1.65) \times 0.021] \text{ for } \epsilon = 3$$

$$C_{FVE} = 1.519 \times [1 + 0.14 \times BLC] + [(MR - 1.65) \times 0.057] \text{ for } \epsilon = 9$$

$$C_{FVE} = 1.783 \times [1 + 0.23 \times BLC] + [(MR - 1.65) \times 0.12] \text{ for } \epsilon = 72$$

10. Compute C_F correlation (K)

$$K = \frac{C_{F\ VAC}}{C_{FVE}}$$

11. Adjust thrust coefficient to nominal ϵ

$$C_{F\ VAC} = 1.311 \times C_{F\ VAC}\ [1 - 0.06 \times BLC] \text{ for } \epsilon = 3$$
$$\epsilon = 72$$

$$C_{F\ VAC} = 1.1738 \times C_{F\ VAC}\ [1 - 0.14 \times BLC] \text{ for } \epsilon = 9$$
$$\epsilon = 72$$

$$C_{F\ VAC} = C_{F\ VAC}\ [1 - 0.23 \times BLC] \text{ for } \epsilon = 72$$
$$\epsilon = 72$$

12. Compute vacuum thrust (F_{VAC})

$$F_{VAC} = F + \epsilon \times A_t \times P_a$$

13. Find stratification C* loss (ΔC^*_{BLC}) from table of ΔC^*_{BLC} vs blc,

mr at blc = BLC
mr = MR

14. Compute C* adjusted for BLC (C^*_{UMR})

$$C^*_{UMR} = C^* - \Delta C^*_{BLC}$$

15. Find stratification specific impulse loss ($\Delta I_{s\ BLC}$) from table of $\Delta I_{s\ BLC}$

vs blc, mr at blc = BLC
mr = MR

16. Compute vacuum specific impulse (I_{s1}) at test MR, BLC

$$I_{s1} = \frac{C_{F\ VAC} \times C^*_{UMR}}{\epsilon = 72 \quad 32.174} + \Delta I_{s\ BLC}$$

17. Find theoretical I_s ($I_{s\ TH}$) from table of $I_{s\ TH}$ vs

mr, P at mr = MR
P = P_{NS}

18. Compute specific impulse efficiency (ηI_s) for test

$$\eta I_s = \frac{I_{s1}}{I_{s\ TH}}$$

19. Compute test vacuum specific impulse ($I_{s\ VT}$)

$$I_{s\ VT} = \frac{C^* \times C_{F\ VAC}}{32.174}$$

20. Find TDK specific impulse ($I_{s\ TDK}$)

from table of $I_{s\ TDK}$ vs mr, P at mr = MR

P = P_{NS}

21. Compute energy release efficiency (η_{ER})

$$\eta_{ER} = \frac{I_{s\ VT} + 40/\dot{W}_T}{I_{s\ TDK}} \times 100 \text{ for } \epsilon = 3$$

$$\eta_{ER} = \frac{I_{s\ VT} + 58/\dot{W}_T}{I_{s\ TDK}} \times 100 \text{ for } \epsilon = 9$$

$$\eta_{ER} = \frac{I_{s\ VT} + 127/\dot{W}_T}{I_{s\ TDK}} \times 100 \text{ for } \epsilon = 72$$

ORBIT MANEUVERING ENGINE TEST DATA SUMMARY

(PERFORMANCE)

TEST # N

Thrust, lb (vac)	$F + 9 \times P_a \times A_t$
Injector end chamber pressure, psia	P_c
Nozzle stagnation pressure, psia	P_{NS}
Mixture ratio	MR
Characteristic Velocity (C*), ft/sec	C*
C* efficiency (overall), percent	$\eta_{C^* \text{ SITE}} \times 100$
C* efficiency (stratified), percent	$\eta_{C^* \text{ VAP,MIX}} \times 100$
Vacuum specific impulse at EPS = 72, sec	I_{sl}
Specific impulse efficiency, percent	$\eta_{I_s} \times 100$
Film coolant flow, percent of total flow	BLC x 100
Total oxidizer flow, lb/sec	$\dot{W}_o$
Total fuel flow, lb/sec	$\dot{W}_F$
Total flow, lb/sec.	$\dot{W}_T$
Oxidizer injector delta P, psi	$P_{OI} - P_c$
Fuel injector delta P, psi	$P_{FI} - P_c$
Fuel injection temperature, F	T_F
Ambient pressure, psia	P_a
Throat area, in^2	A_t
Site thrust coefficient	$C_{F \text{ SITE}}$
Vacuum thrust coefficient	$C_{F \text{ VAC}}$
Vacuum Specific Impulse, sec	I_{sVT}
Predicted thrust coefficient	C_{FVE}
Thrust coefficient correlation	K
Vacuum thrust coefficient at EPS = 72	$C_{F \text{ VAC}}$ $\epsilon = 72$

AUXILIARY DATA

Thrust, lb	I.E. Chamber Pressure, psia	Oxidizer Flowrate, lb/sec	Fuel Flowrate, lb/sec	Cell Pressure, psia
F_A	$P_{c\ 1}$	$\dot{W}_{ox\ 1}$	$\dot{W}_{F\ 1}$	$P_{a\ 1}$
F_B	$P_{c\ 2}$	$\dot{W}_{ox\ 2}$	$\dot{W}_{F\ 2}$	$P_{a\ 2}$